

May 2023

Morphologic Comparisons of Recrystallized and Neocrystallized Fibrous Amphibole Asbestos: Implications for Corresponding Health Risk Potential

Natalie G. Renkes

Follow this and additional works at: <https://digitalscholarship.unlv.edu/thesesdissertations>



Part of the [Environmental Health Commons](#), [Environmental Health and Protection Commons](#), and the [Geology Commons](#)

Repository Citation

Renkes, Natalie G., "Morphologic Comparisons of Recrystallized and Neocrystallized Fibrous Amphibole Asbestos: Implications for Corresponding Health Risk Potential" (2023). *UNLV Theses, Dissertations, Professional Papers, and Capstones*. 4766.

<http://dx.doi.org/10.34917/36114791>

This Thesis is protected by copyright and/or related rights. It has been brought to you by Digital Scholarship@UNLV with permission from the rights-holder(s). You are free to use this Thesis in any way that is permitted by the copyright and related rights legislation that applies to your use. For other uses you need to obtain permission from the rights-holder(s) directly, unless additional rights are indicated by a Creative Commons license in the record and/or on the work itself.

This Thesis has been accepted for inclusion in UNLV Theses, Dissertations, Professional Papers, and Capstones by an authorized administrator of Digital Scholarship@UNLV. For more information, please contact digitalscholarship@unlv.edu.

MORPHOLOGIC COMPARISONS OF RECRYSTALLIZED AND NEOCRYSTALLIZED FIBROUS
AMPHIBOLE ASBESTOS: IMPLICATIONS FOR CORRESPONDING
HEALTH RISK POTENTIAL

By

Natalie G. Renkes

Bachelor of Science- Geology
Grand Valley State University
2016

A thesis submitted in partial fulfillment
of the requirements for the

Master of Science-Geoscience

Department of Geoscience
College of Sciences
The Graduate College

University of Nevada, Las Vegas
May 2023



Thesis Approval

The Graduate College
The University of Nevada, Las Vegas

April 7, 2023

This thesis prepared by

Natalie G. Renkes

entitled

Morphologic Comparisons of Recrystallized and Neocrystallized Fibrous Amphibole
Asbestos: Implications for Corresponding Health Risk Potential

is approved in partial fulfillment of the requirements for the degree of

Master of Science-Geoscience
Department of Geoscience

Brenda Buck, Ph.D.
Examination Committee Chair

Rodney Metcalf, Ph.D.
Examination Committee Member

Pamela Burnley, Ph.D.
Examination Committee Member

David James, Ph.D.
Graduate College Faculty Representative

Alyssa Crittenden, Ph.D.
*Vice Provost for Graduate Education &
Dean of the Graduate College*

Abstract

The presence of naturally-occurring asbestos (NOA) is increasingly concerning for scientists, health and regulatory agencies, and citizens living in impacted areas. It is commonly believed that fibrous amphibole asbestos can only form through neocrystallization. In southern Nevada, NOA occurs as a result of hydrothermal alteration of granitic rock producing fibrous amphibole both as cross-cutting neocrystallized veins and via recrystallization of original magmatic hornblende crystals. Fibers with a greater aspect ratio are known to have increased toxicity. This study measured the maximum length and average width of both neocrystallized and recrystallized fibers to see if the morphologies were similar. Neocrystallized and recrystallized fibers from the McCullough Range, NV were identified using a petrographic microscope, extracted from polished thin sections using a motorized drill, and analyzed using the scanning electron microscope (SEM), and field emission scanning electron microscope (FESEM) with energy dispersive x-ray analysis (EDS). Neocrystallization produced fibers with an average width of $0.53 \pm 0.018 \mu\text{m}$, an average length of $4.26 \pm 0.257 \mu\text{m}$, and an average aspect ratio of 8.7 ± 0.38 . Recrystallization produced fibers with an average width of $0.64 \pm 0.023 \mu\text{m}$, an average length of $7.31 \pm 0.483 \mu\text{m}$, and an average aspect ratio of $13. \pm 0.86$. Multiple statistical analyses, explicitly the Mann-Whitney U-test, confirmed that recrystallized particles more commonly had either statistically similar ($p > 0.05$) or statistically wider ($p < 0.05$) widths, significantly longer lengths, and significantly greater aspect ratios compared to neocrystallized particles of similar mineralogy and chemistry. Because the recrystallization process produces fibers that have greater average aspect ratios, they may be more toxic than those produced through neocrystallization. We hypothesize that the likely reason for this are increased chain width defects resulting from fluctuating conditions during recrystallization. Because hydrothermal alteration and recrystallization of primary minerals is a very common geologic process, this finding may significantly increase the estimated potential of rocks and soils that contain NOA.

Acknowledgements

I would like to acknowledge and thank Chris Bolhuis who first introduced me to the field of geology and taught me how the world has a beautiful way of making one feel insignificant. Thank you to Dr. Steve Maddox and all my Grand Valley State University Geology professors who guided me, built my confidence as a geologist, and filled my geology toolkit with knowledge. Thank you to all my UNLV professors, committee members, and more specifically, my advisors (Dr. Brenda Buck and Dr. Rodney Metcalf) who gave me an immense amount of support, patience, and guidance. I truly could not have finished this thesis without Brenda or Rod's council, advice, and dedication to myself and this research. Thank you to the student interns (Laekyn Kelley, Samantha Lockhart, Tammy Legg, and Anabelle Castro) for helping me with SEM/FESEM imaging and lab work. Thank you to Anay Gomez who taught me how to use our lab. Thanks for the BLM for funding this project (permit #L13AC00237). Lastly, thank you to my friends and family. I truly could not have finished this without your love, support, and understanding.

Dedication

To my friends, family, and advisors. I couldn't have done this without your endless love and support.

Table of Contents

Abstract.....	iii
Acknowledgements.....	iv
Dedication.....	v
Table of Contents.....	vi
List of Tables.....	ix
List of Figures.....	xi
Chapter 1: Introduction.....	1
1.1 What is Asbestos?.....	1
1.2 The Life Cycle of Asbestos.....	2
1.3 Exposure Pathways and Toxicity.....	4
1.4 Morphology of EMPs and Asbestos Fibers.....	5
1.5 Crystallization Processes.....	9
1.6 Geologic Background.....	10
1.7 Hypothesis.....	11
Chapter 2: Methods.....	13
Chapter 3: Results.....	18
3.1 Statistical Analyses.....	18
3.2 Petrographic Analyses.....	18
3.3 Dimensional Analyses of Amphibole Particle Chemistry and Mineralogy.....	19
3.4 Dimensional Analysis of Neocrystallized Vs. Recrystallized Particles.....	20

3.5 Dimensional Analyses by Particle type	20
3.5.1 Dimensional Analysis of Fiber Vs. Bundle Morphology.....	21
3.5.2 Dimensional Analysis of Particle Type with Fiber Width $\leq 1 \mu\text{m}$	22
3.5.3 Particle type with Length $\geq 5 \mu\text{m}$, Width $\leq 1 \mu\text{m}$, and AR $\geq 3:1$	23
3.6 Regulatory and Theorized Dimension Definitions	24
3.6.1 Regulatory Dimension Definitions: OSHA, WHO, EPA	24
3.6.2 Harper’s Theorized Dimension Definition of an Asbestos Fiber.....	26
3.7 Dimensional Analyses of Particle Type Vs. Asbestos Fiber Regulations.....	26
3.8 FESEM Vs. SEM Statistical Analyses.....	28
Chapter 4: Discussion	30
4.1 Amphibole Mineralogy and Petrographic Implications.....	31
4.2 Dimensional and Morphologic Patterns and Implications of Neo-and-Re-crystallization	33
4.2.1 Particle Dimensional Qualification Under Asbestos Standards.....	33
4.2.2 Particle Type Implications	35
4.2.3 Implications for Dimensional Analyses of Particle Type Vs. Asbestos Fiber Standards	38
4.2.4 FESEM Vs. SEM Implications	39
4.3 Previous Regional NOA Studies (Nevada-Arizona).....	40
4.4 Toxicity of Amphibole Particles.....	42
4.4.1 Short Fiber Debate	44
4.4.2 Cleavage Fragment Debate	48
4.4.3 Toxicological Study of Arizona NaFe ³⁺ fibrous Amphiboles	51

4.4.4 Short Fibers and Cleavage Fragments in Las Vegas.....	52
4.5 Chain-Width Defects	54
4.6 Worldly Implications	55
Chapter 5: Conclusion.....	57
5.1 Recrystallization Produces Asbestos Morphologies	57
Appendix A: Tables	58
Appendix B: Figures	97
Appendix C: Supplemental Data.....	138
References.....	139
Curriculum Vitae	149

List of Tables

Table 1. Mineral Names and Formulas of Regulated and Non-Regulated Asbestos. Modified from Perry (2004).....	58
Table 2. Tests of Normality for Particles with an $AR \geq 3:1$ by Crystallization Process*	59
Table 3. Tests of Normality for Log_{10} (Particles) with an $AR \geq 3:1$	60
Table 4(a). Ranks for Log_{10} (All Particles) with an $AR \geq 3:1$ Across Crystallization Process and (b) Test Statistics for Log_{10} (All Particles) with an $AR \geq 3:1$ Across Crystallization Process	61
Table 5(a). Ranks for Log_{10} (Particles) with an $AR \geq 3:1$ Across the Category of Microscopy Method and (b) Test Statistics for Log_{10} (Particles) with an $AR \geq 3:1$ Across the Category of Microscopy Method. ...	62
Table 6(a). Ranks for Log_{10} (SEM Particles) with an $AR \geq 3:1$ Across the Category of Crystallization Process and (b) Test Statistics for Log_{10} (SEM Particles) with an $AR \geq 3:1$ Across the Category of Crystallization Process.....	63
Table 7(a). Ranks for Log_{10} (FESEM Particles) with an $AR \geq 3:1$ Across Crystallization Process and (b) Test Statistics for Log_{10} (FESEM Particles) with an $AR \geq 3:1$ Across Crystallization Process.	64
Table 8. Assigned Mineral Name for All Particles with an $AR \geq 3:1$	65
Table 9. Assigned Mineral Name by Crystallization Process Particles with an $AR \geq 3:1$	66
Table 10. Assigned Mineral Group for All Particles with an $AR \geq 3:1$	67
Table 11. Assigned Mineral Group by Crystallization Process for Particles with an $AR \geq 3:1$	68
Table 12. Statistical Analysis of All Data with an $AR \geq 3:1$	69
Table 13. Bundle Dimensions by Crystallization Type for Data with an $AR \geq 3:1$	70
Table 14. Fiber Dimensions by Crystallization Type for Data with an $AR \geq 3:1$	71
Table 15. Prismatic Crystal Dimensions by Crystallization Type for Data with an $AR \geq 3:1$	72
Table 16. Combined Statistics of Fibers and Bundles with an $AR \geq 3:1$	73
Table 17. Statistical Analysis of All Data with Particle Width $\leq 1 \mu\text{m}$; $AR \geq 3:1$	74
Table 18. Bundle Dimensions by Crystallization Type with Bundle Width $\leq 1 \mu\text{m}$; $AR \geq 3:1$	75

Table 19. Fiber Dimensions by Crystallization Type with Fiber Width $\leq 1 \mu\text{m}$; AR $\geq 3:1$	76
Table 20. Prismatic Crystal Dimensions by Crystallization Type with Prismatic Crystal Width $\leq 1 \mu\text{m}$; AR $\geq 3:1$	77
Table 21. Particles with a L $\geq 5 \mu\text{m}$, W $\leq 1 \mu\text{m}$, AR $\geq 3:1$	78
Table 22. Bundles with a L $\geq 5 \mu\text{m}$, W $\leq 1 \mu\text{m}$, AR $\geq 3:1$	79
Table 23. Fibers with a L $\geq 5 \mu\text{m}$, W $\leq 1 \mu\text{m}$, AR $\geq 3:1$	80
Table 24. Prismatic Crystals with a L $\geq 5 \mu\text{m}$, W $\leq 1 \mu\text{m}$, AR $\geq 3:1$	81
Table 25. Particles That Fit The OSHA Definition of an Asbestos Fiber (L $\geq 5 \mu\text{m}$; AR $\geq 3:1$).....	82
Table 26. Particles That Fit The WHO Definition of an Asbestos Fiber (L $\geq 5 \mu\text{m}$, W $< 3 \mu\text{m}$, AR $\geq 3:1$)	83
Table 27. Particles That Fit The EPA TEM Counting Method Definition of an Asbestos Fiber (L ≥ 0.5 μm , AR $\geq 5:1$).....	84
Table 28. Particles That Fit Harper et al. (2012) definition of an Asbestos Fiber (W $\leq 1 \mu\text{m}$; AR $\geq 3:1$) .	85
Table 29. Bundles That Fit The OSHA Definition of an Asbestos Fiber (L $\geq 5 \mu\text{m}$; AR $\geq 3:1$).....	86
Table 30. Fibers That Fit The OSHA Definition of an Asbestos Fiber (L $\geq 5 \mu\text{m}$; AR $\geq 3:1$).....	87
Table 31. Prismatic Crystals That Fit The OSHA Definition of an Asbestos Fiber (L $\geq 5 \mu\text{m}$; AR $\geq 3:1$)	88
Table 32. Bundles That Fit The WHO Definition of an Asbestos Fiber (L $\geq 5 \mu\text{m}$, W $< 3 \mu\text{m}$, AR $\geq 3:1$)	89
Table 33. Fibers That Fit The WHO Definition of an Asbestos Fiber (L $\geq 5 \mu\text{m}$, W $< 3 \mu\text{m}$, AR $\geq 3:1$)...	90
Table 34. Prismatic Crystals That Fit The WHO Definition of an Asbestos Fiber (L $\geq 5 \mu\text{m}$, W $< 3 \mu\text{m}$, AR $\geq 3:1$)	91
Table 35. SEM Statistics with an AR $\geq 3:1$	92
Table 36. FESEM Statistics with an AR $\geq 3:1$	93
Table 37. Combined SEM and FESEM Statistics with an AR $\geq 3:1$	94
Table 38. Percent of particles in this study with an AR $\geq 3:1$ that fit various asbestos parameters.....	95
Table 39. Percent of particles in this study with an AR $\geq 3:1$ that fit various asbestos fiber definitions. ..	96

List of Figures

Figure 1: The life cycle of commercially and naturally-modified asbestos. Schematic courtesy of Metcalf et al. (2018).	97
Figure 2: Neocrystallized fibrous actinolite in a granitic fracture fill vein cutting through altered plagioclase (Type I). Cross polarized light.	98
Figure 3. Recrystallized fibrous actinolite formed via replacement of magmatic magnesio-hornblende surrounded by altered plagioclase and chlorite (Type III). Cross polarized light.	99
Figure 4. Neocrystallization fiber intergrowth within or on edges of other grains (Type II). Plane polarized light (A) and Cross polarized light (B).	100
Figure 5. Erosion of a granitic pluton within the McCullough Range that contains asbestos minerals....	101
Figure 6. Overview of the field area in McCullough Range, NV.	102
Figure 7. The locations of samples of neocrystallized and recrystallized fibrous amphibole collected January 10, 2018 in McCullough Range, Nevada. Fifteen GPS data points were collected for each sample bag. A total of 46 rocks were collected.	103
Figure 8. Hand sample of blue neocrystallized fibrous amphibole collected in McCullough Range, NV.	104
Figure 9. Hand sample of recrystallized fibrous amphibole collected in McCullough Range, NV.	105
Figure 10. Image of an Undergrad student at UNLV removing subsamples of both neocrystallized and recrystallized fibrous amphibole using a 0.015” diameter motorized drill.	106
Figure 11. Image of neocrystallized naturally-occurring asbestos fibers drilled from a hand sample collected within the McCullough Range, NV.	107
Figure 12. Image of the Scanning Electron Microscope in the EMiL Lab at the University of Nevada, Las Vegas.	108

Figure 13. Image of a prepared neocrystallized FESEM/ SEM sample. Sample prepared by placing the extracted subsamples on a polycarbonate 0.4 μm isopure filter, which was mounted on a plastic base with carbon tape and coated with carbon..... 109

Figure 14. Photo of how we measured a particle using the imageJ program. Measurements were done in the following order (1) scale bar, (2) maximum length, (3) width measurement one, (4) width measurement two, and (5) width measurement three. All imageJ output measurements are done in pixels and can be seen within the length column from the Results section of the imageJ program. Pixels were converted to microns using the “length” results for the scale bar from the imageJ program for each image. After conversion to microns, an average width and aspect ratio were calculated..... 110

Figure 15. Continuous Field Information for Log_{10} (Particle Width) for Particles with an $\text{AR} \geq 3:1$ Across Crystallization Process..... 111

Figure 16. Normal Q-Q Plot of Log_{10} (Neocrystallized Particle Width) for Particles with an $\text{AR} \geq 3:1$ 112

Figure 17. Normal Q-Q Plot of Log_{10} (Recrystallized Particle Width) for Particles with an $\text{AR} \geq 3:1$.. 113

Figure 18. Detrended Normal Q-Q Plot of Log_{10} (Neocrystallized Particle Width) for Particles with an $\text{AR} \geq 3:1$ 114

Figure 19. Detrended Normal Q-Q Plot of Log_{10} (Recrystallized Particle Width) for Particles with an $\text{AR} \geq 3:1$ 115

Figure 20. Continuous Field Information for Log_{10} (Particle Length) for Particles with an $\text{AR} \geq 3:1$ Across Crystallization Process..... 116

Figure 21. Normal Q-Q Plot of Log_{10} (Neocrystallized Particle Length) for Particles with an $\text{AR} \geq 3:1$ 117

Figure 22. Normal Q-Q Plot of Log_{10} (Recrystallized Particle Length) for Particles with an $\text{AR} \geq 3:1$. 118

Figure 23. Detrended Normal Q-Q Plot of Log_{10} (Neocrystallized Particle Length) for Particles with an $\text{AR} \geq 3:1$ 119

Figure 24. Detrended Normal Q-Q Plot of Log_{10} (Recrystallized Particle Length) for Particles with an $\text{AR} \geq 3:1$ 120

Figure 25. Continuous Field Information for Log10 (Particle Aspect Ratio) for Particles with an AR \geq 3:1 Across Crystallization Process.....	121
Figure 26. Normal Q-Q Plot of Log10 (Neocrystallized Particle Aspect Ratio) for Particles with an AR \geq 3:1	122
Figure 27. Normal Q-Q Plot of Log10 (Recrystallized Particle Aspect Ratio) for Particles with an AR \geq 3:1	123
Figure 28. Detrended Normal Q-Q Plot of Log10 (Neocrystallized Particle Aspect Ratio) for Particles with an AR \geq 3:1	124
Figure 29. Detrended Normal Q-Q Plot of Log10 (Recrystallized Particle Aspect Ratio) for Particles with an AR \geq 3:1	125
Figure 30. U-Test formula that will be used to compare neocrystallized (population 1) and recrystallized (population 2) fibrous amphibole fibers to see if they are significantly different or similar.	126
Figure 31. Plan for statistical comparison between neocrystallized and recrystallized fibrous amphiboles for McCullough Range, NV.....	127
Figure 32. NOA formed via replacement of magmatic magnesio-hornblende (left arrow) into NaFe ³⁺ fibrous amphibole (right arrow) asbestos surrounded by altered albite. Fibrous amphibole is intergrown with albite (right edge) along the amphibole pseudomorph boundary. Cross polarized light. Photo courtesy of Rodney Metcalf. Modified from Austin et al. (2019).	128
Figure 33. FESEM (A-D) and SEM (E-F) photomicrographs of neocrystallized fibrous amphibole bundles.	129
Figure 34 (A-C). FESEM photomicrographs of neocrystallized fibrous amphibole fibers.	130
Figure 35. SEM photomicrograph of a neocrystallized prismatic crystal.....	131
Figure 36(A-C). FESEM photomicrographs of recrystallized fibrous amphibole bundles.	132
Figure 37(A-C). FESEM photomicrographs of recrystallized fibrous amphibole fibers.....	133
Figure 38. FESEM photomicrographs of recrystallized prismatic crystal.....	134
Figure 39. SEM EDS analysis of my data set showing particles plotting mainly as calcic amphiboles...	135

Figure 40. A/B) EPMA-WDS analyses from Metcalf et al. (2018). C/D) SEM EDS analyses from Metcalf et al. (2018). All figures show NV samples plotting mainly as calcic amphiboles. 136

Figure 41. All Neocrystallized (open shapes) and recrystallized (solid shapes) amphibole data plotted aspect ratio vs. length. All plots contain both OSHA’s regulatory definition and EPA TEM Counting definition of an asbestos fiber. 137

Chapter 1: Introduction

1.1 What is Asbestos?

Asbestos is a non-scientific term originally designed for industrial, legal, and commercial purposes (Van Gosen, 2007). This term represents a set of specific silicate minerals but is not a mineral name or mineral group (Van Gosen, 2007). In the USA, asbestos is *legally* defined as one or more of the following six minerals: chrysotile (a serpentine mineral); and five fibrous varieties of amphibole minerals including riebeckite (industrial name: crocidolite), cummingtonite-grunerite (industrial name: amosite), anthophyllite, actinolite, and tremolite (Van Gosen, 2007). These minerals were mined and used in numerous products because they have one or more of the following: high tensile strength, resistance to heat and chemical alteration, high flexibility, spinability, low electrical conductivity, and a large surface area (Thompson, 1974; Virta, 2002). Inhalation of these long, thin fibers can cause gastrointestinal cancer, cardiovascular disease; suppressed immune function and autoimmune disorders; lung, larynx, and ovarian cancer; asbestosis, pleural fibrosis, and mesothelioma (Agency for Toxic Substances and Disease Registry, 2001; Camargo et al., 2011; International Agency for Research on Cancer, 2012; Pfau et al., 2017, Shannahan et al., 2012). Additionally, there are several other fibrous minerals that are, or may be, hazardous but are currently not regulated, including other fibrous amphibole minerals (winchite, richterite, arfvedsonite, magnesiohornblende, and fluoro-edenite) erionite, mordenite, talc, wollastonite, and palygorskite (Baumann et al., 2013; Harper, 2008; Meeker et al, 2003; Van Gosen, 2007).

Historically, 90-95% of asbestos mined, worldwide, was serpentine (chrysotile) (Clinkenbeard et al., 2002; Gunter et al., 2007, Harper, 2008). Chrysotile is well known for having the asbestiform crystal habit where fibers are broken down by a mechanical or erosive force into thinner fibers and ultimately fibrils (American Society for Testing and Materials, 1995). Although there is much disagreement regarding the definition of asbestiform (Lowers and Meeker, 2002), in general, asbestiform fibers are long thread-like, or needle-like, fibers that grow in curved, or straight, parallel bundles often displaying splayed ends

(Beard et al., 2001; Lowers and Meeker, 2002). In the asbestos industry, processing was performed on the asbestos ore to crush and sort fibers into sizes appropriate for their uses in commercial products (Clinkenbeard et al., 2002). In these scenarios, primarily chrysotile fibers were defined as having aspect ratios (AR) ranging from 20:1 to 100:1 or individual fibrils measuring less than 0.5 μm in width (Perkins and Harvey, 1993). Because the majority of asbestos mined was chrysotile, the regulatory language, and definitions of ‘asbestos’ and ‘asbestiform’ are biased towards crystal morphologies common to chrysotile, not amphibole (Harper et al., 2008; Metcalf et al., 2018). For example, fibrous amphibole fibers are often straighter and can be shorter compared to the long, curly chrysotile fibers (Plumlee et al., 2006). Because of this, amphibole fibers are able to flow more aerodynamically and penetrate into deeper areas of the lungs (Plumlee et al., 2006). This, among other characteristics, including biopersistence, makes amphibole asbestos more toxic than chrysotile (Plumlee et al., 2006). Unlike chrysotile asbestos, fibrous amphibole fibers tend to be shorter and are also able to more readily penetrate surrounding tissues and membranes, which can trigger cancers like mesothelioma (Plumlee et al., 2006).

1.2 The Life Cycle of Asbestos

Naturally-occurring asbestos (NOA) has recently become a hot topic in medical geology and has gained a great deal of attention from scientists, health agencies, regulatory agencies, and citizens throughout the United States (Harper, 2008; Van Gosen, 2007). The term NOA has been used to describe environmental exposures to asbestos (both regulated and non-regulated fibrous amphibole or serpentine minerals) (Buck et al., 2013; Harper, 2008; Metcalf et al., 2018). NOA is often found in-situ in exposed bedrock that is either disturbed or eroded out of the source rock and transported by geologic processes resulting in talus, sediment, alluvium, soil, and dust containing NOA. Once disturbed by anthropogenic process (i.e., construction, mining, off road vehicles, horseback riding, etc.), NOA then has the potential to be inhaled or ingested, creating an environmental health risk (Buck et al., 2013; Harper, 2008; Metcalf et al., 2018; Van Gosen, 2007). Figure 1 is a schematic of the life cycle of asbestos and explains the differences between

commercially- and naturally-modified asbestos (Metcalf et al., 2018). According to Figure 1, both commercially- and naturally-modified asbestos can result in anthropogenically-disturbed asbestos.

Cases such as Fairfax County, Virginia, El Dorado Hills and Clear Creek management area, California, as well as in other locations discussed in Harper (2008), served as a catalyst for change regarding regulatory definitions of fibrous amphibole and the idea of naturally-occurring asbestos began to gain a great deal of attention (Harper et al., 2008). The recent discovery of naturally-occurring fibrous actinolite in Clark County, NV (Buck et al. 2013) and fibrous NaFe^{3+} amphiboles in Mohave County, AZ (Metcalf and Buck, 2015) has become a topic of concern throughout metropolitan Las Vegas and northwestern Arizona ([News Stories](#)). The fibrous amphibole surrounding Boulder City, Henderson, and eastern Las Vegas is a result of in-situ asbestos-bearing bedrock that is eroded and transported into alluvial fans and eolian deposits in southern Nevada and northwestern Arizona (Buck et al., 2013; Metcalf and Buck, 2015). The fibrous amphibole has the ability to be disturbed either anthropogenically or through geological processes (Figure 1).

In 2014, a reference concentration (RfC) for fibrous Libby amphibole was established by the Environmental Protection Agency (EPA) for non-cancer adverse health effects (US EPA, 2014). An RfC is the maximum dose of a toxicant that can be inhaled without causing a noncancer health effect. Any dose that exceeds the RfC may result in adverse noncancer health effects over a lifetime of exposure. It was found that exposures that exceed 0.00009 PCM fibers/cc per day for a lifetime (defined as 70 years) have significant increased risk of causing adverse non-cancer health effects (US EPA, 2014). Asbestosis, pleural effusions, pleural plaques, and plural thickening are examples of non-cancer effects from cumulative asbestos exposure (Pfau et al., 2017).

Ambient air was recently measured in the El Dorado Basin in, and around, Boulder City, NV (Tetra Tech, 2014). The average airborne concentrations of fibrous amphibole from May 8 through August 10, 2014 (Tetra Tech, 2014) were 2.3 times higher than the EPA RfC (Buck et al., 2016). The presence of fibrous amphiboles in this region poses a potential environmental health risk to those living in Clark and Mohave counties (Buck et al., 2013) by increasing their chances for asbestosis, lung cancer, ovarian cancer,

mesothelioma, auto-immune disorders, and other adverse health effects (Agency for Toxic Substances and Disease Registry, 2001; Camargo et al., 2011; International Agency for Research on Cancer, 2012; NIOSH, 2011; Pfau et al., 2017, Shannahan et al., 2012).

1.3 Exposure Pathways and Toxicity

For any toxicant, including fibrous amphibole, there are five potential pathways for exposure: ingestion, inhalation, eyes, wounds, and direct contact with unbroken skin (Plumlee et al., 2006). For fibrous amphibole, the primary pathway for exposure is inhalation (Plumlee et al., 2006). Amphibole and serpentine asbestos are both silicate minerals. Once inhaled or ingested, it is difficult for organisms to process silicate minerals. When ingested, these silicates concentrate within soft tissues because the body has no, or poor, mechanisms to reject or remove them, a phenomenon known as biopersistence (NIOSH, 2011). Biopersistence of an elongated particle is generally known as the capacity of a particle to stay within the lungs for an extended period of time (NIOSH, 2011). This depends on several factors, including: lung fluid solubility, rates of translocation, alveolar macrophages clearance rate and mucociliary transport, breakage pattern and breakage rate, and deposition rates of elongated particles (NIOSH, 2011). Biopersistence is influenced by the surface area, particle dimension, chemical composition, and surface chemistry of elongated mineral particles (EMPs) (NIOSH, 2011).

One of the many reasons amphibole fibers are more toxic than chrysotile is that amphibole fibers are more biopersistent and can remain in the body for decades (Plumlee et al., 2006). Chrysotile is a sheet silicate whose mineral fibers are rolled into bundles or fibers. When ingested, the body is able to eventually break down chrysotile because the fibers unroll and dissolve due to its sheet-silicate structure. Fibrous amphibole often has an acicular habit with thin, straight fibers that will not dissolve even after decades of exposure due to its multiple chain structure (Plumlee et al., 2006). In addition, the body's immune response differs between these minerals. Chrysotile is known to suppress the human immune system and can lead to proportionally more cases of cancer compared to fibrous amphibole fibers, but the number of persons

affected is much smaller compared to those exposed to fibrous amphibole because of chrysotile predominantly only causing cancer and no other adverse health effects (Pfau, 2017). In contrast, fibrous amphibole fibers are known to induce an over-response to the immune system which can lead to a greater number of cases where individuals experience adverse health effects such as, progressive lamellar pleural thickening (LPT) and several autoimmune diseases including scleroderma, rheumatoid arthritis, and systemic lupus (Pfau et al., 2017). Amphibole asbestos may predominantly cause other adverse health effects as described, but it can still also cause lung cancer and mesothelioma. Once a fiber is inhaled, macrophages within the lungs attempt to expel such fibers. Because amphibole fibers are more biopersistent than chrysotile fibers, and cannot unroll and dissolve, amphibole fibers create more inflammation and scar tissue within the lung. The amphibole fibers are able to create an immunoenhanced response, thus causing the body to attack itself (e.g., autoimmune). The immune system becomes distracted, creating a poor anti-cancer response that may eventually lead to cancer (Pfau et al., 2014, 2016, 2017, 2018).

1.4 Morphology of EMPs and Asbestos Fibers

The toxicity of elongated mineral particles (EMPs) is mainly controlled by crystal morphology, mineralogy, and mineralogy chemistry (NIOSH, 2011). The longer and thinner the fiber, the greater its toxicity (Stanton et al., 1981). This is likely because longer and thinner fibers have greater surface area (Aust et al., 2011), and/or because they may travel to deeper areas within the lung (Aust et al., 2011; NIOSH, 2011). These long, thin fibers often split longitudinally once within the lung, producing an increased number of thinner fibers with an increased aspect ratio (NIOSH, 2011). A mineral fiber is considered an EMP when it has a mean aspect ratio greater than 3:1 (L:D) and can be inhaled according to The World Health Organization (the WHO) standards (Mortureux, 2015). The WHO defines asbestos fibers as those with a minimum length of at least 5 μm , a maximum diameter of 3 μm , and an aspect ratio greater than or equal to 3:1 (WHO Regional Office, 2000).

Upon inhalation, asbestos fibers may be deposited in one of three regions: the extrathoracic region, bronchial region, or the alveolar-interstitial region (NIOSH, 2011). The aerodynamic and thermodynamic properties of airborne particles determine a particle's deposition within the regions listed above (NIOSH, 2011). The aerodynamic diameter of a specific particle is "the diameter of a unit density sphere that has the same settling velocity as a particle in question" of any shape or size (Cooper and Alley, 2011). The diameter and density of an elongated particle dictates the aerodynamic equivalent diameter (AED) of a particle (NIOSH, 2011). For example, a Ping-Pong ball and a golf ball have similar diameters but behave differently when they free-fall because of their densities (Cooper and Alley, 2011). The shape of such particles will impact movement and where they will deposit within the body. Long, thin fibers flow through the air like a javelin spear due to thinner diameters (Cooper and Alley, 2011). Particles with larger diameters and shorter lengths are "blockier" in shape causing them to not flow as efficiently through the air. When an elongated particle is inhaled, its orientation combined with the direction of airflow dictates where the particle will be deposited within the body. Deposition is affected by impaction, interception, sedimentation, and diffusion of the elongated particles (NIOSH, 2011). Insoluble particles, such as asbestos fibers, with AEDs $< 2 \mu\text{m}$ deposit in the lower respiratory tract and have longer retention times than those deposited in the bronchial region, because the alveolar region does not have mucociliary clearance capability (NIOSH, 2011). Diameters and length of particles can be measured, and combined with particle density, an AED can be calculated, in order to predict where particles will be deposited within the human body (Cooper and Alley, 2011).

There is much disagreement within the asbestos community over the "correct" definition of an asbestos fiber (Gunter et al., 2007; Lowers and Meeker, 2002). Many in the asbestos community consider elongated particles "asbestos" when particles have a diameter $< 0.5 \mu\text{m}$ (Lowers and Meeker, 2002; Perkins and Harvey 1993). This definition was used for commercial purposes and does not reflect toxicity (Clinkenbeard et al., 2002). In contrast, health experts consider particles with a diameter $< 3 \mu\text{m}$ potentially toxic since they are respirable (NIOSH, 2011). Issues such as length and diameter for health purposes vs mineralogical purposes, or industrial purposes (Lowers and Meeker, 2002) cast doubt over "what" is

considered “asbestos” and creates great confusion that can affect legal cases, often favoring industry and not the victim (Meeker Vs. Gunter, 2009). For this study it is important to focus on what is considered potentially toxic, which is any particle that has the ability to be inhaled (width < 3 μm) (NIOSH, 2011; WHO Regional Office, 2000).

In order for an amphibole fiber to be *legally* classified as an asbestos fiber by the Environmental Protection Agency using the Transmission Electron Microscopy (TEM) Methods according to the U.S. Codes of Federal Regulations, it must have a minimum length of 0.5 μm and aspect ratio greater than or equal to 5:1 (40 CFR 763 Subpart E, App. A). This is not a definition founded on health purposes, but rather a legal definition that was founded based on the capabilities of the range of fiber dimensions the TEM can detect (40 CFR 763 Subpart E, App. A). In order for an amphibole fiber to be *legally* classified as an asbestos fiber by The United States Occupational Safety and Health Administration (the OSHA) according to the U.S. Codes of Federal Regulations, it must have a minimum length of at least 5 μm and with a mean aspect ratio of 3:1 or greater (29 CFR 1910.1001, subpart Z(b)) (Clinkenbeard et al., 2002; Brownson et al., 2012). This is not a definition founded on health purposes, but rather a legal definition that was founded based on the capabilities of the range of fiber dimensions the Phase Contrast Microscope (PCM) can detect (Addingley, 1966; Boulanger et al., 2014; Clinkenbeard et al., 2002; Dodson et al., 2003; Holmes, 1965; Langer et al., 1978; Lynch, 1970; NIOSH, 1972; Tweedale, 2000). A review of the history of this regulation, which is further discussed in section 4.4.1, claims the definition of a fiber that NIOSH adopted from the UK in 1972, was arbitrarily defined and was not based on health risks but utilitarian purposes (Addingley, 1966; Boulanger et al., 2014; Dodson et al., 2003; Holmes, 1965; Langer et al., 1978). The commercial asbestos industry uses the term asbestiform when referring to fibers that are of a desired morphology for commercial purposes (Van Gosen, 2007; Virta, 2002). A particle does not need to reach commercial standards for an asbestiform particle to be considered asbestos or to be toxic (NIOSH, 2011). The term “asbestiform” was created to describe something that looks like asbestos (NIOSH, 2011), which because the type of asbestos that was mined was largely chrysotile (Clinkenbeard et al., 2002; Harper et al., 2008; Virta, 2002), meant that this term mostly is used to describe the characteristics of chrysotile. Definitions of

asbestos terminology are inconsistent and problematic and must be better defined. Some of the major problems are (1) regulations and definitions are often focused on characteristics of chrysotile, and are incorrectly applied to amphibole minerals, and (2) commercially-modified asbestos particles have been crushed and sorted and their population characteristics will differ from particles that have not undergone that processing. Because not all of these characteristics are tied to health outcomes, it is incorrect to apply some commercial definitions of asbestos when considering health implications. This especially applies to the definitions of ‘asbestiform.’ Meeker et al. (2006) states that any amphibole with a mean aspect ratio greater than 3:1 should be defined as having an “asbestiform” habit. The World Health Organization (the WHO) defines asbestos fibers as those of 5 μm or longer, a diameter $<3 \mu\text{m}$, and a mean aspect ratio of at least 3:1 (WHO Regional Office, 2000; Clinkenbeard et al., 2002). For this study, it is important to focus on what may be considered harmful when inhaled, which is any amphibole particle that has a width less than 3 μm (WHO Regional Office, 2000; Aust et al., 2011; NIOSH, 2011). There is no known, explicit length cutoff tied to health outcomes, other than increased lengths are known to increase toxicity (Aust et al., 2011).

The morphologies of amphibole fibers are a product of the geologic environments in which they form. Economic deposits of fibrous amphibole are thought to be rare, occurring only in specific geologic environments that allow the growth of long, thin, needle-like fibers within veins (Bailey et al., 2004; Tabler, 1916; Virta, 2002; Van Gosen 2007). Fibrous amphibole deposits are often created when a hydrothermal fluid chemically alters a rock in a process known as metasomatism. In order for amphibole fibers to nucleate, high concentrations of magnesium, silica, and water are usually present (Van Gosen, 2007). Asbestos deposits often display evidence of shear as well as an influx of silica-rich hydrothermal fluids (Bailey et al., 2004; Erskine and Bailey, 2018; Virta, 2002) that are driven by regional metamorphic, contact metamorphic, or magmatic hydrothermal fluid processes (Van Gosen, 2007). Geologic environments that often host asbestos are: metamorphosed ultramafic rocks, metasomatized mafic rocks, metamorphosed dolostones, metamorphosed banded iron formations, and metasomatism of alkalic intrusions and carbonatites (Van Gosen, 2007).

1.5 Crystallization Processes

This study will compare two types of fibrous amphibole (1) neocrystallized amphibole (Figure 2) and (2) recrystallized amphibole (Figure 3). Neocrystallization refers to the growth of fibrous amphibole asbestos primarily precipitated from an aqueous solution within fracture-fill veins (Figure 2) or within/ on the edges of other grains (Figure 4) (Austin, 2019; Metcalf et al., 2018). Some researchers believe that fibrous amphibole asbestos can only form through neocrystallization within fracture-fill veins (Figure 2) (Bailey et al., 2004; Lee et al., 2008; Strohmeier et al., 2010; Tabler, 1916; Van Gosen 2007; Virta, 2002). The regulatory nomenclature for asbestos has essentially ignored the distinction between mineral fibers formed from recrystallization versus neocrystallization of amphibole minerals. The term “asbestos” is often only given to one of the five regulated fibrous amphibole minerals that grew within a vein (neocrystallized) (Bailey et al., 2004; Lee et al., 2008; Strohmeier et al., 2010; Tabler, 1916; Van Gosen 2007; Virta, 2002). Because of this, fibrous amphibole formed via recrystallization is not considered asbestos by industry standards and is not regulated. Regulations were written using asbestos fibers disaggregated or liberated from an asbestos ore deposit (Bailey et al., 2004; Gunter et al., 2007) and were not written with NOA in mind (Clinkenbeard et al., 2002; Harper et al., 2008). Recent findings by Metcalf and Buck (2015) and others (Ahn and Buseck, 1991; Akai, 1982; Meeker et al., 2006), show that naturally-occurring fibrous amphibole can form by replacement (Figure 3), which challenges the neocrystallization hypothesis that asbestos can only form within veins. Additionally, Meeker et al (2006) recognized textures within fibrous amphibole from Libby, Montana that suggest fibers formed from recrystallization of pyroxene. These findings increase the possibility that naturally-occurring asbestos may have formed throughout much of the western United States, and many other areas worldwide, where hydrothermal alteration and recrystallization has occurred. As the morphology of asbestos fibers is an important characteristic that strongly affects toxicity (longer and thinner fibers, which have increased surface area, are believed to be significantly more toxic) (Aust et al., 2011; Dodson et al., 2003; Stanton et al., 1981), recrystallized fibrous

amphibole may have the potential to be toxic if morphologies are similar to those of neocrystallization. To date, no study has been conducted to compare the morphologies of recrystallized vs. neocrystallized fibrous amphiboles.

1.6 Geologic Background

As mentioned above, asbestos deposits are generally created from metasomatic replacement of *magnesium-rich* rocks (Van Gosen, 2007). Although, in the case of Clark County, NV and Mohave County, AZ, granitoid rocks hosting fibrous actinolite and NaFe^{3+} amphiboles have low magnesium contents with whole-rock concentrations of <5 wt% (Metcalf and Buck, 2015; Metcalf et al., 2018). During the middle Miocene (17-13 Ma), a belt of granitic plutons (quartz monazite), along the AZ-NV border and parallel to the Colorado River, formed which were then faulted and fractured. These plutons are known as the Boulder City pluton (Nevada) and the Wilson Ridge pluton (Arizona). The Boulder City pluton is a part of the McCullough Range and within this study's field area (Figures 5-7). Around 13.7 ± 0.5 Ma (Wilson Ridge pluton) and 13.96 ± 0.25 Ma (Boulder City pluton), metasomatism occurred, causing a siliceous hydrothermal fluid to invade local granitic rock, producing recrystallized fibrous amphibole (Figure 3 and 9) and neocrystallized fibrous amphibole within veins (Figures 2 and 8) (Metcalf and Buck, 2015; Metcalf et al., 2018). The metasomatism of the granitic pluton occurred at approximately 300 degrees Celsius under low pressure conditions (Metcalf et al., 2018). Metcalf and Buck (2015) bracketed the age of fibrous amphibole mineralization of the Wilson Ridge pluton between 13.7 and 11.7 Ma and suggested the mineralization of the fibrous amphibole in southern Nevada likely occurred within a similar timeframe due to analogous geologic conditions. Both plutons experienced active faulting and uplift during the same period which allowed for a hydrothermal system to provide fluid access to the open fractures within the plutonic host (Metcalf et al., 2018). This hydrothermal system was established within two million years of the Miocene pluton solidification (at 750-900°C) and occurred concurrently as the altered pluton was uplifted and then eroded at the surface, eventually causing the release of asbestos fibers (Metcalf et al.,

2018). The hydrothermal aqueous solutions moved along active faults and fracture zones within the plutonic host and adjacent Precambrian gneisses (Metcalf et al., 2018). Metcalf et al. (2018) also found fracturing of quartz and plagioclase feldspar present in thin sections supporting formation temperatures of $\leq 350^{\circ}\text{C}$. A study conducted by Yau et al. (1986), of the Salton Sea geothermal field in southern California, supports Metcalf et al. (2018) findings and serves as an analog for NOA origins by means of hydrothermal processes (Metcalf et al., 2018). The Salton Sea study found fibrous actinolite along with albite, potassium feldspar, epidote, and chlorite which is nearly identical to the assemblages that we found in this study (Metcalf et al., 2018). The Salton Sea fluid temperatures that produced the fibrous amphibole were around $310\text{-}330^{\circ}\text{C}$ at depth (Metcalf et al., 2018; Yau et al., 1986). Amphibole asbestos was able to form in southern Nevada, because the timing of the active uplift and faulting of the Miocene pluton created an environment for fluid access pathways at the time the solidified plutons were cooling from magmatic temperatures and formation occurred within the temperature range of $\sim 300\text{-}350^{\circ}\text{C}$, at depth, while cooling (Metcalf et al., 2018).

1.7 Hypothesis

To date, no published work has been performed to distinguish between morphology of neocrystallized and recrystallized fibrous amphiboles, which we aim to do in this study. We measured the morphology of fibrous amphibole formed through both recrystallization and neocrystallization, within the same rocks formed from the same hydrothermal event, to see if the resulting fiber shapes and sizes produced were similar. The morphology of asbestos fibers strongly affects toxicity (longer and thinner fibers have greater aspect ratios, increased surface area, and are known to be more toxic (Aust et al., 2011)). We hypothesized that the length to width ratios of neocrystallized and recrystallized fibrous amphibole fibers of similar mineralogy and chemistry will be comparable, and therefore have potentially comparable toxicities. A previous study in southern Nevada found no bimodal distribution in fibrous amphibole particles measured further indicating that both crystallizations processes could produce similar morphologies (Buck et al., 2018). Until now, the claim that fibrous amphibole can only produce toxic

morphologies when grown via neocrystallization has not been questioned. This project will aim to provide evidence that fibrous amphibole grown via recrystallization may have similar morphologies as those formed through neocrystallization and, therefore, have the potential to produce toxic morphologies. To do so, we used rocks collected from the McCullough Range, NV (Figures 5-7) that contains both neocrystallized (Figure 8) and recrystallized fibrous amphibole within the same sample (Figure 9) (confirmed petrographically (Figures 2-4)). If this hypothesis proves to be true, this could significantly increase the number and distribution of naturally-occurring asbestos deposits, and many more people may be unknowingly exposed to hazardous amphibole fibers than we currently recognize (Figure 1).

Chapter 2: Methods

Forty-six rock samples containing both neocrystallized (Figure 8) and recrystallized (Figure 9) amphibole were collected from a set of isolated, closely-spaced outcrops (over a few 100 sq meters) containing highly altered faulted Miocene granitic rock (Figures 5-6) in McCullough Range, NV (Figures 6 and 7) and cut into 69 billets (27 mm x 46 mm). Once prepared, thirty-six billets were sent to Geo Tech Labs in Vancouver B.C., Canada to be made into thin sections (~30 μm thick). All thin sections were analyzed using a petrographic microscope and examined for evidence to identify neocrystallized versus recrystallized fibrous amphiboles (Figures 2-4).

Using a 0.015" diameter motorized drill (Figure 10), we separately removed subsamples of both the neocrystallized and recrystallized fibrous amphiboles from their corresponding billets and further gently broke samples down using a mortar and pestle (Figure 11). In total, 24 samples were analyzed using the Scanning Electron Microscopy (SEM) and Field Emission-Scanning Electron Microscopy (FESEM) with Energy Dispersive Spectroscopy (EDS) (Figure 12) by placing the extracted subsamples on a polycarbonate 0.4 μm isopure filter, which was mounted on a plastic base with carbon tape and coated with carbon (Figure 13) (Meeker et al. 2003; Buck et al., 2013). Analyses using a JSM6700F FESEM and a JSM-5610 SEM with an EDS detector were performed at the University of Nevada, Las Vegas Electron Microanalysis and Imaging Laboratory (EMiL) to count and measure amphibole particles within the carbon-prepared subsamples. Using a marker, the carbon coated sample plates were divided into a four-quadrant grid to assist with particle counting and to prevent repeat analyses (Wylie and Schweitzer, 1982). Once a sample quadrant was scanned and removed, it was not used again. Quantitative identification of amphibole mineralogy was previously performed on samples from this site using Electron Probe Microanalysis (EPMA) with Wavelength Dispersive Spectroscopy (WDS) on polished thin sections (Austin, 2019; Buck et al., 2013; Metcalf et al., 2018).

Problematic issues can arise while using different microscopy methods when identifying fibrous amphibole. Understanding choice of microscopy method is important in relation to the inconsistent, and

problematic definitions of asbestos currently used. There are multiple microscopy instruments that can be used either singularly or in combination to assist in classifying an EMP as fibrous amphibole (Clinkenbeard et al., 2002). These include but are not limited to: phase contrast microscopy (PCM), polarized light microscopy (PLM), scanning electron microscopy (SEM), field-emission scanning electron microscopy (FESEM), electron probe microanalysis (EMPA), transmission electron microscopy (TEM), and X-ray diffraction (XRD) (Clinkenbeard et al., 2002). For this study, use of the PLM and PCM, was avoided because of the problems associated with distinguishing between asbestos and non-asbestos fibers in natural environments, and because the lower resolution is unable to identify many of the particles with widths less than one micron in diameter (Clinkenbeard et al., 2002). Additionally, the TEM was too expensive for this study and wasn't locally convenient. Therefore, both the SEM and FESEM were utilized. These microscopy methods are able to produce images at magnifications that range from 10-10,000x (greater than optical microscopy), display semi-quantitative EDS analysis, have resolutions of 1-5 nm (FESEM) and 10-50 nm (SEM) (Goldstein et al., 2003), can provide information on the presence and dimensions of asbestos in a sample, and the morphology of particles present. Additionally, the SEM is limited by a lower resolution and magnification compared to that of the FESEM (Clinkenbeard et al., 2002; Goldstein et al., 2003; Meeker et al., 2006). Despite this, both the SEM and FESEM are more than sufficient for measuring and identifying fibrous amphibole. The resolution, magnification, mineral identification, and the ability for the SEM-EDS to show surface features make this microscopy method preferable over the PCM and PLM (Clinkenbeard et al., 2002).

Each particle was analyzed for its chemical composition using EDS on the SEM and FESEM. EDS displays qualitative and semi-quantitative chemistry, meaning it can tell us if a fiber is amphibole, but these data are not sufficient to accurately distinguish among amphibole minerals alone. Therefore, the EDS elements collected were then assigned to sites within the amphibole formula to estimate a potential mineral name and group. For this study, we used the amphibole classification system from Leake et al (1997) that is based on nomenclature from the International Mineralogical Association (IMA97). Based on B-site cation occupancy, the amphibole classification system from Leake et al (1997) divided amphiboles into

four main subgroups: sodic amphiboles ($N_{\text{B}} > 1.5$ cations), sodic-calcic amphiboles ($N_{\text{B}} = 0.5-1.5$), calcic amphiboles ($Ca_{\text{B}} \geq 1.5$ cations), and Mg-Fe amphiboles ($[Ca+Na]_{\text{B}} < 1$, $[Mg+Fe]_{\text{B}} > 1$) (Metcalf et al., 2018). These four groups are further subdivided by T-site occupancy, which is the amount of Al^{3+} substituting for Si^{4+} ; the A-site occupancy, and the Mg#, which is defined as $Mg/[Mg + Fe^{2+}]$ per formula (Metcalf et al., 2018). Amphibole composition varies with the chemical environment in which it formed. This classification system was used to assign mineral names and groups to the amphibole particles collected from the FESEM and SEM. Table 1 lists various chemical formulas for fibrous amphiboles that are calcic, sodic, or sodic-calcic in nature.

In total, 3,408 particles were analyzed on the FESEM and SEM with EDS. Of these particles, 2,128 were confirmed amphibole (yes or no). This was determined by using the weight percent oxide data from the FESEM and SEM with EDS to calculate structural formulae for each particle present (Metcalf et al., 2018). In order to calculate wt% oxide data as such, all Fe present was assumed to be Fe^{2+} as discussed in Meeker et al. (2003) (Metcalf et al., 2018). The ideal stoichiometry for amphibole used for this study was “T-site sum ~ 8 , C-site sum ~ 5 , B-site sum ~ 2 , A-site sum < 1 , and total cations of 15-16” (Metcalf et al., 2018). Cation totals and sites for each particle were assessed and assigned only if it passed these 5 cation-site tests. Therefore, this assessment limited particles within this study to those only classified as amphibole by passing the stoichiometry test discussed above (Metcalf et al., 2018). Due to poor FESEM and SEM images that were missing a scale bar, 202 confirmed amphibole particles had to be omitted from the study since they were unmeasurable. Thus, 1,926 particles were analyzed and measured. The number of particles considered were then reduced by filtering for aspect ratios greater than or equal to 3:1 as this is what is considered asbestos morphologies within the field of research (NIOSH, 2011; Clinkenbeard et al., 2002; WHO Regional Office, 2000; 29 CFR 1910.1001, subpart Z(b)). Therefore, in total, 1,525 particles were included in the analyses described within this thesis. The technique described above was utilized as the main method to analyze EDS data from the SEM and FESEM.

Morphology of asbestos fibers is an important factor regarding toxicity (NIOSH, 2011). Using the ImageJ program (Rasband, 2018), photomicrographs collected from the SEM/ FESEM of both

neocrystallized and recrystallized fibrous amphibole particles were measured (length and width), according to the methods presented in Meeker et al. (2003) (Figure 14). Once measured, these particles were then analyzed to see if their resulting morphologies were significantly different by comparing average width, maximum length, and mean aspect ratios (length to width) of fibers. Despite morphology classification nomenclature being inconsistently problematic (Lowe and Meeker, 2002), we attempted to assign “visual shape” or morphology of particles based on Meeker et al. (2003) and Buck et al. (2013). The visual shape describing the morphology of particles includes: (1) *fibers*, (2) *bundles*, or (3) *prismatic crystals*. In this study, we visually identified *fibers* as: particles that are longer than they are wide with no signs of splitting or splayed ends, often having a width less than one micron; *bundles* as: particles that have splayed or splitting ends with individual fibers bundled together; *prismatic crystals* as: blocky crystals with blunt edges with a width often greater than one micron. When identifying particles using SEM and FESEM photomicrographs, particles were classified as a *fiber*, *bundle*, or *prismatic crystal* based on dimension (length, width, and aspect ratio) and, more importantly, the visual representation of the particle. This type of morphology is referred to as “particle type” throughout this thesis. Statistical analyses of particles were also conducted to compare dimensions of particles only. This is often referred to as “particle dimensional analyses” throughout this thesis.

In order to obtain a statistically valid population size, nearly 1000 particles were originally measured from each subsample (Wylie and Schweitzer, 1982). Per Wylie and Schweitzer (1982), they found smaller variations in their regression coefficients for the -120 mesh for a sample size of 750 than they did in their +120 mesh with a sample size of 250. Based on their findings, they suggested that a population size of 250 is valid (Wylie and Schweitzer, 1982). Both parametric and non-parametric analyses were conducted to verify if the two populations, neocrystallized and recrystallized fibrous amphibole, were significantly different ($p < 0.05$) from each other. In addition to testing the two populations of neocrystallized and recrystallized amphibole, an additional two populations were created to test for a discrepancy between the SEM and FESEM. Student’s t-Tests, Two-way Analysis of Variance (ANOVA), and Mann-Whitney U-tests were calculated using SPSS version 28 on both neocrystallized and

recrystallized populations as well as the SEM and FESEM populations. All obtained size distributions were positively (right) skewed and were therefore, not normally distributed. Due to the data not being normally distributed, analyses from the Student's t-test and the Two-way ANOVA were not valid because of the data not meeting assumption of normal distributions (Table 2) (LAERD Statistics, 2018, accessed: 12/07/2022; Sokal and Rohlf, 1969; Wylie and Schweitzer, 1982). If the assumptions are not met for the Student's t-test and data are not normally distributed, a nonparametric test, such as a Mann Whitney U-test, can be calculated to see if the two populations are significantly different ($p < 0.05$) (Sokal and Rohlf, 1969; Wylie and Schweitzer, 1982). For a non-parametric U-test, the datasets do not need to be normally distributed, but the data must be *similarly* distributed and *similarly* shaped in order to compare medians (LAERDStatistics, 2018 accessed: 12/07/2022; Sokal and Rohlf, 1969). Therefore, the datasets also failed the assumptions for the U-tests as the data were not near normally distributed (Table 2) because the distributions were right-skewed. Conducting a \log_{10} transformation of the datasets allowed for an approximate normal distribution to develop. In order to compare medians using a Mann Whitney U-test, data must be *similarly* distributed and *similarly* shaped (LAERDStatistics, 2018 accessed: 12/07/2022; Sokal and Rohlf, 1969). The log-transformation of the datasets caused similar distributions and similar shapes to develop (Table 3; Figures 15-29). This is because once the dataset is transformed to logarithms, the variance of a sample is independent of its mean and in most cases will also remove heteroscedasticity (Sokal and Rohlf, 1969). By log-transforming the data, we were then able to conduct a U-test to see if the neocrystallized and recrystallized populations (Table 4), as well as the FESEM and SEM (Tables 5-7) populations, were statistically similar ($p > 0.05$) or different ($p < 0.05$). Using the methods described in Alder and Roessler (1964) and Sokal and Rohlf (1969), U-tests comparing recrystallized and neocrystallized fibrous amphiboles (as two separate populations) were calculated to see if the morphology varies between the two processes (Figure 30).

Chapter 3: Results

3.1 Statistical Analyses

The following U-tests were calculated to compare the morphologies (lengths, widths, aspect ratios) between the two populations to see if they were significantly different or not: all neocrystallized data vs. all recrystallized data (Table 4), FESEM Vs. SEM data (Table 5), SEM neocrystallized data vs. SEM recrystallized data (Table 6), and FESEM neocrystallized data vs. FESEM recrystallized data (Table 7) (Figure 31). It was found that the FESEM and SEM data were significantly different with the SEM having greater lengths, fatter widths, and similar aspect ratios compared to the FESEM (Table 5). To confirm that microscopy method would not alter my conclusions, a U-test was conducted comparing lengths, widths, and aspect ratios for SEM neocrystallized and SEM recrystallized fibrous amphibole (Table 6) as well as FESEM neocrystallized and FESEM recrystallized fibrous amphibole (Table 7). In both cases it was found that neocrystallized and recrystallized fibrous amphibole were significantly different with recrystallized particles having larger widths, lengths, and aspect ratios (Tables 4-7). Lastly, a U-test was conducted on all data in its entirety to compare widths, lengths, and aspect ratios for neocrystallized and recrystallized fibers to see if they were significantly different. As seen in Table 4, neocrystallized and recrystallized particles were found to be significantly different with recrystallized particles being wider, longer, and having greater aspect ratios.

3.2 Petrographic Analyses

Recrystallized particles formed by replacement were identified petrographically in both plane polarized light (PPL) and cross polarized light (XPL). Replacement of magmatic magnesio-hornblende into fibrous amphibole can be observed recrystallizing within one grain (Figure 32), but more commonly is observed as a grain that has undergone replacement to fibrous amphibole in completion (Figure 3). These grains are identified in PPL by being weakly pleochroic and having a pale green color. Additionally, these

grains are identified in XPL by their second order birefringence colors, having a needle like habit, and are often surrounded by altered plagioclase (Figures 2-4). Neocrystallized fibers can be identified in PPL and XPL as thin, fracture fill veins (several μm to mm wide) often cutting through altered plagioclase (Figure 2). These veins are often filled with very small needle like particles that have crystalized primarily within the vein (Figure 2). Neocrystallized fibers can also be seen growing within or around the edges of other grains (often quartz) petrographically as well (Figure 4).

3.3 Dimensional Analyses of Amphibole Particle Chemistry and Mineralogy

Using both the SEM and FESEM with EDS, 1,525 particles were identified and classified as having amphibole chemistry with aspect ratios $\geq 3:1$ (Tables 10 and 11). The minerals identified, through the methods described in Chapter 2, were actinolite, anthophyllite, edenite, magnesiohornblende, riebeckite, winchite, and unassigned amphibole (Table 8 and 9). As seen in Table 8, 56.1% of all particles were classified as actinolite (average width: $1.2 \pm 0.034 \mu\text{m}$, average length: $7.86 \pm 0.266 \mu\text{m}$, and average aspect ratio: 7.6 ± 0.26). For neocrystallized particles, 67.9% were actinolite (average width: $1.1 \pm 0.042 \mu\text{m}$, average length: $6.19 \pm 0.242 \mu\text{m}$, and average aspect ratio of 6.7 ± 0.23) (Table 9). For recrystallized particles, 46.2% of particles were classified as actinolite (average width: $1.4 \pm 0.056 \mu\text{m}$, an average length of $9.94 \pm 0.495 \mu\text{m}$, and average aspect ratio of 8.8 ± 0.50) (Table 9). An additional 501 particles (33%) were unassigned, meaning we could classify the particle as amphibole but could not definitively assign a mineral name (Table 8).

Amphibole mineral groups present included (1) calcic, (2) Fe-Mg, (3) sodic, (4) sodic-calcic, and (5) sub-calcic (Table 10 and 11). The two largest groups were calcic (57.5% of total particles) and sub-calcic (38% of total particles) (Table 10). Within the neocrystallized group, 64.9% of particles were calcic and 29.9% were sub-calcic (Table 11). The recrystallized group had 51.3% calcic, and 44.7% sub-calcic (Table 11). In nearly all amphibole mineral groups, recrystallized particles had significantly larger average widths, lengths, and aspect ratios compared to neocrystallized particles (Table 11).

3.4 Dimensional Analysis of Neocrystallized Vs. Recrystallized Particles

To reflect current definitions for asbestos morphology, the data presented within this thesis includes any fibrous amphibole particle with an $AR \geq 3:1$. Photomicrographs of 1,525 particles were measured using ImageJ (Rasband, 2018) taken from both the SEM and FESEM with EDS capabilities (Appendix C). Statistical analysis of all data with an $AR \geq 3:1$ indicates that recrystallized particles were significantly different having wider average widths ($1.1 \pm 0.037 \mu\text{m}$), longer lengths ($9.03 \pm 0.341 \mu\text{m}$), and greater aspect ratios ($10. \pm 0.38$) compared to neocrystallized particles (width: $0.94 \pm 0.032 \mu\text{m}$, length: $5.70 \pm 0.191 \mu\text{m}$, and aspect ratio: 7.1 ± 0.19) (Table 12). For all particles in this study, 96% met the criteria to be respirable and 49% of particles had a length $\geq 5 \mu\text{m}$ (Table 38). For neocrystallized particles included within this study, 97% met the criteria to be respirable and 39% had a length $\geq 5 \mu\text{m}$ (Table 38). For recrystallized particles included within this study, 95% met the criteria to be respirable and 73% had a length $\geq 5 \mu\text{m}$ (Table 38). For both neocrystallized and recrystallized fibers, 100% of fibers had widths $< 3 \mu\text{m}$ (Table 14).

3.5 Dimensional Analyses by Particle type

Despite inconsistent rules on descriptions of particle morphology in the literature (Lowers and Meeker, 2002), we assigned one of the following descriptors for each particle: (A) *fibers*, (B) *bundles*, or (C) *prismatic crystals*. In this study, *fibers* are defined as particles that are longer than they are wide with no signs of splitting or splayed ends, often having a width less than one micron. *Bundles* are defined as particles that have splayed or splitting ends with individual fibers bundled together. *Prismatic crystals* are defined as blocky crystals with blunt edges with widths often greater than one micron. *Prismatic crystals* differ from *fibers* as they tend to be more square and blocky compared to the longer, more rectangular shape of a *fiber*. In addition, because these morphologic descriptors are not based on quantifiable metrics, they are largely ‘in the eye of the beholder.’ Thus, in order to decrease internal variability/error, and increase

consistency, we had one person make these morphologic determinations. Figures 33 (A-F), 34 (A-C), 35, 36 (A-C), 37 (A-C), and 38 display FESEM and SEM photomicrographs of neocrystallized and recrystallized *bundles*, *fibers*, and *prismatic crystals* respectively. A greater percentage of *bundles* (58%) identified in this study were formed via recrystallization than neocrystallization (Table 13). A similar percentage of *fibers* identified in this study were present for both neo-and-recrystallization (Table 14). A greater percentage of *prismatic crystals* (53%) identified in this study were formed via neocrystallization compared to recrystallization (Table 15).

Recrystallized *bundles* had similar average widths ($1.4 \pm 0.056 \mu\text{m}$), significantly longer lengths ($10.5 \pm 0.494 \mu\text{m}$), and significantly greater aspect ratios (9.5 ± 0.41) compared to neocrystallized *bundles* (width: $1.2 \pm 0.55 \mu\text{m}$, length: $7.16 \pm 0.295 \mu\text{m}$, and aspect ratio: 6.6 ± 0.20) (Table 13). Recrystallized *fibers* were significantly different having larger widths ($0.64 \pm 0.023 \mu\text{m}$), longer lengths ($7.31 \pm 0.483 \mu\text{m}$), and greater aspect ratios ($13. \pm 0.86$) compared to neocrystallized *fibers* (width: $0.53 \pm 0.018 \mu\text{m}$, length: $4.26 \pm 0.257 \mu\text{m}$, and aspect ratio: 8.7 ± 0.38) (Table 14). Recrystallized *prismatic crystals* were significantly different having larger widths ($1.4 \pm 0.010 \mu\text{m}$), longer lengths ($5.28 \pm 0.366 \mu\text{m}$), and similar aspect ratios (3.9 ± 0.088) compared to neocrystallized *prismatic crystals* (width: $1.1 \pm 0.064 \mu\text{m}$, length: $3.90 \pm 0.249 \mu\text{m}$, and aspect ratio: 3.7 ± 0.078) (Table 15)

3.5.1 Dimensional Analysis of Fiber Vs. Bundle Morphology

The data were further constrained by removing all *prismatic crystals* from the analyses and testing the combined statistics for *fibers* and *bundles* only, as *prismatic crystals* are often labeled by industry as “non-asbestiform” (Gunter et al., 2007, Harper et al., 2012). After removing *prismatic crystals* from the dataset for this analysis, 91% of the data remained. Therefore, 91% of the data was classified as having *fiber* or *bundle* morphology. A greater percentage of *fibers* and *bundles* formed via recrystallization (55%) compared to neocrystallization (45%) (Table 16). Recrystallized *fibers/ bundles* were significantly different having larger widths ($1.1 \pm 0.39 \mu\text{m}$), longer lengths ($9.33 \pm 0.365 \mu\text{m}$), and greater aspect ratios ($11 \pm$

0.41) compared to neocrystallized *fibers/ bundles* (width: $0.93 \pm 0.35 \mu\text{m}$, length: $5.91 \pm 0.209 \mu\text{m}$, and aspect ratio: 7.5 ± 0.205).

3.5.2 Dimensional Analysis of Particle Type with Fiber Width $\leq 1 \mu\text{m}$

Consistently distinguishing between fibers, bundles, and prismatic crystals/cleavage fragments is extremely difficult. Therefore, Harper et al. (2012) suggested that using a criterion for asbestos as a width $< 1 \mu\text{m}$ allowed for greater exclusion of cleavage fragments, and more cross-laboratory consistency in counting, possibly creating an “asbestos-rich” dataset. Following these criteria, an additional analysis was conducted by analyzing particle type with a width $\leq 1 \mu\text{m}$. This analysis consisted of 67% of the original particles with 49% classified as neocrystallized and 51% as recrystallized particles (Table 17). Recrystallized mean width was statistically similar to neocrystallized mean width, with both measuring $0.58 \pm 0.10 \mu\text{m}$ wide (Table 17). Recrystallized particles had significantly longer ($p < 0.05$) lengths ($6.08 \pm 0.264 \mu\text{m}$) and significantly greater aspect ratios ($12. \pm 0.57$) compared to neocrystallized particles ($4.12 \pm 0.140 \mu\text{m}$ and 7.8 ± 0.24 respectively) (Table 17). It is important to note average length decreased when the data were filtered to accommodate a width $\leq 1 \mu\text{m}$. This is most likely the cause of longer bundles no longer being present in the data set due to their widths usually being larger than $1 \mu\text{m}$. This would cause the data to skew toward shorter lengths. Furthermore, the average aspect ratio likely increased because any long fiber that remained in the data set contains a smaller width. A very small width combined with a longer length would create a much higher aspect ratio.

For particles with a width $< 1 \mu\text{m}$, 49% were classified as *fibers* (Table 19), 45% as *bundles* (Table 18), and 6% as *prismatic crystals* (Table 20). In this same analysis, a greater percentage of *fibers* (52%) and *prismatic crystals* (65%) identified formed via neocrystallization compared to recrystallization (48% and 35% respectively) (Tables 19 and 20). A greater percentage *bundles* with a width $< 1 \mu\text{m}$ were formed via recrystallization (56%) compared to neocrystallization (44%) (Table 18). Recrystallized *bundles* were significantly different ($p < 0.05$) having smaller average widths ($0.61 \pm 0.014 \mu\text{m}$), longer lengths ($6.16 \pm$

0.313 μm), and greater aspect ratios ($11. \pm 0.70$) compared to neocrystallized *bundles* (width: 0.66 ± 0.014 μm , length: 4.71 ± 0.231 μm , and aspect ratio: 7.4 ± 0.30) (Table 18). Recrystallized *fibers* had similar widths (0.54 ± 0.016 μm), significantly longer lengths (6.28 ± 0.458 μm) and significantly greater aspect ratios (13.0 ± 0.96) compared to neocrystallized *fibers* (width: 0.49 ± 0.014 μm , length: 3.89 ± 0.195 μm , and aspect ratio: 8.7 ± 0.39) (Table 19). Recrystallized *prismatic crystals* had similar widths (0.73 ± 0.048 μm), similar lengths (2.87 ± 0.246 μm), and similar aspect ratios (3.9 ± 0.15) compared to neocrystallized *prismatic crystals* (width: 0.70 ± 0.033 μm , length: 2.59 ± 0.146 μm , and aspect ratio: 3.7 ± 0.11) (Table 20).

3.5.3 Particle type with Length ≥ 5 μm , Width ≤ 1 μm , and AR $\geq 3:1$

An additional analysis was conducted to filter particle type for the WHO's length (≥ 5 μm) combined with a width ≤ 1 μm rather than 3 μm . By doing so we are combining Harper et al. (2012) criteria for asbestos as a width < 1 μm with the WHO's definition for an asbestos fiber (WHO Regional Office, 2000). This analysis consisted of 21% of the original dataset with 37% classified as neocrystallized and 63% as recrystallized particles (Table 21). Neocrystallized mean width (0.70 ± 0.020 μm) was significantly different having a wider width than recrystallized particles (0.64 ± 0.017 μm) (Table 21). Recrystallized particles were significantly different having longer lengths (10.8 ± 0.525 μm) and greater aspect ratios ($20. \pm 1.2$) compared to neocrystallized particles (8.20 ± 0.391 μm and $13. \pm 0.70$ (respectively) (Table 21). It is important to note that the average length and aspect ratios increased when the data was further filtered to accommodate for a width ≤ 1 μm when compared to the original data. This is most likely due to the data being filtered for a thinner width which caused a fiber-rich data-pool and allowed for fibers of longer lengths to concentrate by eliminating particles with greater widths that are often accompanied by shorter lengths. Furthermore, the average aspect ratio likely increased because any long fiber that remained in the data set contains a smaller width. A very small width combined with a longer length would create a much higher aspect ratio.

In this study, 53% of particles that fit the WHO's definition for an asbestos fiber (WHO Regional Office, 2000) with a $W \leq 1 \mu\text{m}$ were classified as *bundles* (Table 22), 47% as *fibers* (Table 23), and 0% as *prismatic crystals* (Table 24). A greater percentage of *fibers* (63%) and *bundles* (64%) identified in this analysis formed via recrystallization compared to neocrystallization (37% and 36% respectively) (Tables 22 and 23). Zero percent of particles that were classified as *prismatic crystals* fit this dimensional analysis ($L \geq 5 \mu\text{m}$, $W \leq 1 \mu\text{m}$, $AR \geq 3:1$) (Table 24). *Prismatic crystals* likely did not appear because of their widths not fitting the model when combined with the length and width constraints. Using the WHO's definition for an asbestos fiber (WHO Regional Office, 2000) with a $W \leq 1 \mu\text{m}$, recrystallized *bundles* were significantly different ($p < 0.05$) having smaller average widths ($0.64 \pm 0.55 \mu\text{m}$), longer lengths ($10.1 \pm 0.557 \mu\text{m}$), and greater aspect ratios ($19. \pm 1.4$) compared to neocrystallized *bundles* (width: $0.76 \pm 0.024 \mu\text{m}$, length: $8.22 \pm 0.535 \mu\text{m}$, and aspect ratio: $11. \pm 0.64$) (Table 22). Recrystallized *fibers* had similar widths ($0.63 \pm 0.025 \mu\text{m}$), significantly longer lengths ($11.7 \pm 0.921 \mu\text{m}$), and significantly greater aspect ratios ($23. \pm 2.0$) compared to neocrystallized *fibers* (width: $0.63 \pm 0.030 \mu\text{m}$, length: $8.17 \pm 0.578 \mu\text{m}$, and aspect ratio: $15. \pm 1.2$) (Table 23).

3.6 Regulatory and Theorized Dimension Definitions

For nearly all dimensional analyses listed below in section 3.6, recrystallized particles had statistically similar average widths, significantly different lengths, and significantly different aspect ratios compared to neocrystallized. Furthermore, recrystallized particles more commonly fit regulatory dimensional criteria for an asbestos fiber.

3.6.1 Regulatory Dimension Definitions: OSHA, WHO, EPA

The OSHA defines asbestos fibers as particles having a length $\geq 5 \mu\text{m}$ with an aspect ratio $\geq 3:1$ (29 CFR 1910.1001 Subpart Z(b)). The data collected in this study were sorted into neocrystallized and recrystallized data and then filtered to fit the OSHA's regulatory definition of an asbestos fiber based strictly

on fiber dimensions. This analysis consisted of 49% of the original dataset with 36% of the particles classified as neocrystallized and 64% as recrystallized (Table 25). Neocrystallized mean width ($1.5 \pm 0.068 \mu\text{m}$) was statistically similar to recrystallized mean width ($1.5 \pm 0.057 \mu\text{m}$) (Table 25). Recrystallized particles were significantly different having longer lengths ($13.4 \pm 0.509 \mu\text{m}$) and greater aspect ratios ($13. \pm 0.62$) compared to neocrystallized particles ($9.89 \pm 0.357 \mu\text{m}$ and 8.9 ± 0.39 (respectively) (Table 25).

According to the World Health Organization, asbestos fibers are defined as having a length $\geq 5 \mu\text{m}$, width $< 3 \mu\text{m}$, and an aspect ratio $\geq 3:1$ (WHO Regional Office, 2000). The data collected in this study were sorted into neocrystallized and recrystallized data and then filtered to fit the WHO's definition of an asbestos fiber based strictly on fiber dimensions. This analysis consisted of 45% of the original dataset with 37% of the particles classified as neocrystallized and 63% as recrystallized (Table 26). Neocrystallized mean width ($1.3 \pm 0.041 \mu\text{m}$) was statistically similar to recrystallized mean width ($1.2 \pm 0.032 \mu\text{m}$) (Table 26). Recrystallized particles were significantly different having longer lengths ($12.2 \pm 0.425 \mu\text{m}$) and greater aspect ratios ($14. \pm 0.67$) compared to neocrystallized particles ($9.24 \pm 0.324 \mu\text{m}$ and $9.2. \pm 0.41$ (respectively) (Table 26).

The EPA TEM microscopy method defines asbestos fibers as particles having a length $\geq 0.5 \mu\text{m}$ and an aspect ratio $\geq 5:1$ (40 CFR 763 Subpart E, App. A). The data collected in this study were sorted into neocrystallized and recrystallized data and then filtered to fit the EPA TEM microscopy method definition of an asbestos fiber based strictly on fiber dimensions. This analysis consisted of 63% of the original dataset with 42% of the particles classified as neocrystallized and 58% as recrystallized (Table 27). Recrystallized particles were significantly different having larger widths ($0.98 \pm 0.042 \mu\text{m}$), longer lengths ($10.8 \pm 0.477 \mu\text{m}$), and greater aspect ratios ($13. \pm 0.53$) compared to neocrystallized particles (width: $0.79 \pm 0.032 \mu\text{m}$, length: $6.71 \pm 0.281 \mu\text{m}$, and aspect ratio: 9.5 ± 0.27). Compared to data filtered by the WHO and the OSHA definitions, the averages for the EPA TEM microscopy method definition decreased for width and length (Tables 25-27).

3.6.2 Harper's Theorized Dimension Definition of an Asbestos Fiber

Combining the OSHA's and the WHO's aspect ratio dimension of 3:1 with Harper et al. (2012) criteria for asbestos as a width $< 1 \mu\text{m}$, we attempted to create an "asbestos-rich" dataset. We will refer to this as Harper's theorized definition of an asbestos fiber. For this analysis, the data was filtered for a width $\leq 1 \mu\text{m}$ and an aspect ratio $\geq 3:1$ and then sorted by crystallization process. This analysis consisted of 67% of the original dataset with 49% of the particles classified as neocrystallized and 51% as recrystallized (Table 28). Neocrystallized mean width ($0.58 \pm 0.010 \mu\text{m}$) was statistically similar to recrystallized mean width ($0.58 \pm 0.010 \mu\text{m}$) (Table 28). Recrystallized particles were significantly different having longer lengths ($6.08 \pm 0.264 \mu\text{m}$) and greater aspect ratios ($12. \pm 0.57$) compared to neocrystallized particles ($4.12 \pm 0.140 \mu\text{m}$ and $7.8. \pm 0.24$ (respectively) (Table 28).

3.7 Dimensional Analyses of Particle Type Vs. Asbestos Fiber Regulations

To compare assigned particle type and the OSHA regulations for an asbestos fiber (29 CFR 1910.1001 Subpart Z(b)), we created a table that divided all data, neocrystallized data, and recrystallized data into *bundles*, *prismatic crystals*, and *fibers* based on their particle type. The data were then filtered to fit the OSHA regulatory definition of an asbestos fiber, which is based strictly on fiber dimensions ($L \geq 5 \mu\text{m}$ and $AR \geq 3:1$) (29 CFR 1910.1001 Subpart Z(b)). Particle type within this analysis consisted of: (1) *bundles* (69%), (2) *fibers* (25%), and (3) *prismatic crystals* (6%).

In this study, 60% of *bundles* fit the dimensions for the OSHA definition of an asbestos fiber (Table 29). In addition, 69% of all particles that fit this definition were classified as having the *bundle* particle type (Table 29). Recrystallized *bundles* had similar average widths ($1.7 \pm 0.076 \mu\text{m}$), significantly longer lengths ($14.2 \pm 0.668 \mu\text{m}$) and significantly greater aspect ratios ($11. \pm 0.59$) compared to neocrystallized *bundles* (width: $1.7 \pm 0.089 \mu\text{m}$, length: $10.4 \pm 0.421 \mu\text{m}$, and aspect ratio: 7.5 ± 0.31) (Table 29). For particles in this study classified as *fibers*, 35% of them fit the dimensions for the OSHA definition of an asbestos fiber. In addition, 25% of all particles that fit this definition were classified as having the *fiber* particle type (Table

30). Recrystallized *fibers* had similar widths ($0.82 \pm 0.040 \mu\text{m}$), significantly longer lengths ($12.7 \pm 0.840 \mu\text{m}$), and significantly greater aspect ratios ($20. \pm 1.6$) compared to neocrystallized *fibers* (width: $0.75 \pm 0.043 \mu\text{m}$, length: $8.98 \pm 0.779 \mu\text{m}$, and aspect ratio: $14. \pm 1.1$) (Table 30). Of all the particles that were classified as *prismatic crystals* within this study, 34% of them fit the dimensions for the OSHA definition for an asbestos fiber (Table 31). In addition, 6% of all particles that fit this definition were classified as having the *prismatic crystal* particle type (Table 31). Recrystallized *prismatic crystals* had statistically similar widths ($1.9 \pm 0.15 \mu\text{m}$), similar lengths ($7.41 \pm 0.480 \mu\text{m}$), and similar aspect ratios (4.1 ± 0.12) compared to neocrystallized *prismatic crystals* (width: $1.8 \pm 0.14 \mu\text{m}$, length: $6.99 \pm 0.524 \mu\text{m}$, and aspect ratio: 4.0 ± 0.17) (Table 31).

The WHO's definition of an asbestos fiber differs from the OSHA's by constraining fiber dimensions by length, aspect ratio, and width rather than only aspect ratio and length (WHO Regional Office, 2000). Due to the width constraint, one may expect lower values for the average particle dimensions when comparing to the OSHA's definition. In order to compare assigned particle type and the WHO's definition for an asbestos fiber, a table that divided all dimensional neocrystallized and recrystallized data (Table 12) into *bundles*, *prismatic crystals*, and *fibers*, a title given to each particle based on their *visual* particle type (Tables 13-15), was created. The data was then filtered to fit The WHO's definition of an asbestos fiber, based strictly on fiber dimensions ($L \geq 5 \mu\text{m}$, $W < 3 \mu\text{m}$, and $AR \geq 3:1$) (Table 32-34) (WHO Regional Office, 2000). Particle type within this analysis consisted of: (1) *bundles* (66%), (2) *fibers* (28%), and (3) *prismatic crystals* (6%). Of all the particles in this study, 20% of neocrystallized *prismatic crystals*, 49% of neocrystallized *bundles*, and 24% of neocrystallized *fibers* fit the WHO definition of an asbestos fiber (Table 32-34). In contrast, 47% of recrystallized *prismatic crystals*, 57% of recrystallized *bundles*, and 45% of recrystallized *fibers* fit the WHO definition of an asbestos fiber (Table 32-34). Of all the particles that were classified as *bundles* within this study, 54% of them fit the dimensions for the WHO definition of an asbestos fiber. In addition, 66% of all particles that fit the WHO definition were *bundles* (Table 28). Recrystallized *bundles* had statistically similar average widths ($1.4 \pm 0.041 \mu\text{m}$), significantly longer lengths ($12.5 \pm 0.530 \mu\text{m}$), and significantly greater aspect ratios ($12. \pm 0.66$) compared to

neocrystallized *bundles* (width: $1.4 \pm 0.050 \mu\text{m}$, length: $9.54 \pm 0.362 \mu\text{m}$, and aspect ratio: 7.9 ± 0.33) (Table 32). Of all the particles that were classified as *fibers* within this study, 35% of them fit the dimensions for the WHO definition of an asbestos fiber. In addition, 28% of all particles that fit the WHO definition were classified as having the *fiber* particle type (Table 33). Recrystallized *fibers* had statistically similar widths ($0.82 \pm 0.040 \mu\text{m}$), significantly longer lengths ($12.7 \pm 0.840 \mu\text{m}$), and similar aspect ratios ($20. \pm 1.6$) compared to neocrystallized *fibers* (width: $0.75 \pm 0.043 \mu\text{m}$, length: $8.98 \pm 0.780 \mu\text{m}$, and aspect ratio: $14. \pm 1.1$) (Table 33). Of all the particles that were identified as *prismatic crystals* within this study, 32% of them fit the dimensions for the WHO definition of an asbestos fiber. In addition, 6% of all particles that fit the WHO definition were classified as having the *prismatic crystal* particle type (Table 34). Recrystallized *prismatic crystals* had statistically similar widths ($1.7 \pm 0.078 \mu\text{m}$), similar lengths ($7.05 \pm 0.333 \mu\text{m}$), and similar aspect ratios (4.2 ± 0.12) compared to neocrystallized *prismatic crystals* (width: $1.7 \pm 0.11 \mu\text{m}$, length: $6.65 \pm 0.434 \mu\text{m}$, and aspect ratio: 4.0 ± 0.18) (Table 34). It can also be observed that *fiber* dimensions were the same between the OSHA and the WHO definition for *fiber* particle type (Tables 30 and 33). This is because all particles within this study that were identified as a *fiber*, based on its particle type, had a width $< 3 \mu\text{m}$ once filtered for length and aspect ratio. The WHO definition filters for a width $< 3 \mu\text{m}$ but the OSHA does not. Since all particles identified as a *fiber* had a width less than $3 \mu\text{m}$, both the OSHA *fiber* dimensions and the WHO *fiber* dimensions in tables 30 and 33 had the same values, and therefore, the same *fiber* dimensions existed for each comparison.

3.8 FESEM Vs. SEM Statistical Analyses

During data collection, the FESEM required maintenance and was not accessible for most of the data collection process. Due to this, data were obtained using 24 samples on both the FESEM and the SEM. To confirm that microscopy method did not alter results, U-tests were conducted comparing neocrystallized and recrystallized populations for each microscopy method (Figure 31). The results of these statistical analyses are further discussed below. The descriptive statistics for each microscopy method are as follows.

In total, there was 588 particles imaged on the SEM and 937 particles imaged on the FESEM. Particles imaged on the SEM were significantly different ($p < 0.05$) having greater mean widths, longer mean lengths, and similar mean aspect ratios compared to those imaged on the FESEM (Table 37). For both the SEM and the FESEM, recrystallized particles were significantly different ($p < 0.05$) having greater average widths, average lengths, and average aspect ratios as compared to neocrystallized particles (Tables 35-36).

Chapter 4: Discussion

The purpose of this study was to determine if the different formation processes of neocrystallization versus re-crystallization affected amphibole particle morphology, and therefore toxicity. This project tested the null hypothesis that neocrystallized and recrystallized fibrous amphiboles, of similar mineralogy and chemistry, would produce particles of statistically similar lengths, widths, and aspect ratios. Based upon a thorough literature review, we expected to find neocrystallized amphibole particles to be longer, thinner and have greater aspect ratios compared to recrystallized amphiboles because they grew in open fracture-fill veins (Bailey et al., 2004; Van Gosen, 2007; Virta, 2002). It is believed, that under these conditions, fibers are able to nucleate and grow into asbestiform habits (Tabler, 1916; Virta, 2002). Metcalf and Buck (2015) and others (Ahn and Buseck, 1991; Akai, 1982; Meeker et al., 2006) disputed this fact, claiming that fibrous amphibole can also form from recrystallization (Ahn and Buseck, 1991; Akai, 1982; Meeker et al., 2006) of magmatic-magnesio-hornblende (Metcalf and Buck, 2015) from the same hydrothermal fluid that produced neocrystallized fibrous amphibole (Metcalf and Buck, 2015). The intent of this study was, therefore, to compare these two crystallization processes to see if they produce statistically similar dimensions and, therefore, toxicities. Analyzing the data based on dimensional and primary (visual) morphology (Tables 8-34), this study found that recrystallized particles were often statistically similar or different in width, were significantly longer, and had significantly greater aspect ratios compared to neocrystallized particles. This finding challenged both the null hypothesis and expected outcome from the scientific hypothesis. In order to verify if recrystallized particles truly were significantly different compared to neocrystallized particles, a series of U-tests were conducted (Tables 4-7). The U-tests confirmed that recrystallized particles are significantly different and are wider, longer, and have greater aspect ratios than neocrystallized particles (Tables 4-7, 12, 35-37). This finding demonstrates that recrystallized amphiboles meet the criteria for asbestos. Although such deposits may not be economically minable for the production of asbestos, they may still pose a health hazard to people exposed to these fibers through other mechanisms (Figure 1). Since amphibole minerals are abundant and recrystallization is a common process, we predict

that people are being exposed to more amphibole asbestos than previously recognized through many mechanisms of exposure (Figure 1).

4.1 Amphibole Mineralogy and Petrographic Implications

All of the particles used in this study were confirmed amphibole minerals, and the vast majority of these were calcic amphiboles (Figure 39). The EDS results of this study agree with previous research in this field area that used the more sensitive EMPA-WDS analyses and found that the majority of these calcic amphiboles are actinolite (Figure 40, Tables 8-9) (Austin, 2019; Buck et al., 2013; Metcalf et al., 2018). As we collected samples from the same areas in southern Nevada that were described in these studies, no EPMA-WDS analyses were conducted within this thesis project as they were done previously (Figure 40). We collected EDS data to ensure the particles that we were measuring within the thesis were amphibole. Seeing as how EDS chemistry is qualitative to semi-quantitative at best, and our EDS data matches that of the EMPA-WDS analyses previously conducted in our field area, we will be using the mineralogy results from the previous EMPA-WDS analyses. The EPMA-WDS analyses from previous research in southern Nevada composed of 54% actinolite, 33% magnesiohornblende, 2% edenite, and 2% pargasite (Metcalf et al., 2018). The remaining 9% of the dataset was composed of sodic-calcic compositions including winchite, taramite, and magnesiokatophorite (Metcalf et al., 2018) (Figure 40). With mineralogy remaining near constant between neocrystallized and recrystallized particles, we were able to compare their results with more certainty. This allows us to compare “apples to apples” rather than “apples to oranges.” Recrystallized actinolite particles had significantly larger widths, significantly longer lengths, and significantly greater aspect ratios compared to neocrystallized actinolite particles. Because morphology is an important factor for toxicity, the recrystallized actinolite particles, with greater aspect ratios, have a greater potential to be more toxic than the neocrystallized particles (Aust et al., 2011).

These findings combined with the petrographic analyses support the findings from Metcalf et al. (2018) and Austin (2019). These previous studies petrographically verified and defined recrystallized and

neocrystallized fibrous amphibole from southern Nevada (Boulder City pluton) and northwestern Arizona (Wilson Ridge pluton). EPMA analyses and a fluid inclusion study were previously conducted to understand fluid and particle chemistry (Austin, 2019). The Nevada samples from these analyses were collected from the same pluton as those from this study and are therefore comparable. The protolith mineralogy of rocks from the unaltered Nevada samples contained orthoclase, hornblende, plagioclase, biotite, and quartz. The mineralogy of rocks from the altered Nevada samples contained albite (clear and turbid), potassium feldspar veins, quartz veins, epidote, hematite, and chlorite. Fibrous actinolite dominated within thin section as both veins and grains (Metcalf et al., 2018). Austin (2019) and Metcalf et al. (2018) identified three textures of fibrous amphiboles petrographically, including neocrystallization of fibrous amphibole within empty fracture-fill veins (Type I); neocrystallization fiber intergrowth within or on edges of other grains (Type II); and secondary replacement of magmatic amphibole by fibrous amphibole (Type III). These three textures can be observed petrographically within samples in this study and are interpreted to have been crystallized as a result of multiple interactions with the hydrothermal fluid as described in Metcalf et al. (2018) and Austin (2019) (Figures 2-4).

Austin (2019) hypothesized that the alteration from fluids happened in multiple phases. The first phase of fluid and rock interaction can be observed petrographically by plagioclase with sericite alterations and albitization creating turbidity of feldspars that are lacking type II fiber intergrowth (Austin, 2019). At this phase, the fluid was out of equilibrium with rocks. As the fluid moved through the rock, magmatic hornblende ions were removed causing the fluid to become enriched with amphibole building ions, driving it to equilibrium (Austin, 2019). These amphibole building ions within the fluid reacted with primary magnesiohornblende and recrystallized fibrous amphiboles of slightly-varying chemistries. Secondary conversion of magmatic magnesio-hornblende into fibrous actinolite is observed by Metcalf et al. (2018), Austin (2019), and our study. With the remaining fluid now at equilibrium with the secondary amphiboles, the final stages of type I and II neocrystallized alteration occurs simultaneously. As the latter fluid advances through the rock, type I neocrystallization precipitates fibrous amphiboles as fracture-fill veins and type II neocrystallized fibers precipitate on the edges or within surrounding grains (often quartz and feldspar)

(Austin, 2019). For Metcalf et al. (2018) and Austin (2019) samples, the neocrystallized veins can be observed cutting through recrystallized (type III) grains, placing recrystallization before neocrystallization in southern Nevada. The same pattern can be observed petrographically for this study as well (Figures 2-4). A fascinating find from Austin (2019) was that multiple varieties of amphibole can be seen along the length of grains and within one continuous vein. This implies that amphibole chemistry can change along a spectrum within a single fiber from actinolite to a non-regulated amphibole while maintaining its fibrous habit (Austin, 2019). Therefore, amphibole mineralogy is more complicated than the five amphibole asbestos minerals that are currently regulated.

4.2 Dimensional and Morphologic Patterns and Implications of Neo-and-Re-crystallization

4.2.1 Particle Dimensional Qualification Under Asbestos Standards

In order for asbestos to *legally* be classified as an asbestos fiber by The United States Occupational Safety and Health Administration (OSHA), it must be one of the six regulated asbestos minerals and have a minimum length of at least 5 μm with a mean aspect ratio of 3:1 or greater (29 CFR 1910.1001 Subpart Z(b)) (Clinkenbeard et al., 2002). The World Health Organization has a similar asbestos fiber definition with the following dimensions: minimum length of 5 μm or longer, a diameter < 3 μm , and a mean aspect ratio of at least 3:1 (Clinkenbeard et al., 2002; WHO Regional Office, 2000). The WHO definition contains a width criterion as any elongated mineral particle with a width less than 3 μm is respirable according to the WHO Regional Office (2000) and NIOSH (2011).

When strictly considering particle dimension, the initial data (Table 12) were sorted into subcategories based on several regulatory and theorized asbestos definitions, including: (1) OSHA fiber definition (Table 25), (2) WHO fiber definition (Table 26), (3) EPA TEM fiber counting method definition (Table 27), and (4) Harper et al. (2012) theorized definition for asbestos fiber with widths $\leq 1 \mu\text{m}$ (Table 28). We observed that recrystallized processes generally produced larger numbers of particles that fit the criteria for regulatory definitions of asbestos fibers. These recrystallized particles also demonstrated

significantly greater lengths and higher aspect ratios than particles produced from neocrystallized processes (Tables 25-28; Figure 41). In nearly all cases, these particles classified by definitions had statistically similar widths for both neocrystallized and recrystallized particles (Tables 25, 26, and 28). However, for the EPA TEM definition, neocrystallized particles had significantly thinner widths than recrystallized particles (Table 27). In all instances described above, recrystallized particles produced significantly larger lengths and aspect ratios compared to neocrystallized particles. Therefore, recrystallized particles legally fit the regulatory definitions for an asbestos fiber and should be recognized for their potential to produce fibrous morphologies (Figure 41). Recrystallized particles tended to have similar widths as neocrystallized, but had significantly larger lengths and aspect ratios, thus indicating that recrystallized fibrous amphibole has the potential to produce equally or more toxic morphologies than their neocrystallized counterparts. These findings indicate the health risk potential to those who live in metropolitan Las Vegas region may be greater than previously known.

Recrystallized processes produced a greater number of particles that legally fit criteria for asbestos. Tables 38 and 39 divides data by crystallization type to compare various asbestos regulations, definitions, (Table 39) or qualifiers (Table 38). Within this study, 97% of neocrystallized and 95% of recrystallized particles had a width less than $< 3 \mu\text{m}$ and met the criteria to be respirable according to NIOSH (2011) (Table 38); 39% of neocrystallized and 57% of recrystallized particles had a length $\geq 5 \mu\text{m}$, which is a requirement for several asbestos definitions (WHO Regional Office, 2000; 29 CFR 1910.1001 Subpart Z(b)); 40 CFR 763 Subpart E, App. A) (Table 38); 36% of neocrystallized and 52% of recrystallized particles fit the WHO definition for an asbestos fiber (WHO Regional Office, 2000) (Table 39), 39% of neocrystallized and 57% of recrystallized particles fit the OSHA definition of an asbestos fiber (Figure 41) (29 CFR 1910.1001 Subpart Z(b)) (Table 39), and 58% of neocrystallized and 67% of recrystallized particles fit the EPA TEM microscopy method definition of an asbestos fiber (Figure 41) (40 CFR 763 Subpart E, App. A) (Table 39). For the particles that fit the Harper et al. (2012) definition of an asbestos fiber ($W < 1 \mu\text{m}$, $AR \geq 3:1$), recrystallized particles dominated, consisting of 51% of the population (Table 28). For all particles present in this study, a greater percentage of neocrystallized particles (72%) fit the

Harper-theorized definition of an asbestos fiber compared to recrystallized particles (63%) (Table 39). This can be explained because a greater percentage of total neocrystallized particles have thinner widths compared to recrystallized particles (Table 12). When compared to the neocrystallized and recrystallized analyses of the OSHA fiber definition, the WHO fiber definition, and the EPA TEM microscopy method, a larger percentage of particles within this study fit the Harper-theorized definition for an asbestos fiber (Table 39). These findings provide a clear indication that the naturally-occurring fibrous amphibole in Clark County, NV largely fit various definitions of asbestos.

4.2.2 Particle Type Implications

Particles were classified into specific types based on their visual characteristics as seen on the FESEM images: (a) *fiber*, (b) *bundle* and (c) *prismatic crystal*. Particle types (Tables 13-15) were then sorted into several subcategories, including: (1) combined statistics of fiber and bundle morphologies (Table 16), (2) Harper's theorized definition (width $\leq 1 \mu\text{m}$) (Table 18-20), (3) the WHO's definition with a $W \leq 1 \mu\text{m}$ (length $\geq 5 \mu\text{m}$, width $\leq 1 \mu\text{m}$, and AR $\geq 3:1$) (Tables 22-24). For all analyses listed, recrystallized processes produced particles with significantly different ($p < 0.05$) morphologies and dimensions that more commonly fit the criteria for asbestos compared to particles produced from neocrystallized processes. Neocrystallized and recrystallized *bundles* had widths that were not significantly different but recrystallized lengths and aspect ratios were significantly larger (Table 13, 17, 19, 23). Recrystallized *fibers* and the combined statistics of *bundles* and *fibers* had particles with significantly different, greater widths, lengths, and aspect ratios (Tables 14 and 16). Thus, more commonly fitting the different regulatory criteria for asbestos compared to neocrystallized *fibers* and *bundles*. Although recrystallized *prismatic crystals* had lengths and widths that were significantly larger than neocrystallized *prismatic crystals*, the aspect ratios were not significantly different because neocrystallized *prismatic crystals* were both shorter and thinner than recrystallized (Table 15). Overall, we continuously found that recrystallized particles had greater lengths and aspect ratios compared to neocrystallized particles. When

comparing the statistical analyses of all initial neocrystallized and recrystallized data (Table 12) to particle types (Tables 13, 14, 16), particles classified as *bundles* have a greater average thickness, and this is to be expected because these particles are still in the process of breaking into smaller fibers. Particles classified as *fibers* tend to be longer and thinner and have greater aspect ratios because by definition, particles with these visual characteristics are more likely to be classified as a *fiber* instead of a *prismatic crystal*. The overall averaged data from particles classified as *bundles* and *fibers* fit the WHO and OSHA definitions for an asbestos fiber and are a potential health hazard to those living in Clark County, NV (Tables 13, 14, and 16).

Consistently distinguishing between *fibers*, *bundles*, and *prismatic crystals/cleavage fragments* is extremely difficult. Therefore, Harper et al. (2012) suggested that using a criterion for asbestos as a width $< 1 \mu\text{m}$ allowed for greater exclusion of cleavage fragments (explained in further detail in section 4.4.2), and more cross-laboratory consistency in counting, possibly creating an ‘asbestos-rich’ dataset. Following these criteria, an additional analysis was conducted by analyzing particle type with a fiber width $\leq 1 \mu\text{m}$. When particle type was filtered for a width $\leq 1 \mu\text{m}$, it was found that the average particle widths and lengths decreased (Table 17) from the initial neocrystallized and recrystallized observations (Table 12) while average aspect ratios increased. This is consistent with the neocrystallized and recrystallized fiber dimensional outcomes listed above (Table 14). This is likely the case since 92% of *fibers* had a width less than $1 \mu\text{m}$ (Tables 14 and 19), which accounts for a thinner width. Thinner widths can cause an increased aspect ratio, as aspect ratio is calculated with width in the denominator. Dividing by a smaller number will create a larger quotient. Neocrystallized *bundles* with widths $\leq 1 \mu\text{m}$ had significantly larger widths, shorter lengths, and smaller aspect ratios compared to recrystallized *bundles* (Table 18). Recrystallized *bundles* with widths $\leq 1 \mu\text{m}$ more commonly fit this criterion for asbestos compared to neocrystallized *bundles* (Table 18). Neocrystallized and recrystallized *fibers* with widths $\leq 1 \mu\text{m}$ had widths that were not significantly different, with recrystallized lengths and aspect ratios that were significantly larger (Table 19), therefore, this observation supports recrystallized processes producing *fibers* that more commonly fit asbestos criteria. Neocrystallized *particles* more commonly fit Harper et. al. (2012) definition (72%)

compared to recrystallized particles (63%) (Table 39), but recrystallized *particles* had significantly larger lengths and aspect ratios for *bundles* and *fibers* (Tables 18 and 19). Following the suggestion to create an “asbestos rich” dataset from Harper et al. (2012), we found that *bundles* and *fibers* fitting this definition continued the pattern of recrystallized particles more commonly fitting the criteria for asbestos compared to neocrystallized particles.

It should be repeated and noted that we defined a *fiber* as: particles that are longer than they are wide with no signs of splitting or splayed ends, often having a width *less than* one micron; and *prismatic crystals* as: blocky crystals with blunt edges with a width often *greater than* one micron. As stated above, 6% of *prismatic crystals* (Table 20) and 92% of *fibers* (Tables 14 and 19) had a width less than 1 μm . Therefore, despite these definitions, there was clearly some bias and error in our visual classifications. Identifying particle type is not always black and white, and something one may classify as a *fiber* might be classified by another worker as a *prismatic crystal*. In the 8% of cases where we defined a particle with a width greater than 1 μm as a *fiber*, these particles likely had longer lengths and greater aspect ratios that caused us to identify these particles as *fibers* despite the slightly wider widths.

An additional analysis was conducted to filter particle type for the WHO’s length ($\geq 5 \mu\text{m}$) combined with a width $\leq 1 \mu\text{m}$ rather than 3 μm . By doing so we are combining Harper et al. (2012) criteria for asbestos as a width $< 1 \mu\text{m}$ with the WHO’s definition for an asbestos fiber (WHO Regional Office, 2000). For this final analysis (particle type with fiber dimensions of length $\geq 5 \mu\text{m}$, width $\leq 1 \mu\text{m}$, and AR $\geq 3:1$), recrystallized *bundles* had significantly thinner widths compared to neocrystallized *bundles* (Table 22). This was peculiar since we commonly observed that all recrystallized *fibers* and *bundles* had significantly greater widths, lengths, and aspect ratio compared to neocrystallized particles for other analyses listed above. However, these results further support the argument that recrystallized processes produce a greater number of particles that fit the criteria for asbestos based on dimensions. Not only can one observe particle dimensions of recrystallized particle type more commonly fitting asbestos definitions based on dimensions, but one can also observe recrystallized morphology more commonly produces morphologies known to meet asbestos morphological criteria. Recrystallized particles were more

commonly assigned as *bundles* and *fibers* based on their particle type compared to particles formed by neocrystallization (Tables 13, 14, 16, 22, and 23). This could possibly be explained by increased defects within the multiple chain structure of recrystallized amphiboles. As discussed in further detail in section 4.5, the more altered an amphibole, the greater the defects in chains of an anomalous width. We hypothesize that the increase of defects within these multiple chain structures may increase the fibrosity of amphiboles.

When comparing Harper et al., (2012) asbestos fiber definition (Tables 18-20; width $\leq 1 \mu\text{m}$ and AR $\geq 3:1$) to the WHO's definition with a width $\leq 1 \mu\text{m}$ (Tables 22-24; length $\geq 5 \mu\text{m}$, width $\leq 1 \mu\text{m}$; AR $\geq 3:1$), one may expect the data to be similar as both analyses are comparing particles that we identified as *fibers*, *bundles*, or *prismatic crystals* with a width less than or equal to one micron. In actuality, one can observe that the dimensions are drastically different and short, thin fibers concentrate when the data are filtered only by width and AR. When data was filtered by particle type with a width $\leq 1 \mu\text{m}$, and then further filter by length $\geq 5 \mu\text{m}$, the average length and aspect ratio were *drastically* higher. 92% of particles within this study that we identified as a fiber had a width less than one micron. Therefore, filtering for one micron did create a 'fiber rich' dataset that Harper et al., (2012) hypothesized. Despite this analysis successfully creating a 'fiber-rich' dataset, based solely on dimension, it is omitting many particles that are still of asbestos dimensions (widths greater than $1 \mu\text{m}$ but less than $3 \mu\text{m}$) and morphologies. These omitted particles are of respirable widths according to NIOSH, and potentially toxic. Therefore, we do not believe Harper et al. (2012) asbestos fiber definition is efficient in quantifying all asbestos particles that may be present.

4.2.3 Implications for Dimensional Analyses of Particle Type Vs. Asbestos Fiber Standards

Particle type and known asbestos standard dimensional constraints were combined in order to compare and contrast data that are filtered for both of these criteria at once. This was done specifically for the regulatory definitions of the OSHA and the WHO. For these scenarios, the initial data (Table 12) was filtered based on particle type classification and then further sorted to account for the OSHA definition of

a fiber (Table 29, 30, 31) and the WHO definition of a fiber (Table 32, 33, 34). This allowed for the comparison between particles that were visually classified as a *fiber*, *bundle*, or *prismatic crystal* to the dimensions of the OSHA and the WHO. In all instances described, recrystallized *fibers*, *bundles*, and *prismatic crystals* that fit the WHO and the OSHA definitions of an asbestos fiber had dimensions that were either statistically similar to neocrystallized particles or were significantly different (Tables 29-31 and Tables 32-34). Recrystallized *fibers* and *bundles* more commonly fit the regulatory definitions of an asbestos fiber. We were also able to compare how many particles that we classified as *fibers* actually fit the OSHA and the WHO's definition of a fiber based on dimensions. We found that 34.7% (24.4% neocrystallized and 44.9% recrystallized) of what we classified as *fibers* fit the OSHA's and the WHO's definition for an asbestos fiber (Table 30 and 33). We could then compare this to the previous results where the data were only filtered for the OSHA and the WHO dimensional criteria rather than particle type and the regulatory dimensional criteria. We can see by comparing Table 25 and 26 that 48.9% (39.0% neocrystallized and 57.3% recrystallized) of our particles fit the OSHA's definition and 45.0% (36.2% neocrystallized and 52.4% recrystallized) of our particles fit the WHO's definition of an asbestos fiber. Therefore, a larger percentage of particles were classified as a fiber based on the dimensional analysis of the OSHA and the WHO standards compared to when the data was filtered by particle type *and* the WHO and the OSHA fiber dimensions. According to this finding, our visually based classification of fibers, bundles, and prismatic crystals removed particles that would have otherwise been counted as an asbestos fiber by the OSHA and WHO based solely on dimensions. Therefore, dimensional criteria may be a more reliable method to identify fibrous amphibole fibers than visual identification.

4.2.4 FESEM Vs. SEM Implications

Both FESEM/EDS and SEM/EDS were used in this study to confirm amphibole mineralogy (EDS) and to measure particle dimensions. To confirm that microscopy method did not alter my findings, a series of Mann-Whiney U-tests were conducted to compare neocrystallized and recrystallized data between the

SEM and FESEM (Tables 4-7, 35-37). Analyses confirmed that microscopy method did not affect the results: in both the SEM and FESEM analyses, neocrystallized and recrystallized particles were significantly different ($p < 0.05$) with recrystallized fibers having larger average widths (Tables 35-37), lengths (Tables 35-37), and aspect ratios (Tables 35 and 36). Not surprisingly, because FESEM has higher resolution (1-5 nm) compared to the SEM (10-50 nm), the FESEM data skew towards smaller average width and lengths compared to SEM. It should be noted that the SEM and FESEM combined statistics did not have significantly different aspect ratios between neocrystallized and recrystallized particles (Table 37). Aspect ratio is calculated by dividing length by width. A larger length divided by a larger width (SEM) can create an aspect ratio that is similar to a smaller length divided by a smaller width (FESEM), which is what we see in Table 37.

4.3 Previous Regional NOA Studies (Nevada-Arizona)

A previous study (Buck et al., 2013) on the morphology of amphiboles formed in southern Nevada defined a fiber as “individual, narrow, usually very elongated crystals with straight, even edges” (Buck et al., 2013). They found that amphibole *fibers* had average widths of 1.2 μm and average lengths of 27.9 μm (Buck et al., 2013). Amphibole *particles*, which included any fibrous amphibole particle regardless of morphology, had average widths of 3.9 μm and average lengths of 18.1 μm (Buck et al., 2013). Of the samples measured, 69% of amphibole *particles* and 97% of amphibole *fibers* were less than 3 μm in diameter and thus, met the criteria to be respirable. They also found that 100% of all amphibole *fibers* and 97% of all *particles* had an aspect ratio greater than 3:1 (Buck et al., 2013). EPMA analyses were conducted on these samples and 85% were found to be actinolite which is one of the 6 regulated asbestos minerals (Figure 40). This is congruent to our study as a majority of particles plotted as calcic amphiboles and are considered to be actinolite. Furthermore, some of these EPMA analyses were collected directly from this study’s field area and confirm that actinolite was the most prevalent type of fibrous amphibole present.

In this study, similar to Buck et al. (2013), 96% of particles had a width $< 3 \mu\text{m}$ and by design, we only analyzed particles with an aspect ratio $\geq 3:1$ (Table 38). Furthermore, samples from our study were found to have an average particle width of $1.0 \pm 0.025 \mu\text{m}$, average length of $7.51 \pm 0.209 \mu\text{m}$, and average aspect ratio of 8.8 ± 0.23 (Table 12). Despite having slightly different definitions of a fiber, these results are comparable to those found in Buck et al. (2013). It should be noted that particles in this thesis tended to have smaller lengths and widths compared to those within this previous study. This result may be explained by Buck et al. (2013) method of manually separating fibers using a dental tool while we mechanically separate fibers using a motorized drill. This may have caused the fibrous amphibole to break along weakened planes, creating lower dimension averages. Another explanation would be that this study utilized the FESEM/ EDS where Buck et al. (2013) used the SEM/ EDS which has a lower resolution. The higher resolution of the FESEM allows us to see smaller, thinner particles that we wouldn't be able to measure on an SEM. The overall average length, average width, and mean aspect ratio of fibrous amphiboles from southern Nevada fit the OSHA and the WHO definitions for an asbestos fiber in both studies, suggesting a public health concern (Clinkenbeard et al., 2002; Mortureux, 2015).

A more recent report by Buck et al. (2018) conducted research on NOA in southern Nevada. This study split portions of southern Nevada into 11 different regions. Samples from each region were collected, analyzed using the SEM/EDS, and measured using SEM photomicrographs. Buck et al. (2018), defined fibers as particles with a width $\leq 1 \mu\text{m}$ with an aspect ratio $\geq 3:1$. Particles were classified as bundles if they had a width $> 1 \mu\text{m}$ and exhibited evidence of splitting. All other particles within Buck et al. (2018) were classified as prismatic crystals. These dimensional classifications for fibers, bundles, prismatic crystals were the same definitions used within this thesis. The mean dimensional analyses based on particle type for all particles in Buck et al. (2018) consisted of: *bundles* (width: $3.1 \pm 0.3 \mu\text{m}$, length: $27.1 \pm 1.9 \mu\text{m}$, and aspect ratio: 10 ± 0.3); *fibers* (width: $0.7 \pm 0.0 \mu\text{m}$, length: $6.7 \pm 0.1 \mu\text{m}$, and aspect ratio: 9.5 ± 0.2); and *prismatic crystals* (width: $1.9 \pm 0.1 \mu\text{m}$, length: $12.9 \pm 0.5 \mu\text{m}$, and aspect ratio: 7.2 ± 0.2). Comparing the data to these results, *bundles* in this thesis had thinner widths, shorter lengths, and greater aspect ratios (Table 13); *fibers* within this thesis had thinner widths and shorter lengths (Table 14); and *prismatic crystals*

within this thesis had thinner widths, shorter lengths, and smaller aspect ratios (Table 15) than those in Buck et al. (2018). All particles measured within the Buck et al. (2018) had an average width of 1.6 ± 0.1 μm , average length of 12.8 ± 0.4 μm , and average aspect ratio of 8.8 ± 0.1 (Buck et al., 2018). Similar to the particle type comparisons, all particles measured within this thesis had a decrease in average widths and lengths when contrasted to all particles within Buck et al. (2018). This may be attributed to our use of the FESEM, which has a higher resolution than the SEM and allows us to see and measure smaller, thinner particles, skewing the data in this direction. Another potential explanation for this is the work performed for this thesis mechanically separated fibers with a motorized drill, possibly causing fibers to break along weakened planes. Buck et al. (2018) separated fibers manually with a dental tool and may have caused less breakage as a result. These case studies in Nevada and Arizona increase the potential for fibrous amphibole asbestos of potentially toxic morphologies to be inhaled as these findings fit the criteria for an asbestos fiber according to the WHO and OSHA definitions.

4.4 Toxicity of Amphibole Particles

There are six physical characteristics of solids that influence toxicity depending on how the substance is absorbed and deposited within the body. These six characteristics are: (1) mineralogy (chemical composition and mineral structure), (2) size, (3) shape (morphology), (4) glass or crystalline, (5) density, and (6) surface charge (Plumlee et al., 2006). Specifically for asbestos, Aust et al. (2011) found that the most important parameters for toxicity are: (1) particle length, (2) width, (3) aspect ratio, (4) surface chemistry, (5) chemical composition, and (6) particle surface area within the lung (Aust et al., 2011, Dement, 1990; Dodson et al., 2003; Egilman et al., 2019; Plumlee et al., 2006). The toxicity of amphibole vs chrysotile asbestos is an important topic that can be misunderstood. Asbestos definitions and regulations do not differentiate between chrysotile and amphibole chemical composition of fibers, which is important as these minerals cause different auto-immune responses and health effects (Pfau et al., 2017, 2018; Plumlee et al., 2006). Amphibole fibers are much more toxic compared to chrysotile fibers (Plumlee et al., 2006).

This is because chrysotile is less biopersistent than amphibole asbestos and has a sheet-silicate structure. These sheets are rolled into fibers and once inhaled, macrophages within the lungs are able to unroll and dissolve many of these sheets with time (Plumlee et al., 2006). Chrysotile sheets are rolled such that the Mg-O octahedral layer is on the outside which causes the Mg to be easily leached in acidic solutions. Furthermore, chrysotile causes a suppression of an individual's immune system, which increases the likelihood for illness, including cancer (Pfau et al., 2014, 2017, 2018). Amphibole's multiple chain structure forms fibers that are much more difficult to be dissolved, causing amphiboles to be more biopersistent than chrysotile (Plumlee et al., 2006). Additionally, autoimmune reactions are known to occur from amphibole asbestos exposure, causing diseases such as lupus, rheumatoid arthritis, and scleroderma, in addition to other known asbestos diseases and cancers (Pfau et al., 2014, 2017, 2018). Fibrous amphibole particles, which included 100% of particles within this study, are known to be the most biopersistent forms of asbestos (Plumlee et al., 2006). According to NIOSH, any EMP with a width $< 3 \mu\text{m}$ are thoracic-sized and, thus, respirable. EMPs at or below this width is considered to be the most pathogenic (NIOSH, 2011). 100% of *fibers* (Table 14) and 96% of *particles* (Table 38) within this study met the criteria to be respirable by having a width $< 3 \mu\text{m}$. These biopersistent amphibole particles are likely to result in some level of harm as macrophages within the lungs are unable to effectively clear fibers with amphibole crystal structure (NIOSH, 2011). Furthermore, the greater the surface area of amphibole particles, of any shape and size, within the lung, the greater the bio-chemical reaction potential, thus increasing the potential for toxicity (Aust et al., 2011; Dodson et al., 2003).

The findings within this thesis fit parameters for toxicity described by Aust et al. (2011) and indicate that the naturally-occurring fibrous amphibole in Clark County, NV largely fit various definitions of asbestos dimensions, is one of the six regulated asbestos minerals (actinolite), and therefore, pose a potential health concern for those living in surrounding area. We consistently found that particles produced from recrystallization more commonly fit the criteria for regulatory asbestos dimensions and morphologies by having significantly longer lengths and greater aspect ratios compared to those produced from neocrystallization particles (Tables 12-37). Thus, recrystallized fibrous amphiboles have the potential to be

just as toxic, if not more toxic, than their neocrystallized counterparts. The above findings indicate that hornblende recrystallized into fibrous actinolite (and other fibrous amphiboles), by hydrothermal alteration, may also produce toxic morphologies.

4.4.1 Short Fiber Debate

The Stanton hypothesis (fibers $> 8 \mu\text{m}$ in length and ≤ 0.25 in diameter) suggests that the longer and thinner the fiber, the more toxic it may be (Stanton et al., 1981). Current regulations, definitions, and counting methods for asbestos particles have length cut-offs of $5 \mu\text{m}$ (29 CFR 1910.1001 subpart Z(b); WHO Regional Office, 2000). Aust et al. (2011) acknowledged this and concluded that particles fitting the Stanton hypothesis would produce a larger surface area within the lungs, but particles with lengths $< 5 \mu\text{m}$ *cannot* be excluded from those that are known to cause health effects. It was stated that more studies must be conducted to understand *all* sizes and shapes of Respirable Elongated Mineral Particles (REMP) from environmental exposures. REMPs have widths less than $3.5 \mu\text{m}$ in diameter and sizes of REMP impact clearance and translocation of particles reaching the lungs (Aust et al., 2011). Shorter particles are inhaled in greater numbers than longer particles. This causes shorter particles to accumulate in greater numbers within the lungs despite having faster clearance rates (Aust et al., 2011). Some evidence suggests that damage to lung tissue must arise soon after exposure and short particles that have high clearance capabilities may still cause damage (NIOSH, 2011). Thus, a greater number of shorter particles have the potential for greater overall bio-chemical reaction potential (Aust et al., 2011; Dodson et al., 2003) because of their larger surface area within the lung compared to longer fibers (Aust et al., 2011). As long as a large enough quantity of amphibole particles are inhaled, the overall surface area of these particles within the lungs will dictate toxicity (Aust et al., 2011; Dodson et al., 2003).

A similar study concluded that asbestos particles, regardless of length, produced a pathological response and caused cases of mesothelioma (Dodson et al., 2003). These authors recommend caution when excluding asbestos on the basis of length, as they still have the potential to contribute to asbestos related

diseases (Dodson et al., 2003). Dodson et al. (2003) also noted that the authors of the Stanton Hypothesis found relatively high correlations of the probability of pleural sarcoma for fibers $< 1.5 \mu\text{m}$ in diameter and lengths $> 4 \mu\text{m}$ in addition to the high probability found for longer, thinner particles (Dodson et al., 2003). A review of fiber size and toxicity conducted by Boulanger et al. (2014) had similar conclusions. They observed that many previous studies did not assess the toxicity of short asbestos fibers but rather, following current asbestos fiber dimension standards, assessed toxicity using a length cut-off of $5 \mu\text{m}$ (Boulanger et al., 2014; Dodson et al., 2003). This review led authors to the realization that the $5 \mu\text{m}$ length limit is not based on scientific evidence but rather is a limit put in place based on the reliability of the PCM, which decreases below this length (Boulanger et al., 2014). According to Boulanger et al. (2014), short asbestos fibers should not be ruled out when concerning toxicity. Therefore, the length of asbestos particles may not hold as much weight as others previously recognized and, because this, the total combined surface area of particles in the lung with respirable widths ($< 3 \mu\text{m}$), regardless of morphology, are much more important when predicting toxicity than individual lengths of respirable particles (Aust et al., 2011; Dodson et al., 2003; NIOSH, 2011).

The PCM is one of the cheapest methods for asbestos detection (Clinkenbeard et al., 2002). Despite this method not being able to detect particles present at higher resolutions, it has been adopted as the main method for asbestos detection because it is quite inexpensive compared to other microscopy methods that are able to detect at higher resolutions (TEM or FESEM) (Boulanger et al., 2014; Clinkenbeard et al., 2002; Dodson et al., 2003). The size restrictions for asbestos particles including requiring a length $> 5 \mu\text{m}$ and aspect ratio $> 3:1$ can be first traced back to early United Kingdom regulations (between 1957-1965) that were eventually adopted by the United States in 1972 (Holmes, 1965; NIOSH, 1972). According to Addingley (1966) and Langer et al. (1970), the length $> 5 \mu\text{m}$ was selected based on the usefulness and practicality of the PCM and was originally adopted from studies conducted by the Asbestos Research Council (ARC). The filter membranes used at the time to prepare samples for the PCM had a pore size of 0.45 microns and appeared to be “quite adequate for trapping fibers in the lengths range of 5-100 microns” (Holmes, 1965). The author of this paper, Stephen Holmes, was a scientist for Turner Brothers Asbestos (T

&N), one of top three asbestos firms responsible for about 60% of all UK asbestos production in the 1950s (Tweedale, 2000). In 1956, T & N reached out to other main asbestos factories in the region (British Belting and Cape Asbestos) calling for the need for collaborative research on asbestos and formed the Asbestos Research Council (Tweedale, 2000). Therefore, the ARC was founded in 1957 by the top UK asbestos industry leaders who accounted for nearly all UK production of asbestos (Tweedale, 2000).

Scientists, including Stephen Holmes, and physicians that published work for ARC were most all members of the leading asbestos firms (Tweedale, 2000). By the 1980's, the ARC had published 200 papers, of which only seven researched dust counting and control, only three researched epidemiology, and only two discussed the environmental impact of asbestos (Tweedale, 2000). Although the ARC was aware of the negative health effects associated with asbestos workers as early as 1930 (Merewether and Price, 1930), most all publications tended to steer clear of controversial epidemiology and toxicology research (Tweedale, 2000). Despite the ARC's range of authorship being low, their lack of research into epidemiology and toxicology, and their clear conflict of interest (Tweedale, 2000), the United Kingdom adopted the ARC's definition of a fiber as an index of exposure that was based on the ARC's PCM asbestos detection methods (Holmes, 1965).

The ARC's PCM method for asbestos detection used the definition of an asbestos fiber as a $L > 5 \mu\text{m}$ and $AR > 3:1$ (Holmes, 1965). As mentioned before, the length selection of the ARC fiber definition was based on the capabilities of the filter membrane and PCM detection. Furthermore, the aspect ratio definition resulted from "...the definition of a fiber being *arbitrarily* taken as a particle whose length was at least three times its diameter" (Holmes, 1965). We believe Holmes (1965), who conducted research on behalf of T&N and the ARC, was the first to mention such dimensions in published literature. The language used in Holmes (1965) made it seem that such dimensions were previously defined by the ARC sometime between its founding, in 1957, and its publication. Our literature review failed to return previously published literature that mentioned such dimensions before 1965. As far as we are aware, this is the earliest publication that mentions the reasonings behind the use for such dimensions, which were arbitrarily placed. The British definition became the standard for the United States regulation for asbestos length and aspect ratio after

NIOSH was founded in 1970 (NIOSH, 1972). Therefore, the fiber definitions the United States adopted, and is still using today, were created, and defined by the top three major asbestos producers in the late 1950s and early 1960's (Holmes, 1965; Tweedale, 2000) and were not based upon health implications. According to NIOSH (1972) this fiber definition was only meant to be in place until, "(1) more definitive information on the biologic response of asbestos including the agent (s) and dose-response data on different lengths of fiber is available, (2) the spectrum of fiber lengths encountered in industry by types of asbestos and operations is ascertained, and (3) more precise epidemiologic data are developed" (NIOSH, 1972). Now that more information on the pathogenicity of short fibers has become available (examples present in Aust et al., 2011; Boulanger et al., 2014; Dodson et al., 2003; Langer et al., 1978), NIOSH must re-evaluate their fiber definition, used as an index-of-exposure, for asbestos criteria standards since 1972 to include particles of shorter dimensions.

According to Boulanger et al. (2014), the fiber dimension regulations the USA adopted, affected the sizes of asbestos particles reported in publications that caused pathogenic effects. Such studies often used a length cut-off of 5 μm causing short fiber pathogenic effects to not be recorded (Boulanger et al., 2014). Because the length and aspect ratio regulations are based on microscopy limitations and have no health implications (Boulanger et al., 2014; Dodson et al., 2003; Holmes, 1965; Langer et al., 1978; Lynch, 1970), this definition should not have been used in studies evaluating the dimensions of fibers that may have a biological response within the human body. There is no evidence that can definitively confirm that short fibers, less than 5 microns in length, do not cause negative health outcomes. Several studies show that small fibers make up a large portion of the fiber burden in human lung tissue and are very likely implicated in human disease (Aust et al., 2011, Boulanger et al., 2014, Dodson et al., 2003; Langer et al., 1971, 1973, 1978; Miller et al., 1975; Pooley et al., 1970). Other previous research likely lacks the accounts of short fibers causing a biological response as they were often excluded or ignored in data collection because of the existence of our current, out-of-date regulation (Boulanger et al., 2014; Dodson et al., 2003; Holmes, 1965) and the cost of obtaining data using TEM or SEM methods. The above history and supported literature of the asbestos fiber definition should therefore be revaluated based on health risk.

4.4.2 Cleavage Fragment Debate

There is great debate over whether fibrous amphibole cleavage fragments and short amphibole fibers pose a potential health hazard and if they should be included within the regulatory language for asbestos (Harper et al., 2008, Harper et al., 2012; NIOSH, 1990). Cleavage fragments occur when a mechanical or erosive force causes a mineral to break, or split, along a definite crystalline plane. The asbestos industry and OSHA currently do not define amphibole cleavage fragments as asbestos and do not consider such fragments toxic (29 CFR 1910.1001). However, Meeker et al, 2006 and Buck et al., 2013 point out that one cannot distinguish between prismatic crystals and cleavage fragments when measuring airborne asbestos concentrations because one cannot tell if a crystal grew (prismatic crystal) or was broken (cleavage fragment) since the crystalline planes are the same. Others argue that any particle that cannot be identified as a bundle or a fiber according to the commercial definitions of asbestos, should be referred to as cleavage fragments (Gunter et al., 2007, Harper et al., 2012). They use characteristics common to chrysotile (mean aspect ratio greater than 20:1, high flexibility, high tensile strength) and argue that amphibole cleavage fragments do not have an ‘asbestiform’ habit. Therefore, the asbestos and rock/ mineral industry believes cleavage fragments should not be included within the regulatory policy for asbestos fibers (Gunter et al., 2007, Harper et al., 2012, Lowers and Meeker, 2002). These definitions were designed with commercially-modified *chrysotile* in mind, which does not experience cleavage, thus it is argued that such definitions are not appropriate for fibrous amphibole asbestos.

Recent findings by the French agency for food, environmental and occupation health & safety (ANSES) suggest cleavage fragments may be toxic (Mortureux, 2015). According to their study, there is no authenticated scientific toxicological data that confirms cleavage fragments, with the dimensional criteria of an inhalable EMP presented by the WHO ($L > 5 \mu\text{m}$; $D < 3 \mu\text{m}$ and $L:D > 3:1$), do not pose a health hazard (Mortureux, 2015). The study concluded that cleavage fragments from non-asbestiform amphiboles should not be distinguished from asbestiform particles when regarding health effects because these fibers

are meeting the WHO dimensional requirements ($L > 5 \mu\text{m}$; $D < 3 \mu\text{m}$ and $L:D > 3:1$) for fibers capable of being inhaled (Mortureux, 2015). This study also implied that ‘asbestiform’ and ‘non-asbestiform’ particles occur on a spectrum making such divisions unreliable. Therefore, current regulations regarding asbestos fiber toxicity should encompass cleavage fragments until data suggest otherwise.

Some studies have claimed the ability to identify asbestos cleavage fragments via microscope (Gunter et al., 2007, Harper et al., 2008, 2012). To date, there is no microscopy instrumentation that can definitively classify an asbestos particle as a cleavage fragment. Morphology classification using microscopy is inconsistently problematic, meaning there is a visual bias between users. For instance, what one person may classify as a prismatic crystal, someone else may classify as a fiber. There is no defined universal method for visually identifying morphology of asbestos particles from photomicrographs. The definitions for an asbestos fiber by the WHO and the OSHA are focused on dimensional characteristics (width, length, and AR). These dimensional characteristics are applied when defining the visual particle type of a particle (fiber, bundle, or prismatic crystal). As mentioned earlier, there are hundreds of definitions for a fiber, bundle, and prismatic crystal based on dimensional characteristics (Lowers and Meeker, 2002). It can be near impossible to understand the significance of findings within papers that do not define what definitions are being used because of these inconsistently problematic definitions. Additionally, there is no way to tell if the particle under the microscope broke into these morphologies or grew this way. It is because of these issues stated above that we did not attempt to identify any particles as cleavage fragments within this study. The only way to tell if a particle is a cleavage fragment and not a crystal is if you broke it yourself because cleavage breaks along crystal planes.

Short fibers cannot be excluded from causing negative health outcomes (Aust et al., 2011; Boulanger et al., 2014; Dodson et al., 2003;) and cleavage fragments can fit both short fiber dimensions and fiber dimensions outlined by WHO (Mortureux, 2015) and OSHA. Therefore, we cannot conclude that cleavage fragments are not toxic. Cleavage fragments are merely broken amphibole particles along definite crystalline planes, so they still have the potential to fit the OSHA, the WHO, short asbestos fiber ($L < 5 \mu\text{m}$, $W < 3 \mu\text{m}$, $AR > 3:1$), and other varying definitions of asbestos. Furthermore, if a cleavage fragment

has amphibole surface chemistry/ chemical composition and is a REMP it has the potential to be toxic according to Aust et al. (2011). Because of this, cleavage fragments have the potential to increase the surface area of amphibole particles within the lung and thus increase the potential for a biological response (Aust et al., 2011). It should be noted that longer, thinner fibers are known to be more toxic than shorter fibers because of their increased surface area and shape (Aust et al., 2011; NIOSH, 2011). Moreover, NIOSH (2011) agrees with ANSES and Aust et al. (2011) in that asbestos cleavage fragments cannot be excluded from our current definitions of asbestos. According to NIOSH (2011), the NIOSH recommended exposure limit (REL) for asbestos was revised in 1990 to include ‘nonasbestiform’ particles and cleavage fragments. This revision was in result of epidemiological studies of worker populations that were exposed to ‘nonasbestiform’ particles, including cleavage fragments, in which evidence suggested a risk of lung cancer (NIOSH, 2011). Despite NIOSH concerns, the OSHA does not currently include cleavage fragments, as asbestos or toxic, including even those that fit within the dimensions of the OSHA’s definition of an asbestos fiber (29 CFR 1910.1001) (NIOSH, 2011).

As discussed in Davis et al. (1991) and cited in Dodson et al. (2003), all tremolite samples that were injected into rats, regardless of their morphology and length, had some potential to produce mesothelioma. This included samples with particles that had thicker fiber widths, were “morphologically consistent with cleavage fragments,” and those with few “asbestiform fibers” present (Davis et al., 1991; Dodson et al., 2003). The latter, producing tumors in 70% of rats, combined with the risk potential of mesothelioma (Davis et al., 1991; Dodson et al., 2003) suggests that regardless of fiber length, morphology, and/or the presence of cleavage fragments and “non-asbestiform” particles, negative health outcomes are still possible. Therefore, non-regulated fibers, including cleavage fragments, may pose health risks (Davis et al., 1991; Dodson et al., 2003). The French agency for food, environmental and occupation health & safety (ANSES) agreed with this statement and concluded that particles that currently fall outside of the U.S. OSHA asbestos regulations (i.e. short fibers with $L < 5\mu\text{m}$, $W < 3\mu\text{m}$, and $AR > 3:1$ and cleavage fragments that fit the WHO definition for an asbestos fiber ($L > 5$, $W < 3$ and $AR > 3:1$)) can produce

asbestos morphologies (Mortureux, 2015). Therefore, many particles that fall outside of U.S. regulations are toxic and pose a potential health hazard.

4.4.3 Toxicological Study of Arizona NaFe^{3+} fibrous Amphiboles

A previous study by Pfau et al. (2017) inserted NaFe^{3+} amphibole fibers collected from the Wilson Ridge pluton in northwestern Arizona and Libby, Montana into mice to compare what health effects, if any, occurred. The health disaster that occurred in Libby, Montana that negatively affected thousands of people from chronic exposure of winchite and tremolite asbestos is well known (Beaven, 2014; Harper et al., 2008; Meeker et al., 2006; Pfau et al., 2012 and 2014). The amphibole asbestos was an associated mineral within vermiculite that was mined outside of Libby for decades and used in gardens, playground, and buildings throughout the community (Pfau et al., 2017). Chronic exposure to the Libby amphibole resulted in fibrosis, pleural plaques, cancer, autoimmune diseases, and other various health effects (Pfau et al., 2014).

According to Pfau et al. (2017), the Libby and Arizona mineralogy were similar and was mainly composed of winchite (70% Libby and 69% Arizona). The similarity in mineralogy allowed Pfau et al. (2017) to compare health effects of mice by inserting a fibrous amphibole sample from Libby, Montana (mean aspect ratio 8.4 ± 0.7) and northwestern Arizona (mean aspect ratio 16.7 ± 0.9) into mice (Pfau et al., 2017). A very low $3 \mu\text{g}$ dose of each sample was injected into each mouse. This was the lowest dose yet studied and was chosen to simulate an environmental exposure to NOA (Pfau et al., 2017). After 7 months, mice that were exposed to either sample were found to have chronic immune dysfunction, lung fibrosis, and pleural fibrosis (Pfau et al., 2017). Pfau et al. (2017) concluded autoimmune disorders and pulmonary disease is an associated risk for environmental exposures to NOA.

The morphology of the Arizona amphibole fibers had an average length of $9.0 \pm 0.7 \mu\text{m}$, average width of $0.7 \pm 0.1 \mu\text{m}$, and average aspect ratio of $18.2 \pm 1.1 \mu\text{m}$ (Pfau et al., 2017). This differs from this thesis as samples from our study were found to have an average particle width of $1.0 \pm 0.025 \mu\text{m}$, average length of $7.51 \pm 0.209 \mu\text{m}$, and average aspect ratio of 8.8 ± 0.23 (Table 12). The northwestern Arizona

samples were mainly composed of winchite where samples evaluated for this thesis were mainly composed of actinolite. Furthermore, 56% of particles were assigned as having an actinolite composition and 4% as winchite (Table 8). It should be noted that these percentages are a result of particle mineralogy of *all* individual particles within this thesis collected from multiple rock samples, not the composition of a single, “bulk” sample prepared using a dental tool to separate fibers from a rock for the injection into mice. Both this thesis and Buck et al. (2018), found that sodic and sodic-calcic amphiboles tend to be thinner and have greater aspect ratios compared to calcic amphiboles (Table 10). Therefore, it is likely that mineralogy affects dimensions of fibrous amphibole which may be why the northwestern Arizona samples have dimensions that are much larger than the samples measured within this thesis. Despite differing mineralogy, the mean aspect ratio from this thesis (8.8 ± 0.23) is similar to the Libby sample’s mean aspect ratio that was injected into mice (8.4 ± 0.7 (Pfau et al., 2017)). Additionally, similar geologic processes that produced the Arizona fibrous amphibole produced the fibrous amphibole within our field area.

Libby asbestos is a known toxin and the only known reference concentration for asbestos available for noncancerous outcomes was created from fibrous amphibole asbestos in Libby, Montana. This reference concentration (RfC) is 0.00009 fibers per cubic centimeter and has been exceeded in areas known to have NOA (U.S. EPA, 2014). This RfC was created for Libby amphibole and may translate to other types of amphibole asbestos (Pfau et al., 2014 and 2017). The similar aspect ratios between the Libby sample that was injected into mice and the samples evaluated in this thesis, may indicate that the negative health outcome findings from Pfau et al. (2017) apply to southern Nevada. Therefore, it is possible that many people in southern Nevada are being unknowingly exposed to fibrous amphibole that have the potential to cause negative health outcomes.

4.4.4 Short Fibers and Cleavage Fragments in Las Vegas

Particles within this study mainly included short fibers, with 66% having a length $\leq 5 \mu\text{m}$ (Table 38), and were identified as bundles, fibers, and prismatic crystals (likely including cleavage fragments) based

on their particle type. Despite this, bundles and prismatic crystals identified also fit the dimensions for the OSHA and the WHO's definition for an asbestos fiber. Therefore, nomenclature and identification of fibers, bundles, and prismatic crystals are also inconsistently problematic within literature. To add complexity to these problematic issues, the OSHA and the WHO definitions for what is considered an asbestos fiber are insufficient when concerning health. This is because they are only counting particles with lengths $\geq 5 \mu\text{m}$ as asbestos as they are using the more cost-effective method of the PLM which cannot see fibers $< 5 \mu\text{m}$. There have been multiple studies and reviews that state that short asbestos fibers ($< 5 \mu\text{m}$) and cleavage fragments have the potential to cause asbestos related diseases and should be more effectively regulated (Aust et al., 2011; Boulanger et al., 2014, Dodson et al., 2003; Mortureux, 2015; NIOSH, 2011). These short asbestos particles whether identified as bundles, prismatic crystals, cleavage fragments, or fibers, are REMF, thus depositing within the respiratory tract, and therefore have the potential to be toxic (Aust et al., 2011; Boulanger et al., 2014, Dodson et al., 2003; NIOSH, 2011). Furthermore, we would argue that definitions of a 'fiber,' 'bundle,' and 'prismatic crystal' should also be designed only with health in mind. Many argue that bundles and prismatic crystals are not as toxic as fibers because of their fatter widths (Gunter et al., 2008). If dimensions of prismatic crystals, bundles, and cleavage fragments fit within a dimensional health parameter for an asbestos 'fiber' (according to OSHA), they should also be considered toxic despite their visual shape. Additionally, after being deposited in the lung, bundles are able to split longitudinally, producing an increased number of thinner fibers with an increased aspect ratio as a result (NIOSH, 2011). As long as a particle has a width less than $3 \mu\text{m}$ it is respirable according to NIOSH and poses a health concern because particles with amphibole chemistry are known to be biopersistent (Plumlee et al., 2006; NIOSH, 2011). Current definitions, such as the WHO and the OSHA definition of an asbestos fiber, should therefore be modified to read, "...definition of an asbestos particle," as any particle that fits dimensional criteria for asbestos (length, width, AR) and has an amphibole or serpentine chemical composition are toxic (Aust et al., 2011). Therefore, a specific morphologic, dimensional guideline for what is considered an asbestos particle, regardless of particle type, based solely on health, must be used, and established as the main definition of an asbestos particle. Many would disagree with this statement as

industry still uses such terms to describe the habit of their commercial asbestos (Gunter et al., 2007; Lowers and Meeker, 2002). To solve this issue, using the term “commercially-modified asbestos” would help classify the particle morphology of which one is speaking. Furthermore, the mining and use of asbestos throughout the world is declining and will likely continue to decline because of its toxicity (Allen et al., 2018). This would support my claim that definitions of an asbestos particle, designed with health in mind, should dominate the ‘official’ language for asbestos definitions and nomenclature.

4.5 Chain-Width Defects

The original hypothesis in this study proposed that the length, width, and aspect ratios of neocrystallized and recrystallized fibrous amphibole, of similar chemistries, would have similar dimensions and morphologies. After conducting \log_{10} transformations on this dataset, a Mann-Whitney U-test was calculated. As mentioned above, in nearly all cases, we found recrystallized particles had statistically similar widths, significantly longer lengths, and significantly greater aspect ratios than neocrystallized fibrous amphibole. This finding was unexpected and has potentially dangerous implications. The fibrous amphibole within this study formed from hydrothermal alteration of magmatic hornblende into fibrous actinolite within granitic rock. This implies that hornblende residing within granite, that has been hydrothermally altered, has the potential for asbestos morphologies of hazardous lengths, widths, and aspect ratios. This finding has increased the scope of potential NOA sites around the world.

A potential hypothesis to explain this discrepancy is that chain width defects, within highly altered amphibole, created asbestos of fibrous morphologies. According to Veblen et al. (1977) and Ahn and Buseck (1991), recrystallisation of hornblende can create highly altered biopyriboles that will result in the creation of defects within the chains of amphibole. This was proven to cause fibrous amphibole crystals to be disaggregated into smaller subgrains and broken into finer fibers through structural defects (Ahn and Buseck, 1991). TEM results in multiple studies have verified that the combination of elongated amphibole fibers splitting along the C-axis, planar defects tending to occur along (110) and (100) causing

misorientation, and an increasing of chains, and errors within these chains, will all contribute to the development of bundles and fibers, which will increase the fibrosity of amphibole (Ahn and Buseck, 1991, Veblen et al., 1977). Not only will amphiboles break along their original cleavage planes, but they will also break along chains of uncharacteristic widths. Breakage along the latter plane is the cause of the fibrosity within amphiboles (Veblen et al., 1997). We believe that the recrystallization of magmatic hornblende into fibrous actinolite created such an environment where chain width defects flourished allowing for breakage along chains of anomalous width. This would then create a fibrous amphibole that is highly altered compared to that of neocrystallized amphibole, which occurred from the primary crystallization of actinolite within empty veins. The latter is less altered causing a decrease in chain width defects and thus fibrosity. This process would potentially explain why we found the morphologies of recrystallized fibrous amphibole to be significantly different than that of neocrystallized amphibole within this study. Future research must be done by studying defects within the chains of these amphiboles using TEM analyses to confirm this hypothesis.

4.6 Worldly Implications

Recrystallized asbestos is produced when hydrothermal fluids, containing amphibole building ions in solution, interact with magmatic hornblende causing the precipitation of fibrous amphibole to occur through replacement (Austin, 2019; Metcalf et al., 2018). Deposits that underwent such reactions have the potential to contain recrystallized fibrous amphibole. We are now aware that many people in southern Nevada, and elsewhere, are potentially being unknowingly exposed to hazardous amphibole fibers that were previously unrecognized. Amphibole is a commonly-associated mineral in felsic rocks and hydrothermal alteration is a common process. Therefore, we conclude, that the potential for individuals to be exposed through industrial/ commercial asbestos as well as naturally-occurring asbestos (NOA) is greater than originally thought (Figure 1). It is commonly believed that asbestos can only form in fracture-fill veins and not as recrystallized fibrous amphibole (Bailey et al., 2004; Tabler, 1916; Van Gosen 2007; Virta, 2002).

The research conducted in this thesis concluded that recrystallization has the ability to produce amphibole of asbestos dimensions and morphologies. Therefore, the life cycle of asbestos minerals (Figure 1) includes the risk of inhalation from the release of both primarily crystallized (neocrystallized) and recrystallized amphibole. As such, there is an increased risk of exposure to those living in southern Nevada and other locations where hydrothermal alteration of amphiboles occurred.

In 2019 alone, roughly 2.7 million tons of dimension stone were sold and used in the U.S. for construction of buildings, furniture, monuments, and decorative objects (U.S.G.S., 2020). Within the U.S., dimension stone is mined by 197 companies operating in 251 quarries in 34 states, 18% of this being granite (U.S.G.S., 2020). Moreover, 1.53 billion tons of crushed stone, of which 6% is granite, was produced and sold by 1,430 companies operating in 3,440 quarries within all 50 states (U.S.G.S., 2020). Workers within these quarries, and their families, therefore, have the potential for primary and secondary exposure to asbestos fibers if hydrothermal alteration of hornblende is present within the granite (Figure 1). Information regarding quarries that are mining rocks with hydrothermally altered amphibole must be compiled. Furthermore, it would be useful for hydrothermally altered granite to be identified and mapped on a U.S. and global basis. A future thesis project could estimate the percentages of hydrothermally altered granite in the United States by creating a risk assessment map of quarries and other NOA deposits using GIS. Utilizing GIS would allow for a future student to estimate potential populations being exposed. This work could also stimulate new studies to determine or verify if these potentially hazardous areas do contain fibrous amphiboles.

Chapter 5: Conclusion

5.1 Recrystallization Produces Asbestos Morphologies

This project tested the null hypothesis that recrystallized and neocrystallized fibrous amphibole particles, of similar chemistry, would have similar dimensions and morphologies. As recrystallization was previously recognized as a process that did not constitute the formation of asbestos (Bailey et al., 2004; Tabler, 1916; Van Gosen 2007; Virta, 2002), we expected neocrystallization to produce particles of asbestos morphologies more often than recrystallization. Multiple statistical analyses, explicitly the Mann-Whitney U-test, confirmed that recrystallized particles more commonly had statistically similar or significantly wider widths, significantly longer lengths, and significantly greater aspect ratios (Tables 4-7, 8-37) compared to neocrystallized particles. The ample evidence and supporting literature provided demonstrates that recrystallization of amphibole, from a hydrothermal fluid, can produce fibrous asbestos morphologies and dimensions that fit regulatory criteria for an asbestos fiber by OSHA, more often than neocrystallization. We hypothesize that the recrystallization of magmatic hornblende into fibrous actinolite allowed for chain width defects to flourish, increasing the fibrosity of the recrystallized particles and explaining our statistical analyses and results. Because width, length, aspect ratio and surface area are all important controls for toxicity (Aust et al., 2010), the results of this study suggest that fibrous amphibole formed through recrystallization may be as toxic or more toxic than fibrous amphiboles formed through neocrystallization. As hornblende is a common mineral within the earth's crust and recrystallization and hydrothermal alteration are common processes, we believe many more people are being exposed to potentially hazardous morphologies of naturally-occurring amphibole asbestos than previously recognized (Figure 1).

Appendix A: Tables

Table 1. Mineral Names and Formulas of Regulated and Non-Regulated Asbestos. Modified from Perry (2004).

Commerical Name	Mineral Name	Mineral Group	Regulated?	Chemical Formula
Chrysotile	Chrysotile	Serpentine	Yes	$(\text{Mg, Fe})_6(\text{OH})_8\text{Si}_4\text{O}_{10}$
Anthophyllite	Anthophyllite	Amphibole	Yes	$(\text{Mg, Fe})_2(\text{OH})_2\text{Si}_8\text{O}_{22}$
Amosite	Grunerite	Amphibole	Yes	$\text{Fe}^{2+}_7\text{Si}_8\text{O}_{22}(\text{OH})_2$
Amosite	Commingtonite	Amphibole	Yes	$\text{Mg}_7\text{Si}_8\text{O}_{22}(\text{OH})_2$
Gedrite	Gedrite	Amphibole	No	$\text{Mg}_5\text{Al}_2\text{Si}_6\text{Al}_2\text{O}_{22}(\text{OH})_2$
Actinolite	Actinolite	Calcic Amphibole	Yes	$\text{Ca}_2\text{Fe}_5(\text{OH})_2\text{Si}_8\text{O}_{22}(\pm\text{Mg})$
Tremolite	Tremolite	Calcic Amphibole	Yes	$\text{Ca}_2\text{Mg}_5(\text{OH})_2\text{Si}_8\text{O}_{22}(\text{Fe})$
edenite	edenite	Calcic Amphibole	No	$\text{NaCa}_2\text{Mg}_5\text{Si}_7\text{AlO}_{22}(\text{OH})_2$
Magnesiohornblende	Magnesiohornblende	Calcic Amphibole	No	$\text{Ca}_2(\text{Mg}_4(\text{Al, Fe}^{3+})\text{Si}_7\text{AlO}_{22}(\text{OH})_2$
Magnesio-arfvedsonite	Magnesio-arfvedsonite	Sodic Amphibole	No	$\text{NaNa}_2(\text{Mg}_4\text{Fe}^{3+})\text{Si}_8\text{O}_{22}(\text{OH})_2$
magnesioriebeckite	magnesioriebeckite	Sodic Amphibole	No	$\text{Na}_2(\text{Mg}_3\text{Fe}^{3+}_2)\text{Si}_8\text{O}_{22}(\text{OH})_2$
Crocidolite	Riebeckite	Sodic Amphibole	Yes	$\text{Na}_2(\text{Fe}^{3+})_2(\text{Fe}^{2+})_3(\text{OH})_2\text{Si}_8\text{O}_{22}(\pm\text{Mg})$
Richterite	Richterite	Sodic-Calcic Amphibole	No	$\text{Na}(\text{Ca, Na})\text{Mg}_5\text{Si}_8\text{O}_{22}(\text{OH})_2$
Winchite	Winchite	Sodic-Calcic Amphibole	No	$(\text{Ca, Na})\text{Mg}_4(\text{Al, Fe}^{3+})\text{Si}_8\text{O}_{22}(\text{OH})_2$

Table 2. Tests of Normality for Particles with an AR \geq 3:1 by Crystallization Process *

	Crystallization Process	Kolmogorov-Smirnov ^a			Shapiro-Wilk		Sig.
		Statistic	df	Sig.	Statistic	df	
Width (μm)	Neocrystallization	.195	698	<.001	.677	698	< .001
	Recrystallization	.177	827	<.001	.702	827	< .001
Length (μm)	Neocrystallization	.182	698	<.001	.714	698	< .001
	Recrystallization	.204	827	<.001	.644	827	< .001
Aspect Ratio	Neocrystallization	.206	698	<.001	.704	698	< .001
	Recrystallization	.258	827	<.001	.585	827	< .001

*The null hypothesis for this test of normality is the data are normally distributed. The null hypothesis is rejected if the Sig. value is below 0.05. Therefore, the data are not normally distributed and a Student's t-Test or a 2-way ANOVA parametric analyses cannot be used.

Table 3. Tests of Normality for Log₁₀ (Particles) with an AR ≥ 3:1

	Crystallization Process	Kolmogorov-Smirnov ^a			Shapiro-Wilk		Sig.
		Statistic	df	Sig.	Statistic	df	
Log ₁₀ (Width (μm))	Neocrystallization	.046	698	.001	.996	698	.076
	Recrystallization	.036	827	.013	.996	827	.038
Log ₁₀ (Length (μm))	Neocrystallization	.047	698	.001	.993	698	.001
	Recrystallization	.048	827	.000	.993	827	.001
Log ₁₀ (Aspect Ratio)	Neocrystallization	.090	698	.000	.938	698	.000
	Recrystallization	.093	827	.000	.928	827	.000

Table 4(a). Ranks for Log₁₀ (All Particles) with an AR ≥ 3:1 Across Crystallization Process and (b) Test Statistics for Log₁₀ (All Particles) with an AR ≥ 3:1 Across Crystallization Process

Table 4(a). Ranks for Log₁₀ (All Particles) with an AR ≥ 3:1 Across Crystallization Process*

	Crystallization Process	N	Mean Rank	Sum of Ranks
Log ₁₀ (Width (μm))	Neocrystallization	698	717.12	500550.50
	Recrystallization	827	801.72	663024.50
	Total	1525		
Log ₁₀ (Length (μm))	Neocrystallization	698	655.53	457563.00
	Recrystallization	827	853.70	706012.00
	Total	1525		
Log ₁₀ (Aspect Ratio)	Neocrystallization	698	694.98	485096.00
	Recrystallization	827	820.41	678479.00
	Total	1525		

Table 4(b). Test Statistics for Log₁₀ (All Particles) with an AR ≥ 3:1 Across Crystallization Process*

	Log ₁₀ (Width (μm))	Log ₁₀ (Length (μm))	Log ₁₀ (Aspect Ratio)
Mann-Whitney U	256599.500	213612.000	241145.000
Wilcoxon W	500550.500	457563.000	485096.000
Z	-3.738	-8.755	-5.542
Asymp. Sig. (2-tailed)*	.000	.000	.000

*The mean ranks for recrystallized particles are higher than neocrystallized for all cases. Asymp. Sig. < 0.05, so we reject the null hypothesis that mean width, length, and aspect ratio are the same between neocrystallized and recrystallized particles.

Table 5(a). Ranks for Log₁₀(Particles) with an AR ≥ 3:1 Across the Category of Microscopy Method and (b) Test Statistics for Log₁₀(Particles) with an AR ≥ 3:1 Across the Category of Microscopy Method.

Table 5(a). Ranks for Log₁₀(Particles) with an AR ≥ 3:1 Across the Category of Microscopy Method*

	Microscopy Method	N	Mean Rank	Sum of Ranks
Log ₁₀ (Width (μm))	SEM	588	954.29	561121.50
	FESEM	937	642.96	602453.50
	Total	1525		
Log ₁₀ (Length (μm))	SEM	588	913.00	536846.50
	FESEM	937	668.87	626728.50
	Total	1525		
Log ₁₀ (Aspect Ratio)	SEM	588	740.25	435266.00
	FESEM	937	777.28	728309.00
	Total	1525		

Table 5(b). Test Statistics for Log₁₀(Particles) with an AR ≥ 3:1 Across the Category of Microscopy Method*

	Log ₁₀ (Width (μm))	Log ₁₀ (Length (μm))	Log ₁₀ (Aspect Ratio)
Mann-Whitney U	163000.500	187275.500	262100.000
Wilcoxon W	602453.500	626728.500	435266.000
Z	-13.439	-10.537	-1.598
Asymp. Sig. (2-tailed)*	.000	.000	.110

*The mean ranks for recrystallized particles are higher than neocrystallized for all length and width. Asymp. Sig. < 0.05 for mean width and length but not AR. We reject the null hypothesis that mean width and length are similar between neocrystallized and recrystallized particles, but not AR.

Table 6(a). Ranks for Log₁₀ (SEM Particles) with an AR ≥ 3:1 Across the Category of Crystallization Process and (b) Test Statistics for Log₁₀ (SEM Particles) with an AR ≥ 3:1 Across the Category of Crystallization Process.

Table 6(a). Ranks for Log₁₀ (SEM Particles) with an AR ≥ 3:1 Across the Category of Crystallization Process*

	Crystallization Process	N	Mean Rank	Sum of Ranks
Log ₁₀ (Width (μm))	Neocrystallization	344	253.66	87260.50
	Recrystallization	244	352.07	85905.50
	Total	588		
Log ₁₀ (Length (μm))	Neocrystallization	344	235.25	80925.00
	Recrystallization	244	378.04	92241.00
	Total	588		
Log ₁₀ (Aspect Ratio)	Neocrystallization	344	263.28	90568.00
	Recrystallization	244	338.52	82598.00
	Total	588		

Table 6(b). Test Statistics for Log₁₀ (SEM Particles) with an AR ≥ 3:1 Across the Category of Crystallization Process*

	Log ₁₀ (Width (μm))	Log ₁₀ (Length (μm))	Log ₁₀ (Aspect Ratio)
Mann-Whitney U	27920.500	21585.000	31228.000
Wilcoxon W	87260.500	80925.000	90568.000
Z	-6.923	-10.042	-5.292
Asymp. Sig. (2-tailed)*	.000	.000	.000

*The mean ranks for recrystallized particles are higher than neocrystallized for all cases. Asymp. Sig. < 0.05, so we reject the null hypothesis that mean width, length, and aspect ratio are the same between neocrystallized and recrystallized particles.

Table 7(a). Ranks for Log₁₀ (FESEM Particles) with an AR ≥ 3:1 Across Crystallization Process and (b) Test Statistics for Log₁₀ (FESEM Particles) with an AR ≥ 3:1 Across Crystallization Process.

Table 7(a). Ranks for Log₁₀ (FESEM Particles) with an AR ≥ 3:1 Across the Category of Crystallization Process*

	Crystallization Process	N	Mean Rank	Sum of Ranks
Log ₁₀ (Width (μm))	Neocrystallization	354	422.31	149498.50
	Recrystallization	583	497.35	289954.50
	Total	937		
Log ₁₀ (Length (μm))	Neocrystallization	354	389.47	137871.00
	Recrystallization	583	517.29	301582.00
	Total	937		
Log ₁₀ (Aspect Ratio)	Neocrystallization	354	440.03	155770.50
	Recrystallization	583	486.59	283682.50
	Total	937		

Table 7(b). Test Statistics^a for Log₁₀ (FESEM Particles) with an AR ≥ 3:1 Across the Category of Crystallization Process*

	Log ₁₀ (Width (μm))	Log ₁₀ (Length (μm))	Log ₁₀ (Aspect Ratio)
Mann-Whitney U	86663.500	75036.000	92935.500
Wilcoxon W	149498.500	137871.000	155770.500
Z	-4.115	-7.010	-2.554
Asymp. Sig. (2-tailed)	.000	.000	.011

*The mean ranks for recrystallized particles are higher than neocrystallized for all cases. Asymp. Sig. < 0.05, so we reject the null hypothesis that mean width, length, and aspect ratio are the same between neocrystallized and recrystallized particles.

Table 8. Assigned Mineral Name for All Particles with an AR \geq 3:1.

Assigned Mineral Name	n	% Composition	Mean Width (μm)	Mean Length (μm)	Mean Aspect Ratio
Actinolite	856	56.13%	1.2 \pm 0.034	7.86 \pm 0.266	7.6 \pm 0.26
Anthophyllite	2	0.13%	0.28 \pm 0.12	1.79 \pm 0.216	9.8 \pm 3.7
Edenite	4	0.26%	3.3 \pm 2.5	32.1 \pm 26.0	6.1 \pm 1.3
Mg-hbl	94	6.16%	0.80 \pm 0.051	7.78 \pm 0.934	10. \pm 1.0
Riebeckite	2	0.13%	0.41 \pm 0.0070	6.62 \pm 3.53	16. \pm 8.5
Unassigned	501	32.85%	0.87 \pm 0.038	7.08 \pm 0.326	10. \pm 0.45
Winchite	66	4.33%	0.62 \pm 0.072	4.38 \pm 0.412	10. \pm 1.4
All Particles	1525	100.00%	1.0 \pm 0.025	7.51 \pm 0.209	8.8 \pm 0.23

Table 9. Assigned Mineral Name by Crystallization Process Particles with an AR \geq 3:1.

Crystallization Process	Assigned Mineral Name	n	% Composition	Mean Width (μm)	Mean Length (μm)	Mean Aspect Ratio
Neocrystallized Particles	Actinolite	474	67.9%	1.1 \pm 0.042	6.19 \pm 0.242	6.7 \pm 0.23
	Anthophyllite	2	0.3%	0.28 \pm 0.12	1.79 \pm 0.216	9.8 \pm 3.7
	Edenite ⁺	2	0.3%	0.29 \pm 0.042	1.49 \pm 0.545	4.8 \pm 1.2
	Mg-hblld	36	5.2%	0.63 \pm 0.062	5.05 \pm 0.486	8.6 \pm 0.67 ⁺
	Riebeckite	0	0.0%	-	-	-
	Unassigned	149	21.3%	0.70 \pm 0.058	4.86 \pm 0.401	7.8 \pm 0.40
	Winchite ⁺	35	5.0%	0.62 \pm 0.075	3.82 \pm 0.430	7.6 \pm 0.82
	All Particles	698	100.00%	0.94 \pm 0.032	5.70 \pm 0.191	7.1 \pm 0.19
Recrystallized Particles	Actinolite [*]	382	46.2%	1.4 \pm 0.056	9.94 \pm 0.495	8.8 \pm 0.50
	Anthophyllite	0	0.0%	-	-	-
	Edenite ⁺	2	0.2%	6.3 \pm 3.9	62.6 \pm 42.0	7.3 \pm 1.9
	Mg-hblld [*]	58	7.0%	0.91 \pm 0.069 [*]	9.47 \pm 1.44 [*]	12. \pm 1.6 ⁺
	Riebeckite	2	0.2%	0.41 \pm 0.0070	6.62 \pm 3.53	16. \pm 8.5
	Unassigned [*]	352	42.6%	0.94 \pm 0.047	8.02 \pm 0.423	11. \pm 0.61
	Winchite ⁺	31	3.7%	0.62 \pm 0.13	5.01 \pm 0.712	13. \pm 2.7
	All Particles	827	100.00%	1.1 \pm 0.037	9.03 \pm 0.341	10. \pm 0.38

*Indicates which mineral is significantly different ($p < 0.05$) using a Mann-Whitney U-Test

+Indicates which mineral is not significantly different ($p > 0.05$) using a Mann-Whitney U-Test

Table 10. Assigned Mineral Group for All Particles with an AR \geq 3:1

Mineral Group	n	% Composition	Mean Width (μm)	Mean Length (μm)	Mean Aspect Ratio
Calcic group	877	57.51%	1.2 ± 0.036	8.08 ± 0.302	7.9 ± 0.23
Fe-Mg group	1	0.07%	0.10 ± 0.00	1.48 ± 0.000	$15. \pm 0.00$
Sodic group	2	0.13%	0.41 ± 0.0071	6.62 ± 3.53	$16. \pm 8.5$
Sodic-Calcic group	66	4.33%	0.62 ± 0.072	4.38 ± 0.412	$10. \pm 1.4$
Sub-Calcic	579	37.97%	0.88 ± 0.034	7.00 ± 0.295	9.9 ± 0.40
All Particles	1525	100.00%	1.0 ± 0.025	7.51 ± 0.209	8.8 ± 0.23

Table 11. Assigned Mineral Group by Crystallization Process for Particles with an AR \geq 3:1

Crystallization Process	Mineral Group	n	% Composition	Mean Width (μm)	Mean Length (μm)	Mean Aspect Ratio
Neocrystallized Particles	Calcic group	453	64.90%	1.1 ± 0.043	6.12 ± 0.243	6.7 ± 0.238
	Fe-Mg group	1	0.14%	0.10 ± 0.00	1.48 ± 0.00	$15. \pm 0.00$
	Sodic group	0	0%	-	-	-
	Sodic-Calcic group ⁺	35	5.01%	$0.62 \pm 0.076^+$	$3.82 \pm 0.437^+$	$7.6 \pm 0.84^+$
	Sub-Calcic	209	29.94%	0.73 ± 0.049	5.14 ± 0.342	7.8 ± 0.33
	All Particles	698	100.00%	0.94 ± 0.032	5.70 ± 0.191	7.1 ± 0.19
Recrystallized Particles	Calcic group [*]	424	51.27%	$1.3 \pm 0.057^*$	$10.2 \pm 0.550^*$	$9.2 \pm 0.50^*$
	Fe-Mg group	0	0%	-	-	-
	Sodic group	2	0.24%	0.41 ± 0.0071	6.62 ± 3.53	$16. \pm 8.5$
	Sodic-Calcic group ⁺	31	3.75%	$0.62 \pm 0.13^+$	$5.01 \pm 0.724^+$	$13. \pm 2.7^+$
	Sub-Calcic [*]	370	44.74%	$0.96 \pm 0.046^*$	$8.06 \pm 0.411^*$	$11. \pm 0.59^*$
	All Particles	827	100.00%	1.1 ± 0.037	9.03 ± 0.341	$10. \pm 0.38$

*Indicates which crystallization process is significantly different ($p < 0.05$) for each mineral group using a Mann-Whitney U-Test

+Indicates which crystallization process is not significantly different ($p > 0.05$) using a Mann-Whitney U-Test

Table 12. Statistical Analysis of All Data with an AR \geq 3:1

Crystallization Process	n	Mean Width (μm)	Mean Length (μm)	Mean Aspect Ratio
Neocrystallized Particles	698	0.94 ± 0.032	5.70 ± 0.191	7.1 ± 0.19
Recrystallized Particles*	827	$1.1 \pm 0.037^*$	$9.03 \pm 0.341^*$	$10. \pm 0.38^*$
All Particles	1525	1.0 ± 0.025	7.51 ± 0.209	8.8 ± 0.23

*Indicates which crystallization process is significantly different ($p < 0.05$) using a Mann-Whitney U-Test

Table 13. Bundle Dimensions by Crystallization Type for Data with an AR \geq 3:1

Crystallization Process	n	Mean Width (μm)	Mean Length (μm)	Mean Aspect Ratio
Neocrystallized Bundles	356	1.2 \pm 0.055 ⁺	7.16 \pm 0.295	6.6 \pm 0.20
Recrystallized Bundles	491	1.4 \pm 0.056 ⁺	10.5 \pm 0.494 [*]	9.5 \pm 0.41 [*]
All Bundles	847	1.3 \pm 0.040	9.07 \pm 0.317	8.3 \pm 0.26

*Indicates which crystallization process is significantly different ($p < 0.05$) using a Mann-Whitney U-Test

+Indicates which crystallization process is not significantly different ($p > 0.05$) using a Mann-Whitney U-Test

Table 14. Fiber Dimensions by Crystallization Type for Data with an AR \geq 3:1

Crystallization Process	n	Mean Width (μm)	Mean Length (μm)	Mean Aspect Ratio
Neocrystallized Fibers	271	0.53 ± 0.018	4.26 ± 0.257	8.7 ± 0.38
Recrystallized Fibers*	274	$0.64 \pm 0.023^*$	$7.31 \pm 0.483^*$	$13. \pm 0.86^*$
All Fibers	545	0.59 ± 0.015	5.79 ± 0.282	$11. \pm 0.48$

*Indicates which crystallization process is significantly different ($p < 0.05$) using a Mann-Whitney U-Test

Table 15. Prismatic Crystal Dimensions by Crystallization Type for Data with an AR \geq 3:1

Crystallization Process	n	Mean Width (μm)	Mean Length (μm)	Mean Aspect Ratio
Neocrystallized Prismatic Crystals	71	1.1 \pm 0.064	3.90 \pm 0.249	3.7 \pm 0.078 ⁺
Recrystallized Prismatic Crystals	62	1.4 \pm 0.10 [*]	5.28 \pm 0.366 [*]	3.9 \pm 0.088 ⁺
All Prismatic Crystals	133	1.2 \pm 0.059	4.54 \pm 0.224	3.8 \pm 0.059

*Indicates which crystallization process is significantly different ($p < 0.05$) using a Mann-Whitney U-Test

+Indicates which crystallization process is not significantly different ($p > 0.05$) using a Mann-Whitney U-Test

Table 16. Combined Statistics of Fibers and Bundles with an AR \geq 3:1

Crystallization Process	n	Mean Width (μm)	Mean Length (μm)	Mean Aspect Ratio
Neocrystallized Particles	627	0.93 ± 0.35	5.91 ± 0.209	7.5 ± 0.20
Recrystallized Particles*	765	$1.1 \pm 0.39^*$	$9.33 \pm 0.365^*$	$11. \pm 0.41^*$
All Particles	1392	1.0 ± 0.027	7.79 ± 0.226	9.2 ± 0.25

*Indicates which crystallization process is significantly different ($p < 0.05$) using a Mann-Whitney U-Test

Table 17. Statistical Analysis of All Data with Particle Width $\leq 1 \mu\text{m}$; AR $\geq 3:1$

Crystallization Process	n	Mean Width (μm)	Mean Length (μm)	Mean Aspect Ratio
Neocrystallized Particles	503	$0.58 \pm 0.010^+$	4.12 ± 0.140	7.8 ± 0.24
Recrystallized Particles	520	$0.58 \pm 0.010^+$	$6.08 \pm 0.264^*$	$12. \pm 0.57^*$
All Particles	1023	0.58 ± 0.0070	5.12 ± 0.154	9.9 ± 0.32

*Indicates which crystallization process is significantly different ($p < 0.05$) using a Mann-Whitney U-Test

+Indicates which crystallization process is not significantly different ($p > 0.05$) using a Mann-Whitney U-Test

Table 18. Bundle Dimensions by Crystallization Type with Bundle Width $\leq 1 \mu\text{m}$; AR $\geq 3:1$

Crystallization Process	n	Mean Width (μm)	Mean Length (μm)	Mean Aspect Ratio
Neocrystallized Bundles	204	$0.66 \pm 0.014^*$	4.71 ± 0.231	7.4 ± 0.30
Recrystallized Bundles*	257	0.61 ± 0.014	$6.16 \pm 0.313^*$	$11. \pm 0.70^*$
All Bundles	461	0.63 ± 0.0010	5.52 ± 0.205	9.6 ± 0.42

*Indicates which crystallization process is significantly different ($p < 0.05$) using a Mann-Whitney U-Test

Table 19. Fiber Dimensions by Crystallization Type with Fiber Width $\leq 1 \mu\text{m}$; AR $\geq 3:1$

Crystallization Process	n	Mean Width (μm)	Mean Length (μm)	Mean Aspect Ratio
Neocrystallized Fibers	259	$0.49 \pm 0.014^+$	3.89 ± 0.195	8.7 ± 0.39
Recrystallized Fibers	241	$0.54 \pm 0.016^+$	$6.28 \pm 0.458^*$	$13. \pm 0.96^*$
All Fibers	500	0.51 ± 0.011	5.04 ± 0.248	$11. \pm 0.52$

*Indicates which crystallization process is significantly different ($p < 0.05$) using a Mann-Whitney U-Test

+Indicates which crystallization process is not significantly different ($p > 0.05$) using a Mann-Whitney U-Test

Table 20. Prismatic Crystal Dimensions by Crystallization Type with Prismatic Crystal Width $\leq 1 \mu\text{m}$; AR $\geq 3:1$

Crystallization Process	n	Mean Width (μm)	Mean Length (μm)	Mean Aspect Ratio
Neocrystallized Prismatic Crystals ⁺	40	$0.70 \pm 0.033^+$	$2.59 \pm 0.146^+$	$3.7 \pm 0.11^+$
Recrystallized Prismatic Crystals ⁺	22	$0.73 \pm 0.048^+$	$2.87 \pm 0.246^+$	$3.9 \pm 0.15^+$
All Prismatic Crystals	62	0.71 ± 0.028	2.69 ± 0.129	3.8 ± 0.089

+Indicates which crystallization process is not significantly different ($p > 0.05$) using a Mann-Whitney U-Test

Table 21. Particles with a $L \geq 5 \mu\text{m}$, $W \leq 1 \mu\text{m}$, $AR \geq 3:1$

Crystallization Process	n	% Particles Fitting Definition	Mean Width (μm)	Mean Length (μm)	Mean Aspect Ratio
Neocrystallized Particles	116	16.6%	$0.70 \pm 0.020^*$	8.20 ± 0.391	$13. \pm 0.70$
Recrystallized Particles	201	24.3%	0.64 ± 0.017	$10.8 \pm 0.525^*$	$20. \pm 1.2^*$
All Particles	317	20.8%	0.66 ± 0.013	9.85 ± 0.369	$18. \pm 0.84$

*Indicates which crystallization process is significantly different ($p < 0.05$) using a Mann-Whitney U-Test

Table 22. Bundles with a $L \geq 5 \mu\text{m}$, $W \leq 1 \mu\text{m}$, $AR \geq 3:1$

Crystallization Process	n	% Bundles Fitting Definition	% Particles Classified as Bundles	Mean Width (μm)	Mean Length (μm)	Mean Aspect Ratio
Neocrystallized Bundles	61	17.1%	52.6%	$0.76 \pm 0.024^*$	8.22 ± 0.535	$11. \pm 0.64$
Recrystallized Bundles	107	21.8%	53.2%	0.64 ± 0.022	$10.1 \pm 0.557^*$	$19. \pm 1.4^*$
All Bundles	168	19.8%	53.0%	0.68 ± 0.017	9.40 ± 0.408	$16. \pm 0.94$

*Indicates which crystallization process is significantly different ($p < 0.05$) using a Mann-Whitney U-Test

Table 23. Fibers with a $L \geq 5 \mu\text{m}$, $W \leq 1 \mu\text{m}$, $AR \geq 3:1$

Crystallization Process	n	% Fibers Fitting Definition	% Particles Classified as Fibers	Mean Width (μm)	Mean Length (μm)	Mean Aspect Ratio
Neocrystallized Fibers	55	20.3%	47.4%	$0.63 \pm 0.30^+$	8.17 ± 0.578	$15. \pm 1.2$
Recrystallized Fibers	94	34.3%	46.8%	$0.63 \pm 0.025^+$	$11.7 \pm 0.921^*$	$23. \pm 2.0^*$
All Fibers	149	27.3%	47.0%	0.63 ± 0.019	10.4 ± 0.634	$20. \pm 1.4$

*Indicates which crystallization process is significantly different ($p < 0.05$) using a Mann-Whitney U-Test

+Indicates which crystallization process is not significantly different ($p > 0.05$) using a Mann-Whitney U-Test

Table 24. Prismatic Crystals with a $L \geq 5 \mu\text{m}$, $W \leq 1 \mu\text{m}$, $AR \geq 3:1$

Crystallization Process	n	% Prismatic Crystals Fitting Definition	% Particles Classified as Prismatic Crystals	Mean Width (μm)	Mean Length (μm)	Mean Aspect Ratio
Neocrystallized Prismatic Crystals	0	0.00%	0.00%	-	-	-
Recrystallized Prismatic Crystals	0	0.00%	0.00%	-	-	-
All Prismatic Crystals	0	0.00%	0.00%	-	-	-

Table 25. Particles That Fit The OSHA Definition of an Asbestos Fiber ($L \geq 5 \mu\text{m}$; $AR \geq 3:1$)

Crystallization Process	n	% Particles Fitting Definition	Mean Width (μm)	Mean Length (μm)	Mean Aspect Ratio
Neocrystallized Particles	272	39.0%	$1.5 \pm 0.068^+$	9.89 ± 0.357	8.9 ± 0.39
Recrystallized Particles	474	57.3%	$1.5 \pm 0.057^+$	$13.4 \pm 0.509^*$	$13. \pm 0.62^*$
All Particles	746	48.9%	1.5 ± 0.044	12.1 ± 0.354	$12. \pm 0.43$

*Indicates which crystallization process is significantly different ($p < 0.05$) using a Mann-Whitney U-Test

+Indicates which crystallization process is not significantly different ($p > 0.05$) using a Mann-Whitney U-Test

Table 26. Particles That Fit The WHO Definition of an Asbestos Fiber ($L \geq 5 \mu\text{m}$, $W < 3 \mu\text{m}$, $AR \geq 3:1$)

Crystallization Process	n	% Particles Fitting Definition	Mean Width (μm)	Mean Length (μm)	Mean Aspect Ratio
Neocrystallized Particles	253	36.2%	$1.3 \pm 0.041^+$	9.24 ± 0.324	9.2 ± 0.41
Recrystallized Particles	433	52.4%	$1.2 \pm 0.032^+$	$12.2 \pm 0.425^*$	$14. \pm 0.67^*$
All Particles	686	45.0%	1.2 ± 0.025	11.1 ± 0.300	$12. \pm 0.46$

*Indicates which crystallization process is significantly different ($p < 0.05$) using a Mann-Whitney U-Test

+Indicates which crystallization process is not significantly different ($p > 0.05$) using a Mann-Whitney U-Test

Table 27. Particles That Fit The EPA TEM Counting Method Definition of an Asbestos Fiber ($L \geq 0.5 \mu\text{m}$, $AR \geq 5:1$)

Crystallization Process	n	% Particles Fitting Definition	Mean Width (μm)	Mean Length (μm)	Mean Aspect Ratio
Neocrystallized Particles	404	57.9%	0.79 ± 0.032	6.71 ± 0.281	9.5 ± 0.27
Recrystallized Particles*	551	66.6%	$0.98 \pm 0.042^*$	$10.8 \pm 0.477^*$	$13. \pm 0.53^*$
All Particles	955	62.6%	0.90 ± 0.028	9.10 ± 0.307	$12. \pm 0.33$

*Indicates which crystallization process is significantly different ($p < 0.05$) using a Mann-Whitney U-Test

Table 28. Particles That Fit Harper et al. (2012) definition of an Asbestos Fiber ($W \leq 1 \mu\text{m}$; $AR \geq 3:1$)

Crystallization Process	n	% Particles that fit definition	Mean Width (μm)	Mean Length (μm)	Mean Aspect Ratio
Neocrystallized Particles	503	72.1%	$0.58 \pm 0.010^+$	4.12 ± 0.140	7.8 ± 0.24
Recrystallized Particles	520	62.9%	$0.58 \pm 0.010^+$	$6.08 \pm 0.264^*$	$12. \pm 0.57^*$
All Particles	1023	67.1%	0.58 ± 0.007	5.12 ± 0.154	9.9 ± 0.32

*Indicates which crystallization process is significantly different ($p < 0.05$) using a Mann-Whitney U-Test

+Indicates which crystallization process is not significantly different ($p > 0.05$) using a Mann-Whitney U-Test

Table 29. Bundles That Fit The OSHA Definition of an Asbestos Fiber ($L \geq 5 \mu\text{m}$; $AR \geq 3:1$)

Crystallization Process	n	% Bundles Fitting Definition	% Particles Classified as Bundles	Mean Width (μm)	Mean Length (μm)	Mean Aspect Ratio
Neocrystallized Bundles	191	53.7%	70.2%	$1.7 \pm 0.089^+$	10.4 ± 0.421	7.5 ± 0.31
Recrystallized Bundles	321	65.4%	67.7%	$1.7 \pm 0.076^+$	$14.2 \pm 0.668^*$	$11. \pm 0.59^*$
All Bundles	512	60.4%	68.6%	1.7 ± 0.058	12.8 ± 0.454	9.9 ± 0.40

*Indicates which crystallization process is significantly different ($p < 0.05$) using a Mann-Whitney U-Test

+Indicates which crystallization process is not significantly different ($p > 0.05$) using a Mann-Whitney U-Test

Table 30. Fibers That Fit The OSHA Definition of an Asbestos Fiber ($L \geq 5 \mu\text{m}$; $AR \geq 3:1$)

Crystallization Process	n	% Fibers Fitting Definition	% Particles Classified as Fibers	Mean Width (μm)	Mean Length (μm)	Mean Aspect Ratio
Neocrystallized Fibers	66	24.4%	24.3%	$0.75 \pm 0.043^+$	8.98 ± 0.779	$14. \pm 1.1^+$
Recrystallized Fibers	123	44.9%	25.9%	$0.82 \pm 0.040^+$	$12.7 \pm 0.840^*$	$20. \pm 1.6^+$
All Fibers	189	34.7%	25.3%	0.80 ± 0.030	11.4 ± 0.625	$18. \pm 1.2$

*Indicates which crystallization process is significantly different ($p < 0.05$) using a Mann-Whitney U-Test

+Indicates which crystallization process is not significantly different ($p > 0.05$) using a Mann-Whitney U-Test

Table 31. Prismatic Crystals That Fit The OSHA Definition of an Asbestos Fiber ($L \geq 5 \mu\text{m}$; $AR \geq 3:1$)

Crystallization Process	n	% Prismatic Crystals Fitting Definition	% Particles Classified as Prismatic Crystals	Mean Width (μm)	Mean Length (μm)	Mean Aspect Ratio
Neocrystallized Prismatic Crystals ⁺	15	21.1%	5.5%	$1.8 \pm 0.14^+$	$6.99 \pm 0.524^+$	$4.0 \pm 0.17^+$
Recrystallized Prismatic Crystals ⁺	30	48.4%	6.3%	$1.9 \pm 0.15^+$	$7.41 \pm 0.480^+$	$4.1 \pm 0.12^+$
All Prismatic Crystals	45	33.8%	6.0%	1.8 ± 0.11	7.27 ± 0.366	4.1 ± 0.10

+Indicates which crystallization process is not significantly different ($p > 0.05$) using a Mann-Whitney U-Test

Table 32. Bundles That Fit The WHO Definition of an Asbestos Fiber ($L \geq 5 \mu\text{m}$, $W < 3 \mu\text{m}$, $AR \geq 3:1$)

Crystallization Process	n	% Bundles Fitting Definition	% Particles Classified as Bundles	Mean Width (μm)	Mean Length (μm)	Mean Aspect Ratio
Neocrystallized Bundles	173	48.6%	68.4%	$1.4 \pm 0.050^+$	9.54 ± 0.362	7.9 ± 0.33
Recrystallized Bundles	281	57.2%	64.9%	$1.4 \pm 0.041^+$	$12.5 \pm 0.530^*$	$12. \pm 0.66^*$
All Bundles	454	53.6%	66.2%	1.4 ± 0.032	11.4 ± 0.362	$10. \pm 0.44$

*Indicates which crystallization process is significantly different ($p < 0.05$) using a Mann-Whitney U-Test

+Indicates which crystallization process is not significantly different ($p > 0.05$) using a Mann-Whitney U-Test

Table 33. Fibers That Fit The WHO Definition of an Asbestos Fiber ($L \geq 5 \mu\text{m}$, $W < 3 \mu\text{m}$, $AR \geq 3:1$)

Crystallization Process	n	% Fibers Fitting Definition	% Particles Classified as Fibers	Mean Width (μm)	Mean Length (μm)	Mean Aspect Ratio
Neocrystallized Fibers	66	24.4%	26.1%	$0.75 \pm 0.043^+$	8.98 ± 0.780	$14. \pm 1.1^+$
Recrystallized Fibers	123	44.9%	28.4%	$0.82 \pm 0.040^+$	$12.7 \pm 0.840^*$	$20. \pm 1.6^+$
All Fibers	189	34.7%	27.6%	0.80 ± 0.030	11.4 ± 0.625	$18. \pm 1.2$

*Indicates which crystallization process is significantly different ($p < 0.05$) using a Mann-Whitney U-Test

+Indicates which crystallization process is not significantly different ($p > 0.05$) using a Mann-Whitney U-Test

Table 34. Prismatic Crystals That Fit The WHO Definition of an Asbestos Fiber ($L \geq 5 \mu\text{m}$, $W < 3 \mu\text{m}$, $AR \geq 3:1$)

Crystallization Process	n	% Prismatic Crystals Fitting Definition	% Particles Classified as Prismatic Crystals	Mean Width (μm)	Mean Length (μm)	Mean Aspect Ratio
Neocrystallized Prismatic Crystals ⁺	14	19.7%	5.5%	$1.7 \pm 0.11^+$	$6.65 \pm 0.434^+$	$4.0 \pm 0.18^+$
Recrystallized Prismatic Crystals ⁺	29	46.8%	6.7%	$1.7 \pm 0.078^+$	$7.05 \pm 0.333^+$	$4.2 \pm 0.12^+$
All Prismatic Crystals	43	32.3%	6.3%	1.7 ± 0.063	6.92 ± 0.267	4.1 ± 0.10

+Indicates which crystallization process is not significantly different ($p > 0.05$) using a Mann-Whitney U-Test

Table 35. SEM Statistics with an AR \geq 3:1

Crystallization Process	n	Mean Width (μm)	Mean Length (μm)	Mean Aspect Ratio
Neocrystallized Particles	344	1.1 \pm 0.051	6.87 \pm 0.321	6.7 \pm 0.24
Recrystallized Particles *	244	1.6 \pm 0.085*	14.1 \pm 0.893*	10. \pm 0.60*
All Particles	588	1.3 \pm 0.047	9.85 \pm 0.440	8.2 \pm 0.30

*Indicates which crystallization process is significantly different ($p < 0.05$) using a Mann-Whitney U-Test

Table 36. FESEM Statistics with an AR \geq 3:1

Crystallization Process	n	Mean Width (μm)	Mean Length (μm)	Mean Aspect Ratio
Neocrystallized Particles	354	0.76 ± 0.038	4.57 ± 0.192	7.5 ± 0.29
Recrystallized Particles *	583	$0.92 \pm 0.035^*$	$6.92 \pm 0.261^*$	$10. \pm 0.48^*$
All Particles	937	0.86 ± 0.026	6.03 ± 0.182	9.1 ± 0.32

*Indicates which crystallization process is significantly different ($p < 0.05$) using a Mann-Whitney U-Test

Table 37. Combined SEM and FESEM Statistics with an AR \geq 3:1

Microscopy Method	n	Mean Width (μm)	Mean Length (μm)	Mean Aspect Ratio
SEM	588	$1.3 \pm 0.047^*$	$9.85 \pm 0.440^*$	$8.2 \pm 0.30^+$
FESEM	937	0.86 ± 0.026	6.03 ± 0.182	$9.1 \pm 0.32^+$
Both Microscopy Methods	1525	1.0 ± 0.025	7.51 ± 0.209	8.8 ± 0.23

*Indicates which microscopy method is significantly different ($p < 0.05$) using a Mann-Whitney U-Test

+Indicates which microscopy method is not significantly different ($p > 0.05$) using a Mann-Whitney U-Test

Table 38. Percent of particles in this study with an AR \geq 3:1 that fit various asbestos parameters.

Crystallization Process	% of Particles with a Width $<$ 3 μm (Respirable)	% of Particles with an AR \geq 3:1	% of Particles with a Length \geq 5 μm (Visible to PCM)	% of Particles with a W $<$ 3 μm and AR \geq 3:1 μm
Neocrystallized	97%	100%	39%	97%
Recrystallized	95%	100%	57%	95%
All Particles	96%	100%	49%	96%

Table 39. Percent of particles in this study with an AR \geq 3:1 that fit various asbestos fiber definitions.

Crystallization Process	% of Particles that Fit Harper et al. (2012) Definition	% of Particles that Fit WHO Definition	% of Particles that Fit OSHA Definition	% of Particles that Fit EPA TEM Method Definition
Neocrystallized	72%	36%	39%	58%
Recrystallized	63%	52%	57%	67%
All Particles	67%	45%	49%	63%

Appendix B: Figures

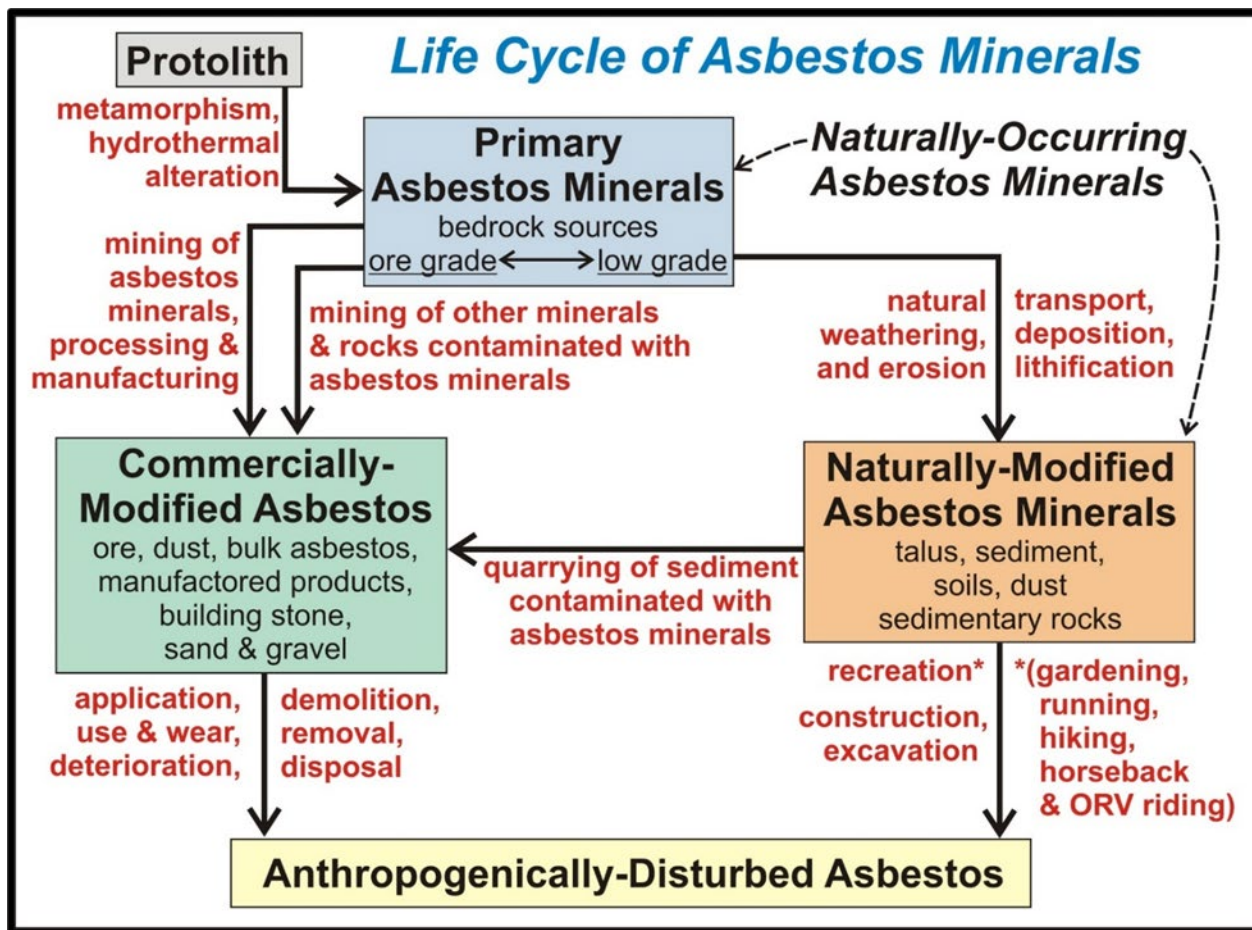


Figure 1: The life cycle of commercially and naturally-modified asbestos. Schematic courtesy of Metcalf et al. (2018).

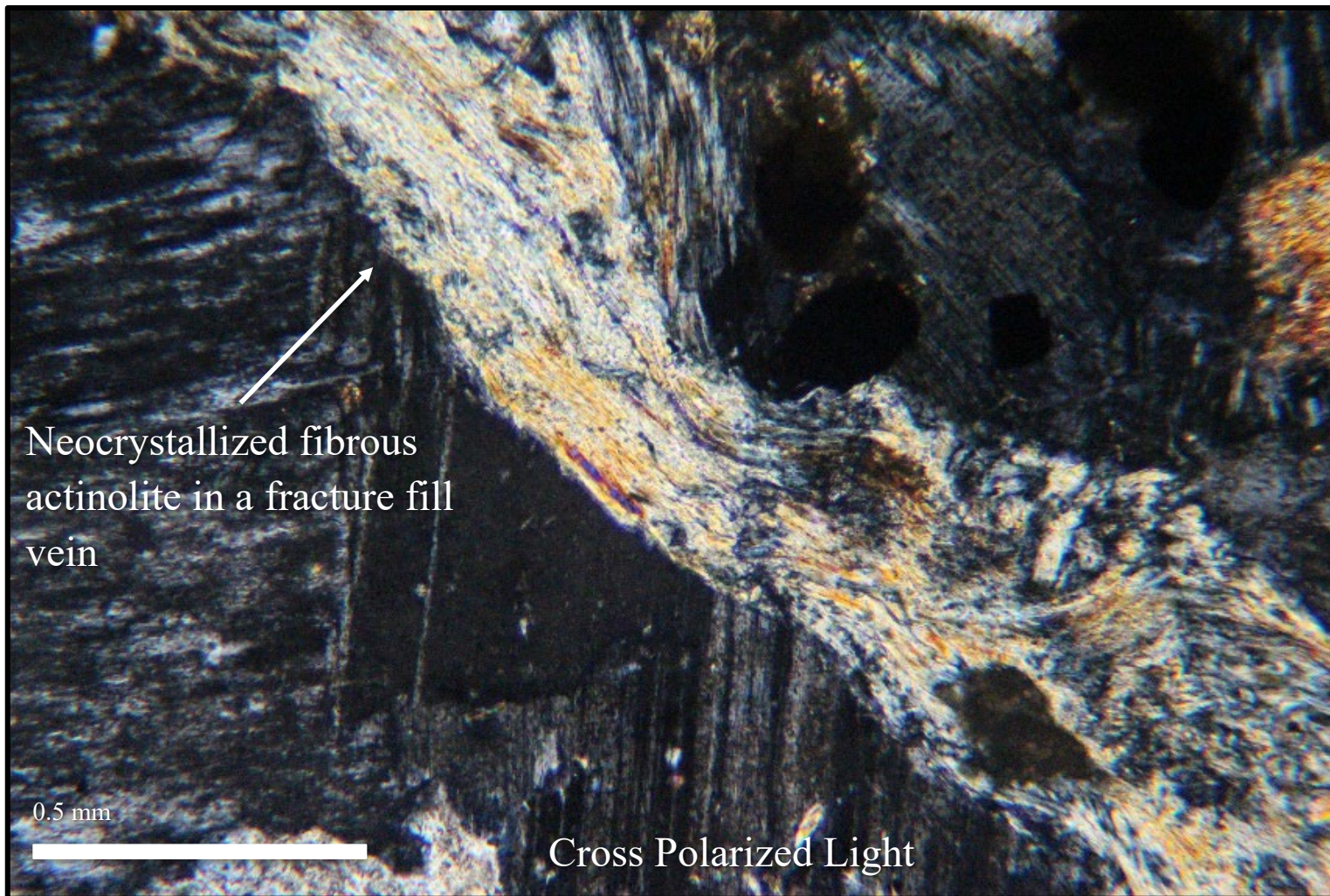


Figure 2: Neocrystallized fibrous actinolite in a granitic fracture fill vein cutting through altered plagioclase (Type I). Cross polarized light.

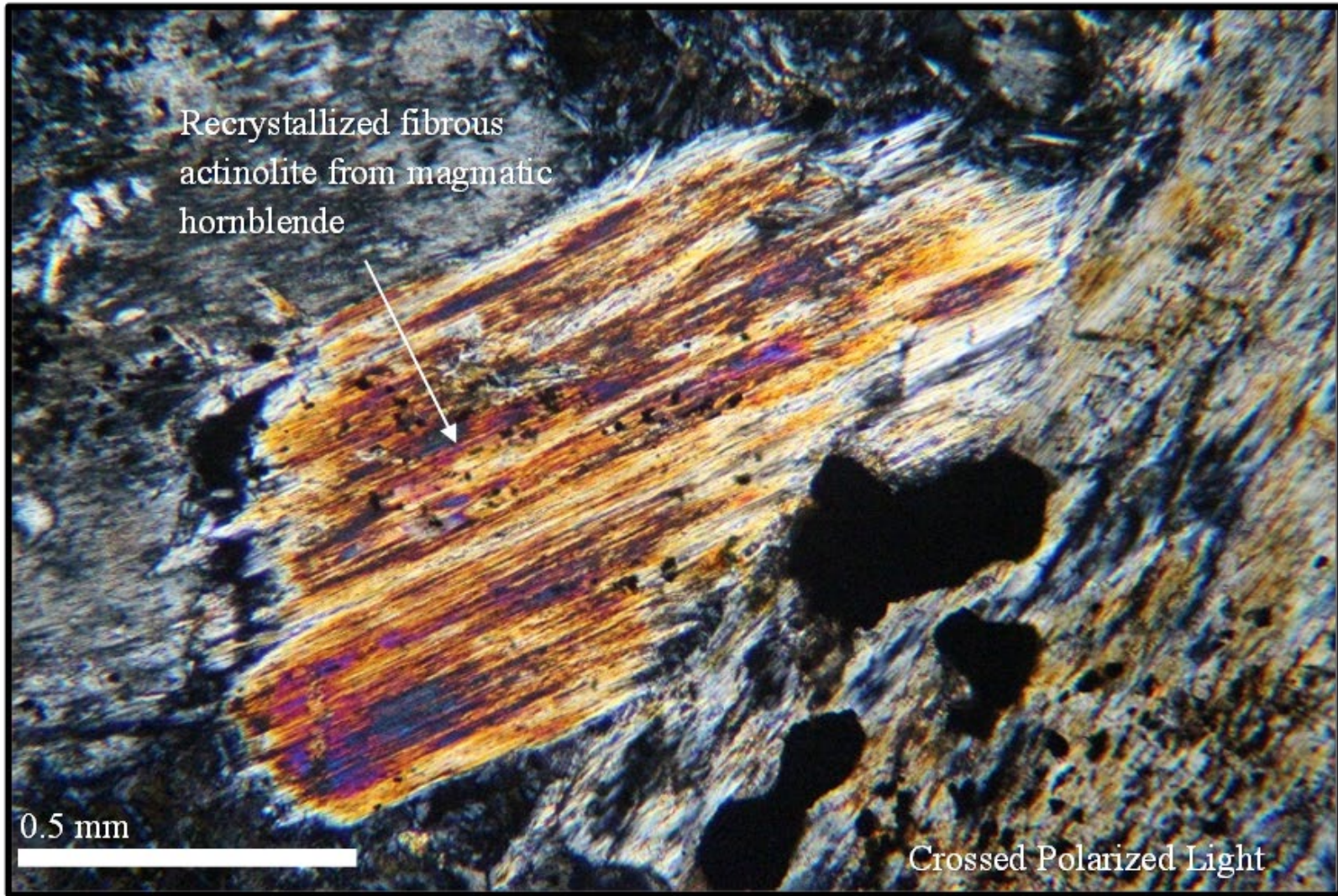


Figure 3. Recrystallized fibrous actinolite formed via replacement of magmatic magnesio-hornblende surrounded by altered plagioclase and chlorite (Type III). Cross polarized light.

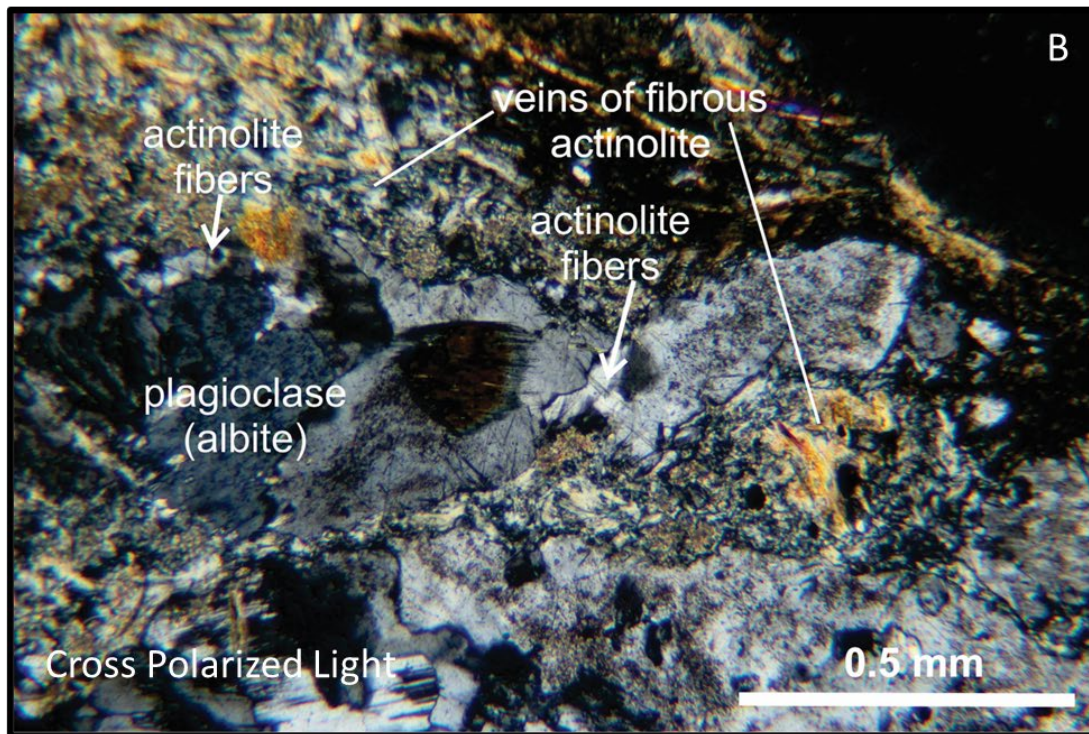
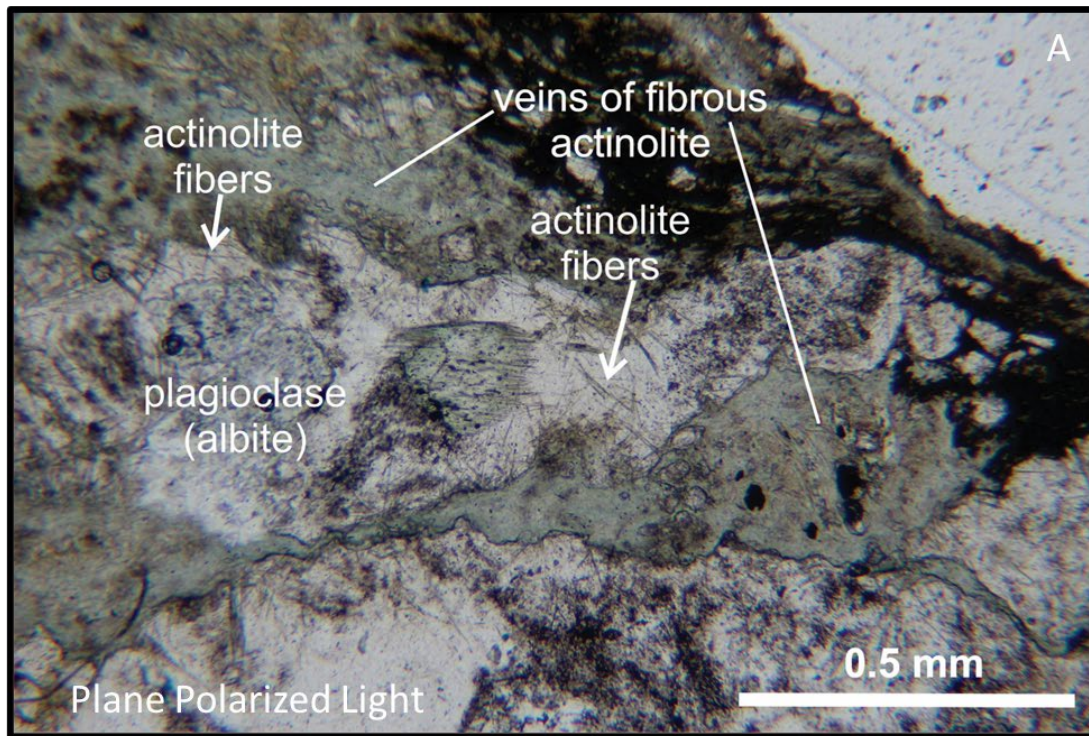


Figure 4. Neocrystallization fiber intergrowth within or on edges of other grains (Type II). Plane polarized light (A) and Cross polarized light (B).

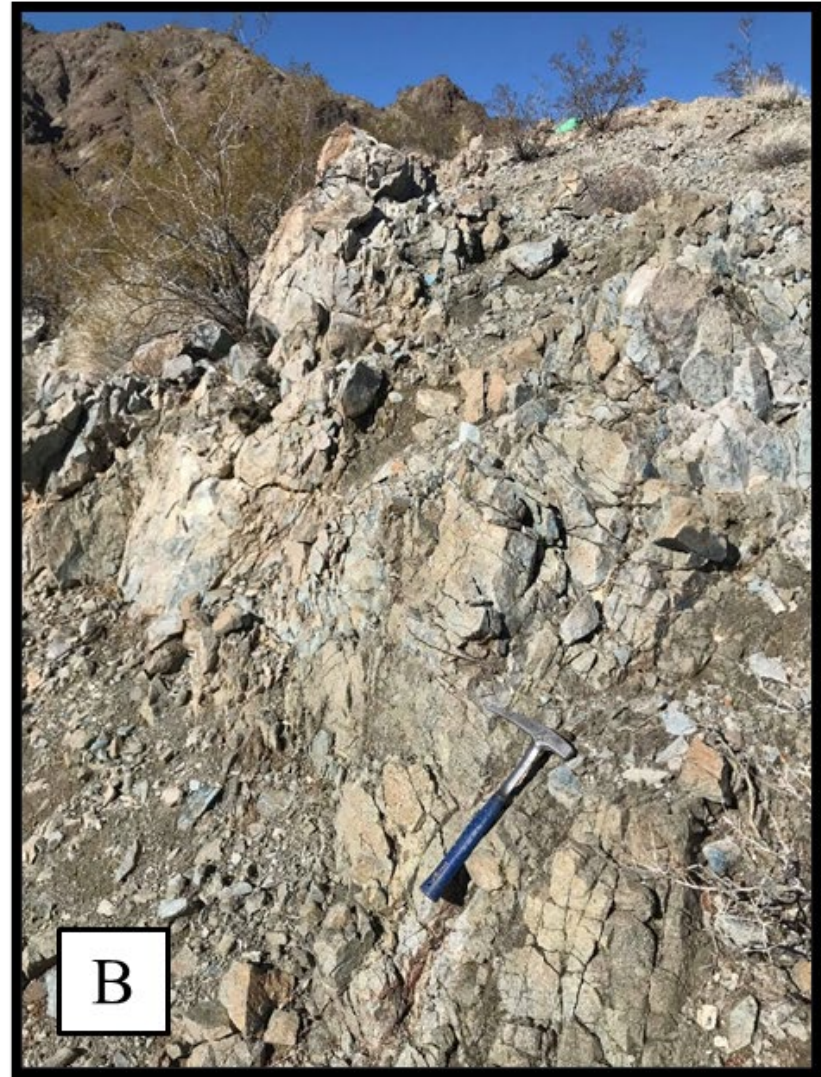
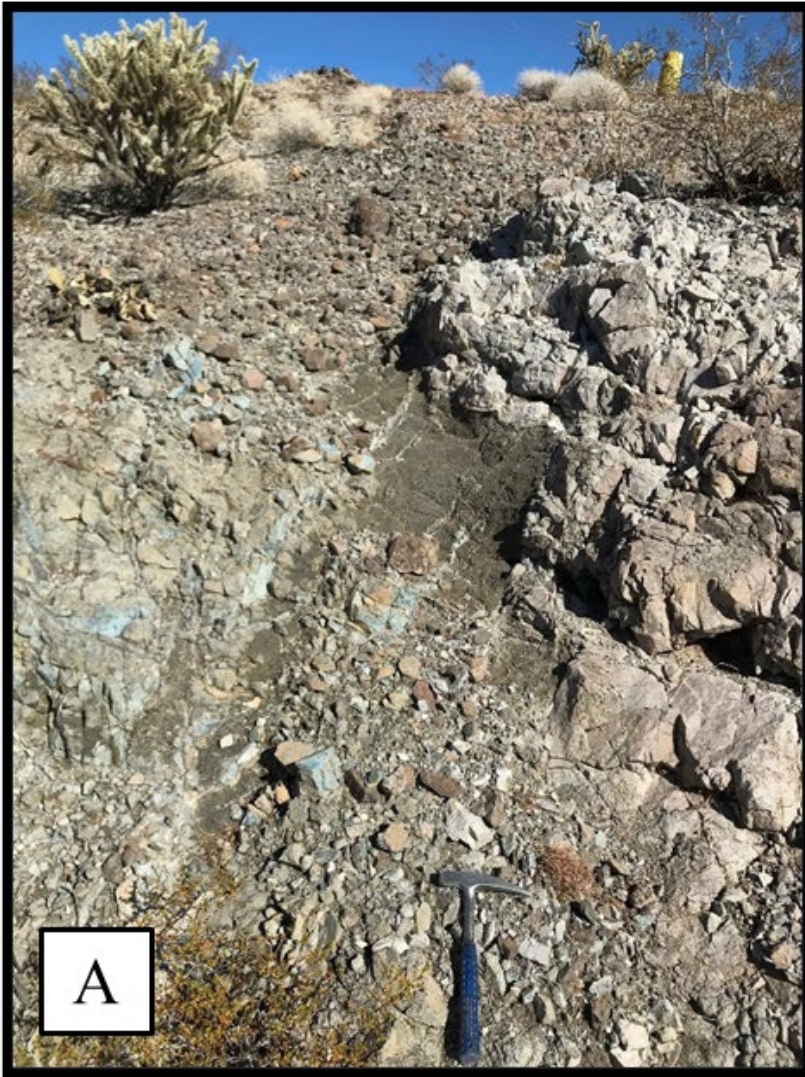


Figure 5. Erosion of a granitic pluton within the McCullough Range that contains asbestos minerals.

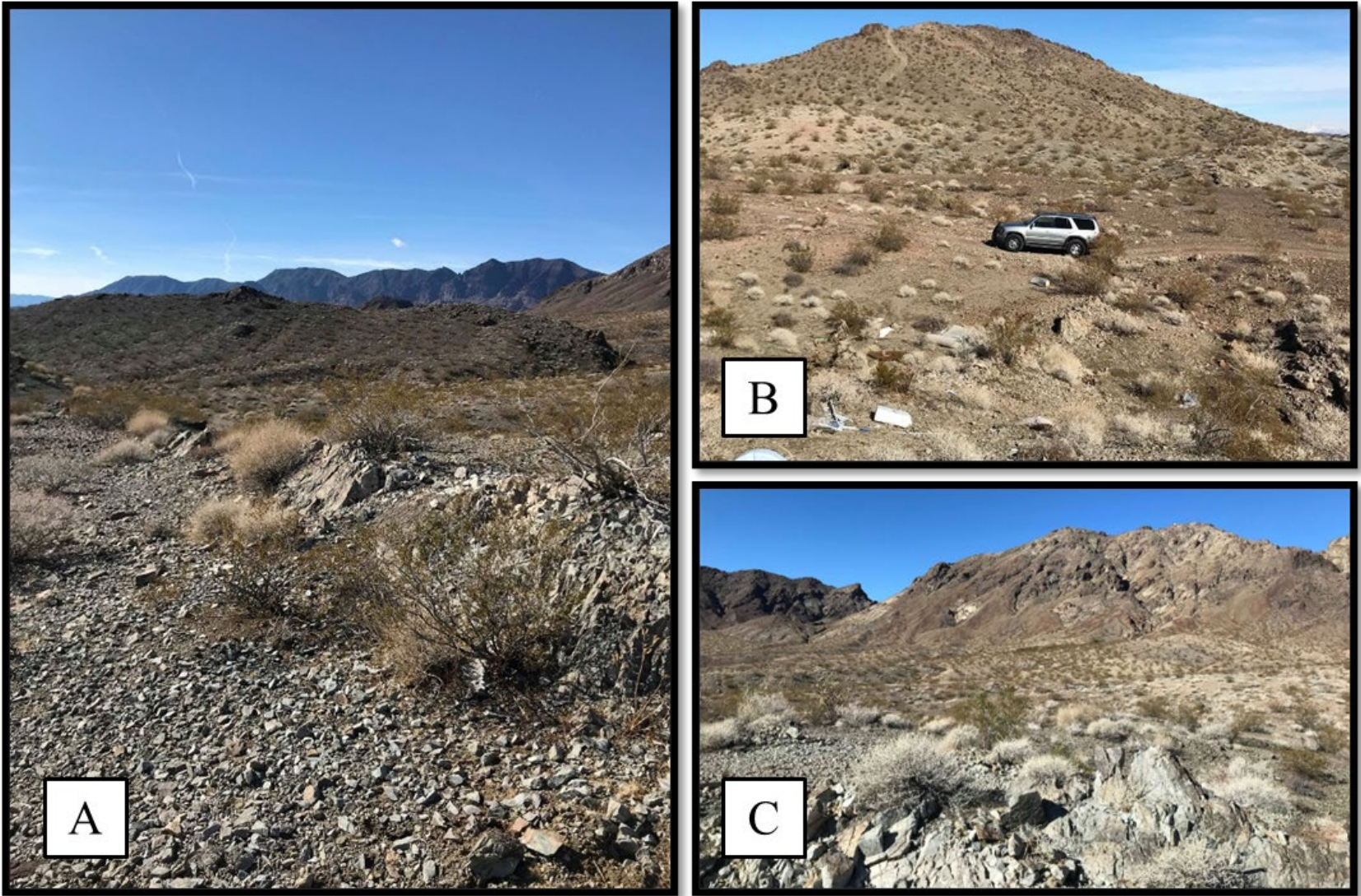


Figure 6. Overview of the field area in McCullough Range, NV.

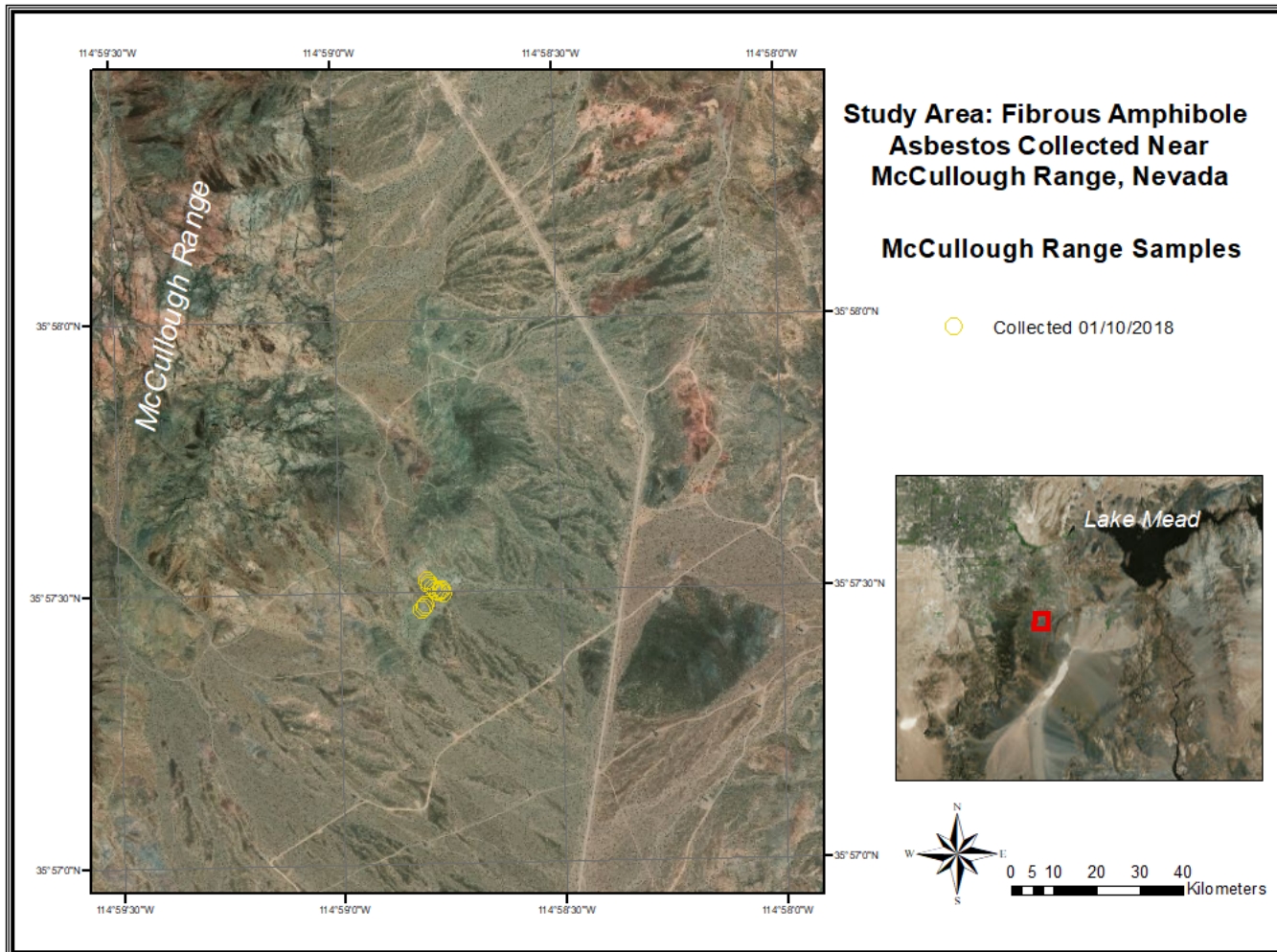


Figure 7. The locations of samples of neocrystallized and recrystallized fibrous amphibole collected January 10, 2018 in McCullough Range, Nevada. Fifteen GPS data points were collected for each sample bag. A total of 46 rocks were collected.



Figure 8. Hand sample of blue neocrystallized fibrous amphibole collected in McCullough Range, NV.



Figure 9. Hand sample of recrystallized fibrous amphibole collected in McCullough Range, NV.



Figure 10. Image of an Undergrad student at UNLV removing subsamples of both neocrystallized and recrystallized fibrous amphibole using a 0.015” diameter motorized drill.

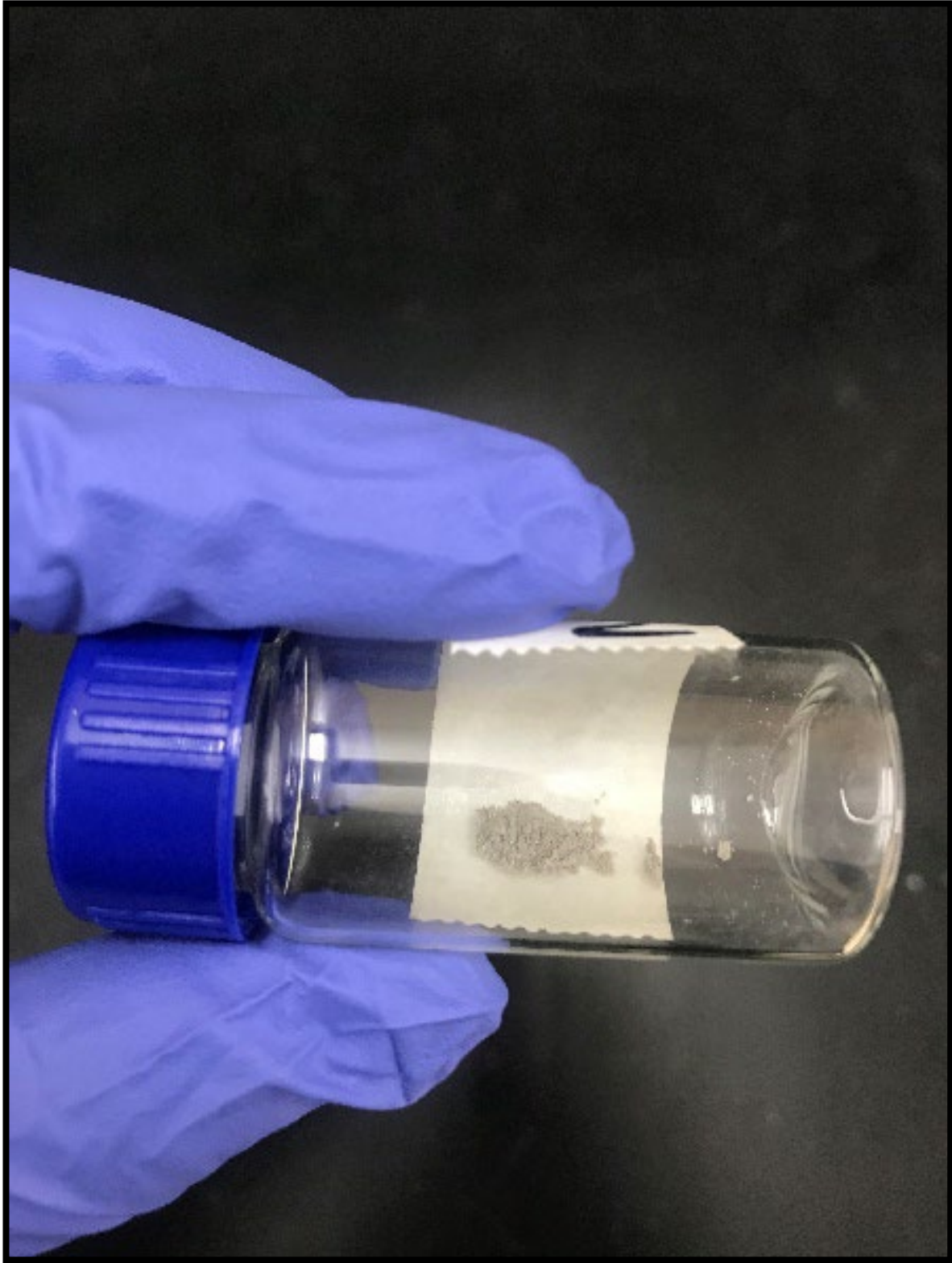


Figure 11. Image of neocrystallized naturally-occurring asbestos fibers drilled from a hand sample collected within the McCullough Range, NV.

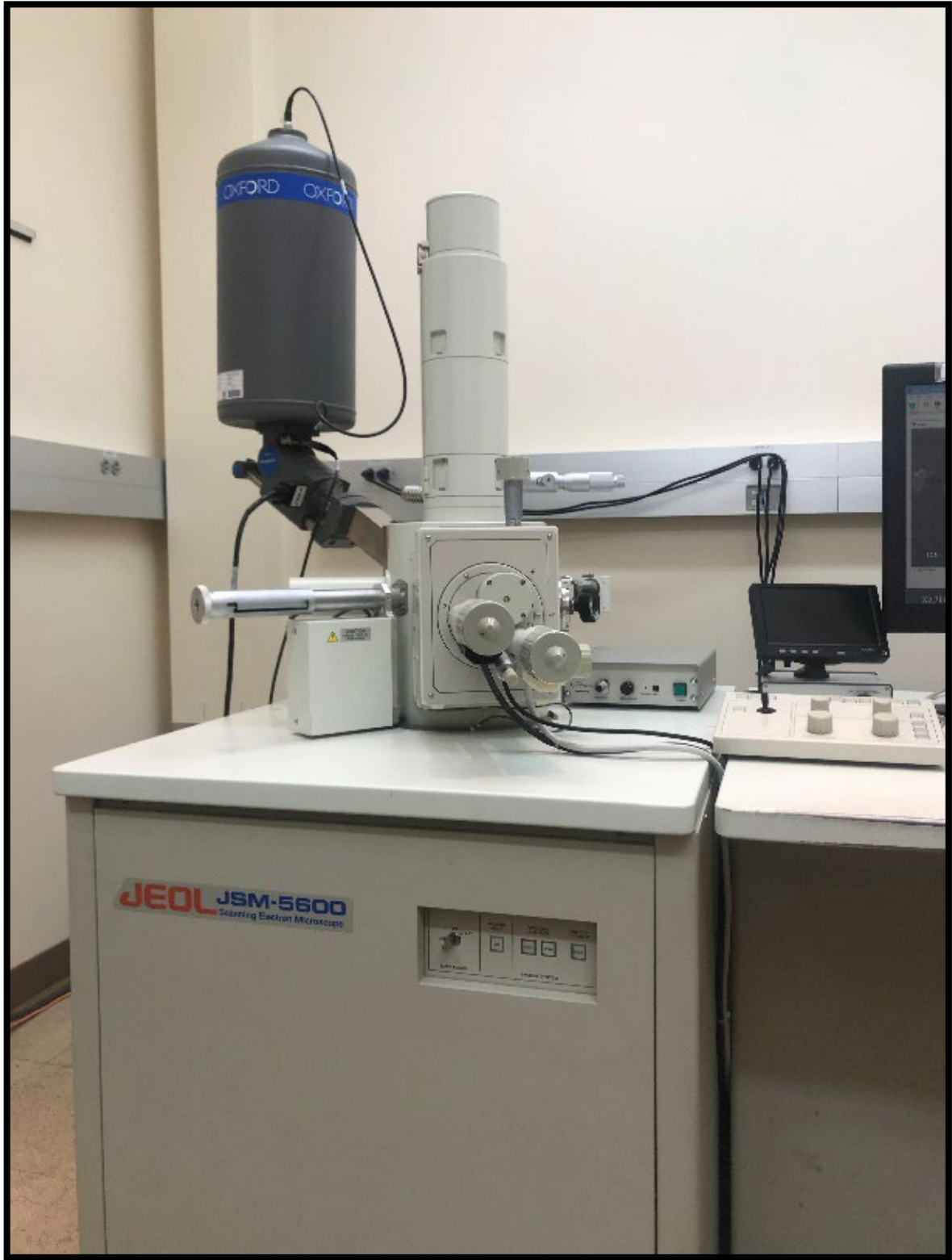


Figure 12. Image of the Scanning Electron Microscope in the EMiL Lab at the University of Nevada, Las Vegas.



Figure 13. Image of a prepared neocrystallized FESEM/ SEM sample. Sample prepared by placing the extracted subsamples on a polycarbonate 0.4 μm isopure filter, which was mounted on a plastic base with carbon tape and coated with carbon.

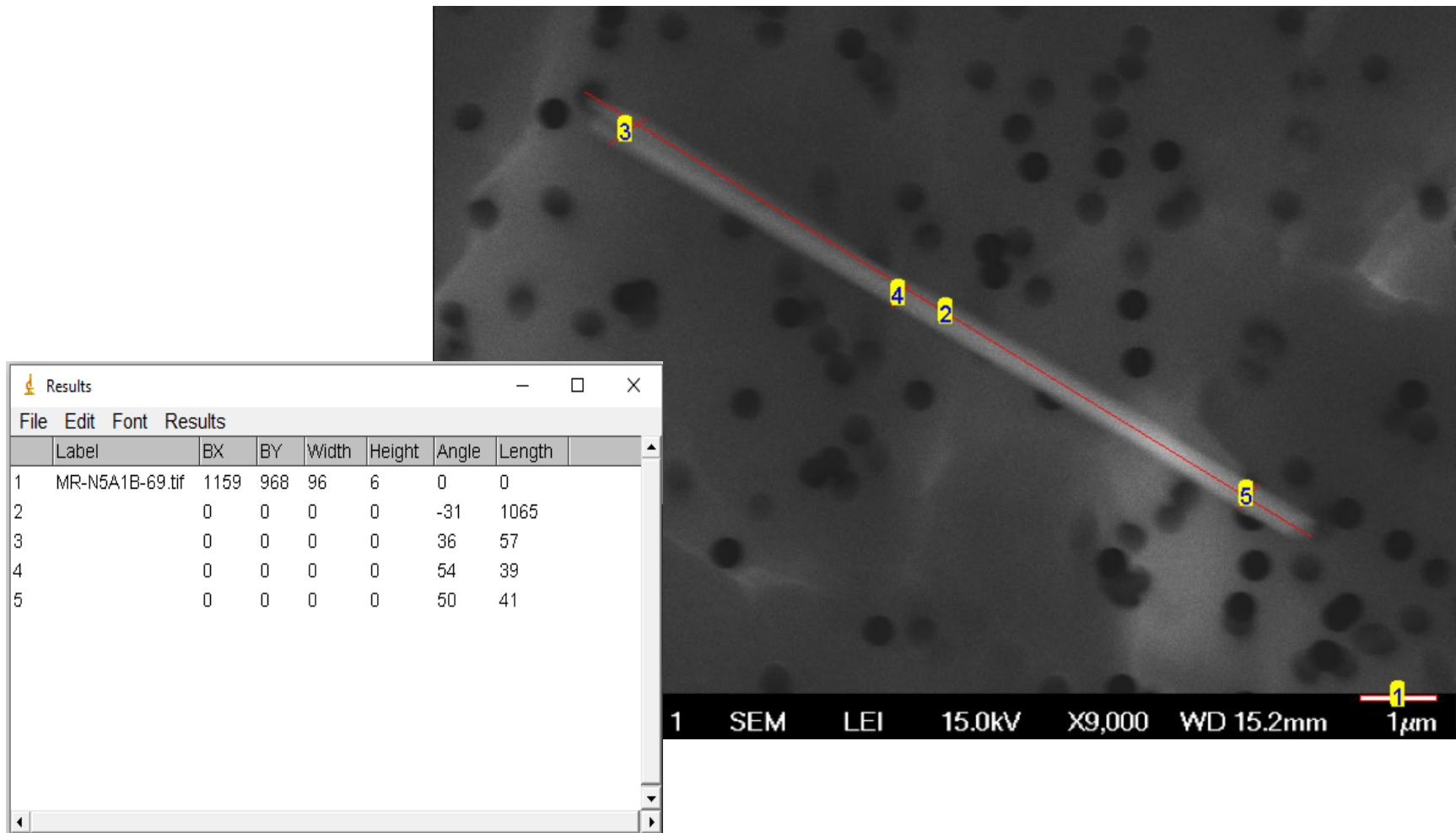


Figure 14. Photo of how we measured a particle using the imageJ program. Measurements were done in the following order (1) scale bar, (2) maximum length, (3) width measurement one, (4) width measurement two, and (5) width measurement three. All imageJ output measurements are done in pixels and can be seen within the length column from the Results section of the imageJ program. Pixels were converted to microns using the “length” results for the scale bar from the imageJ program for each image. After conversion to microns, an average width and aspect ratio were calculated.

**Continuous Field Information for Log10 (Particle Width)
for Particles With an AR \geq 3:1**

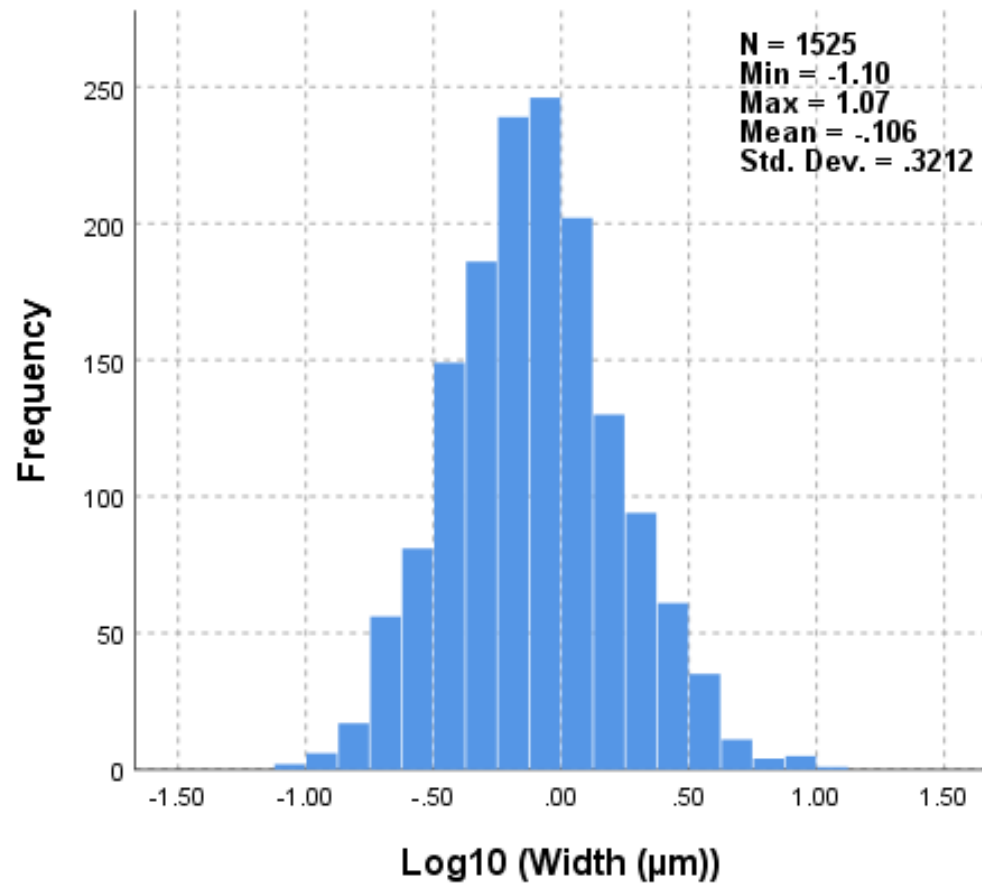


Figure 15. Continuous Field Information for Log₁₀ (Particle Width) for Particles with an AR \geq 3:1 Across Crystallization Process

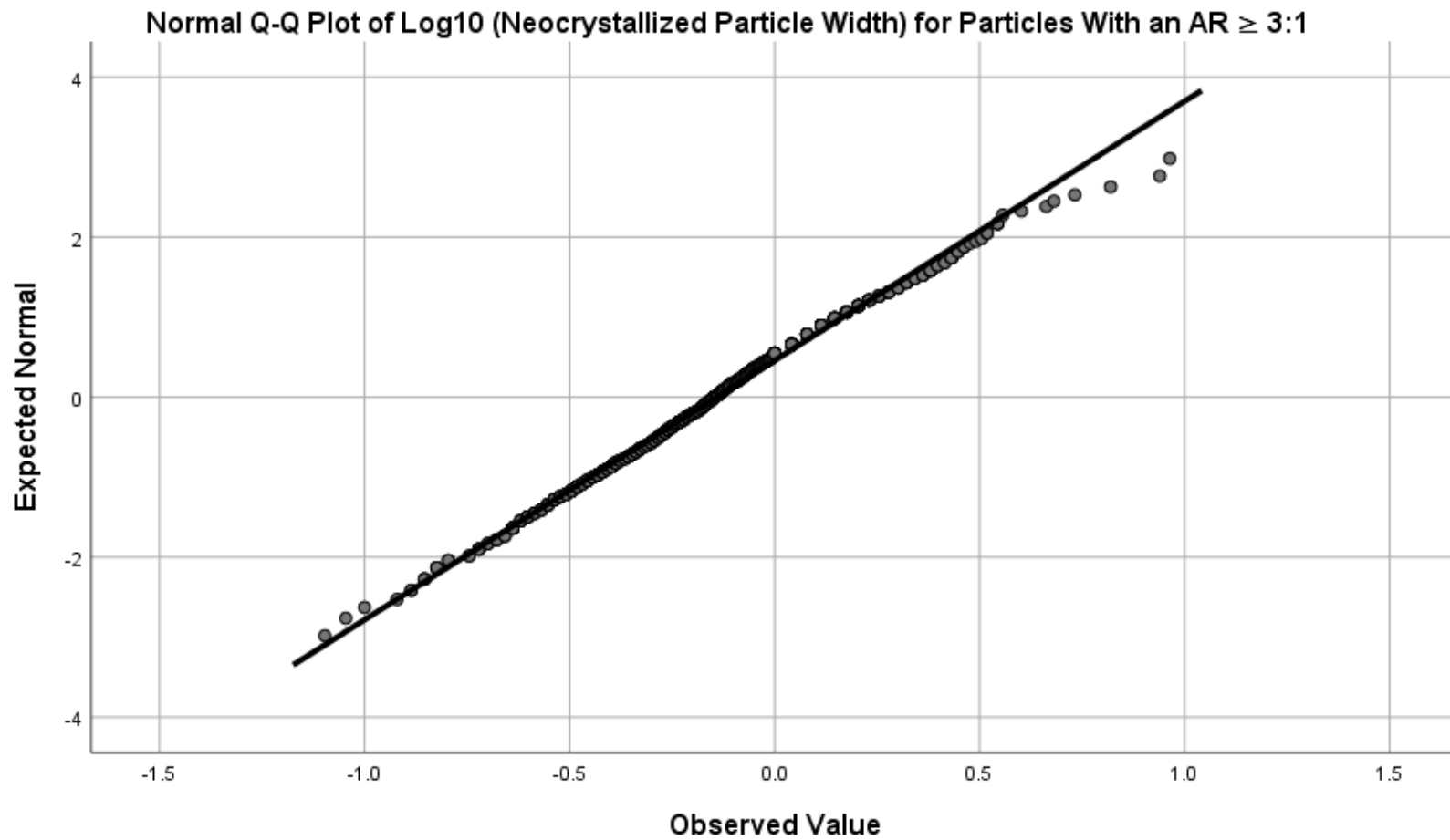


Figure 16. Normal Q-Q Plot of Log10 (Neocrystallized Particle Width) for Particles with an AR \geq 3:1

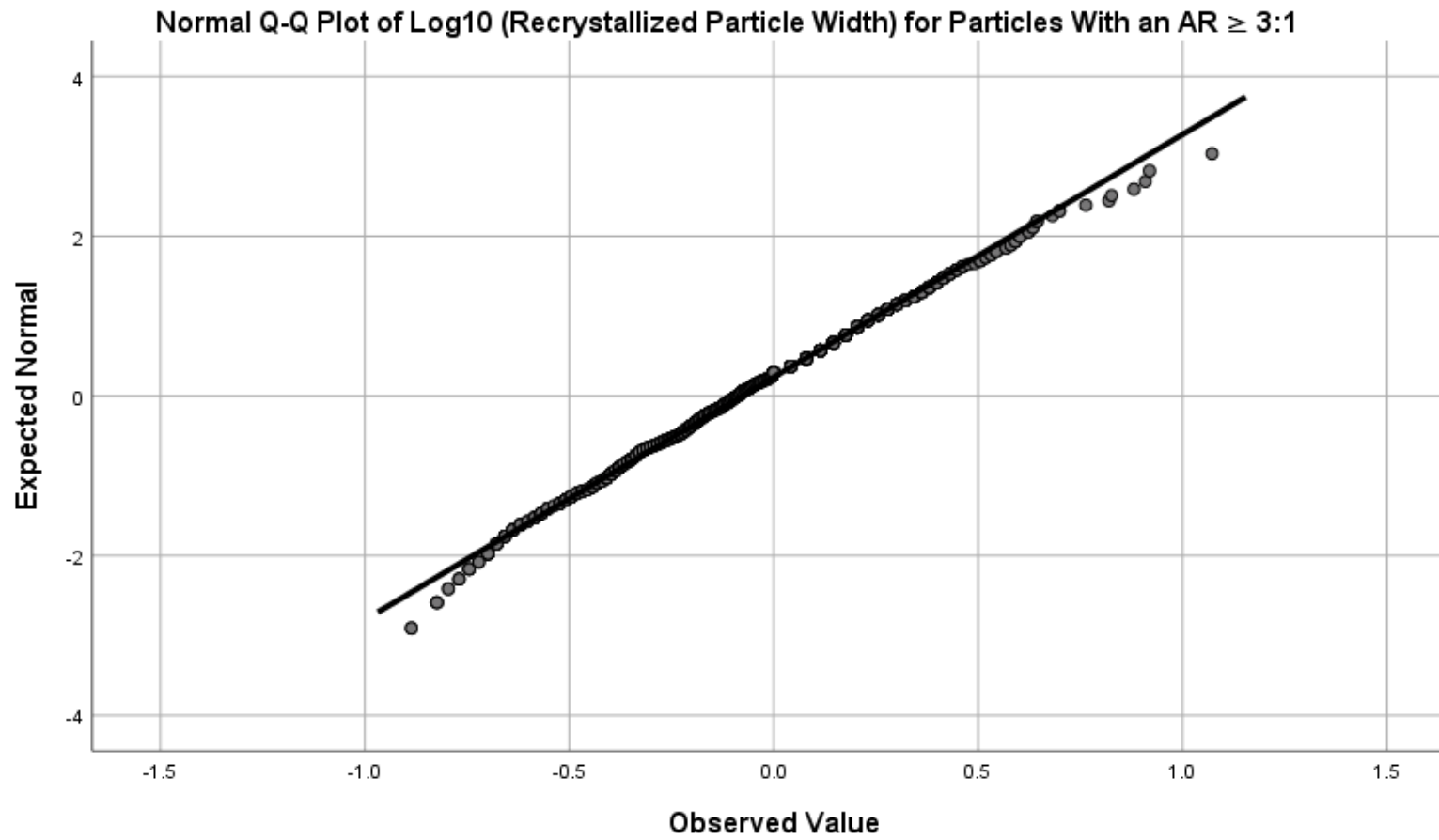


Figure 17. Normal Q-Q Plot of Log10 (Recrystallized Particle Width) for Particles with an AR \geq 3:1

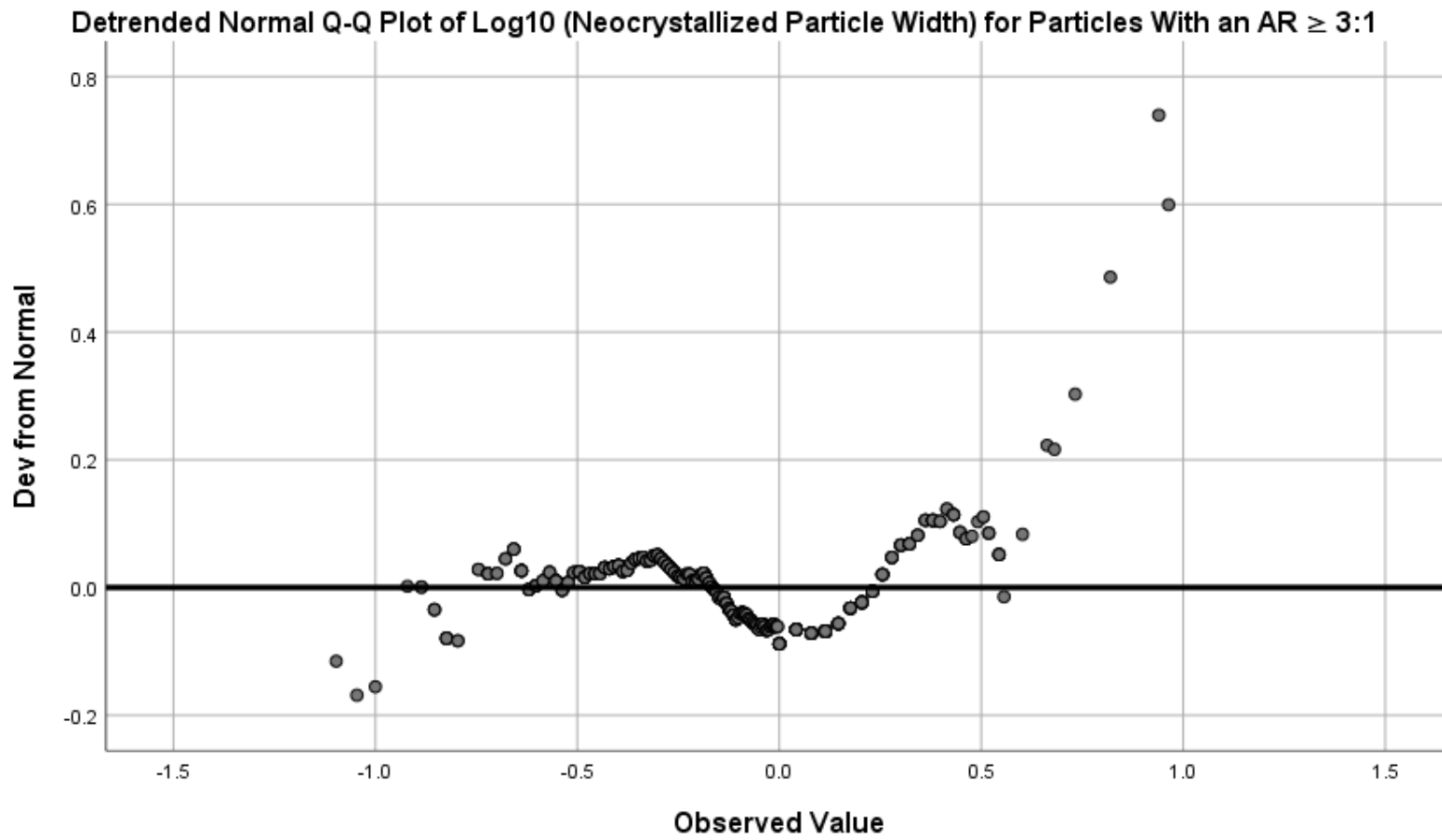


Figure 18. Detrended Normal Q-Q Plot of Log10 (Neocrystallized Particle Width) for Particles with an AR $\geq 3:1$

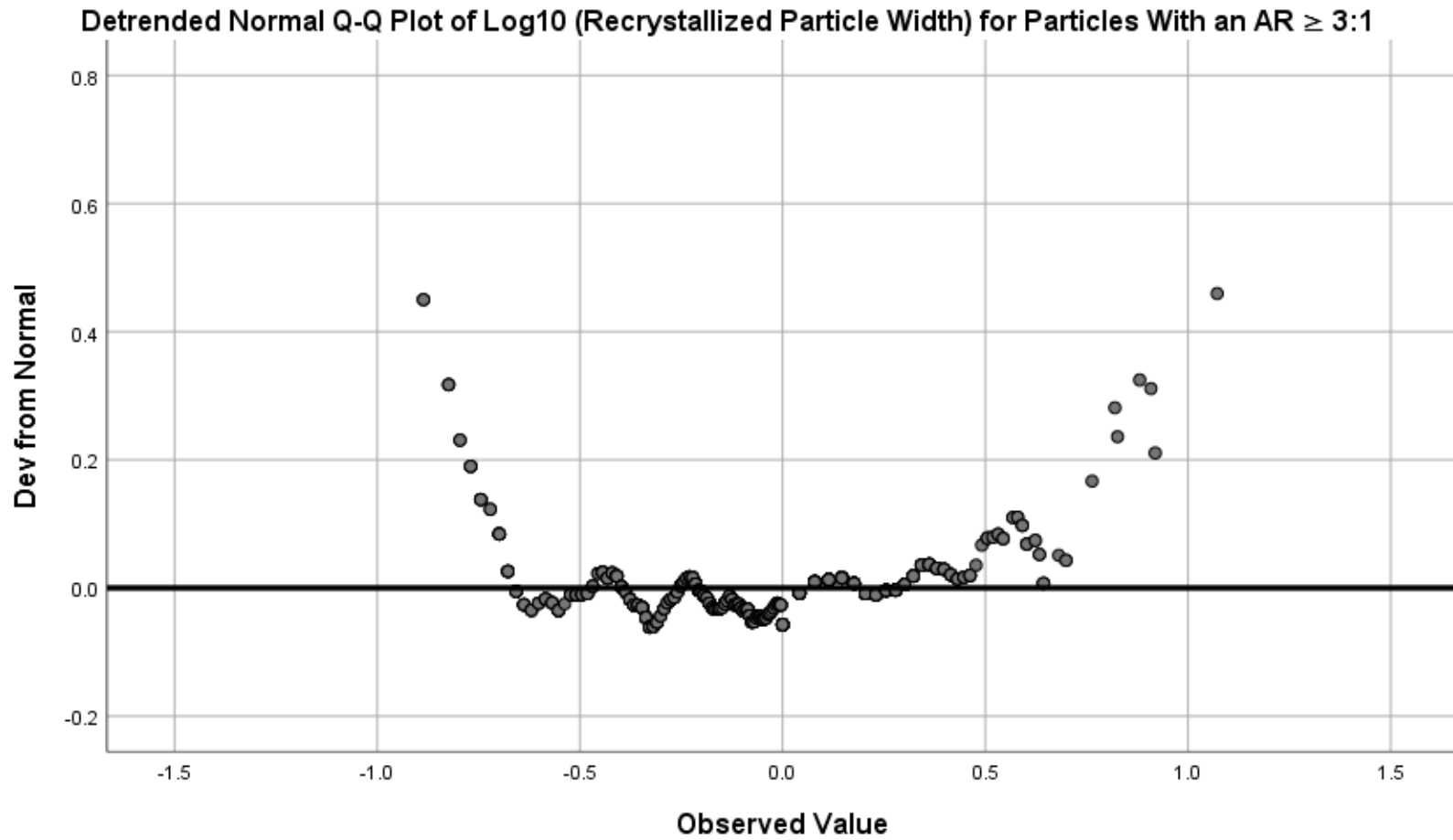


Figure 19. Detrended Normal Q-Q Plot of Log10 (Recrystallized Particle Width) for Particles with an AR \geq 3:1

**Continuous Field Information for Log10 (Particle Length)
for Particles With an AR \geq 3:1**

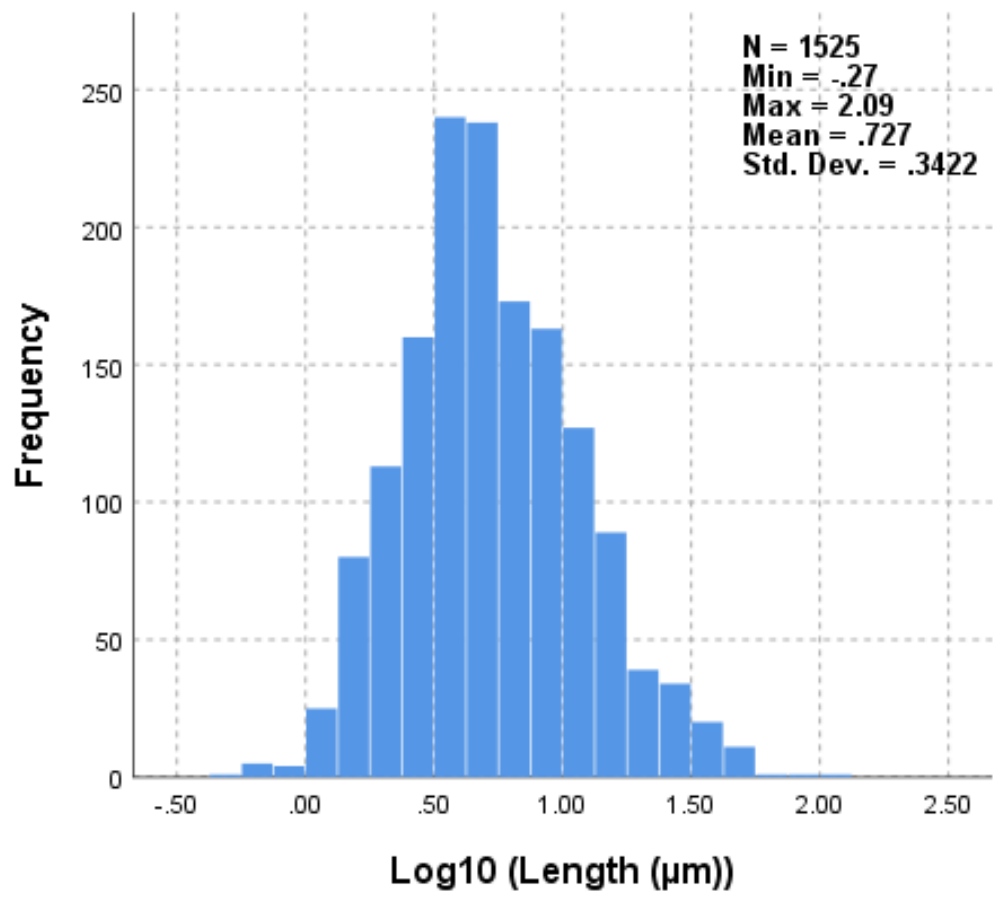


Figure 20. Continuous Field Information for Log10 (Particle Length) for Particles with an AR \geq 3:1 Across Crystallization Process

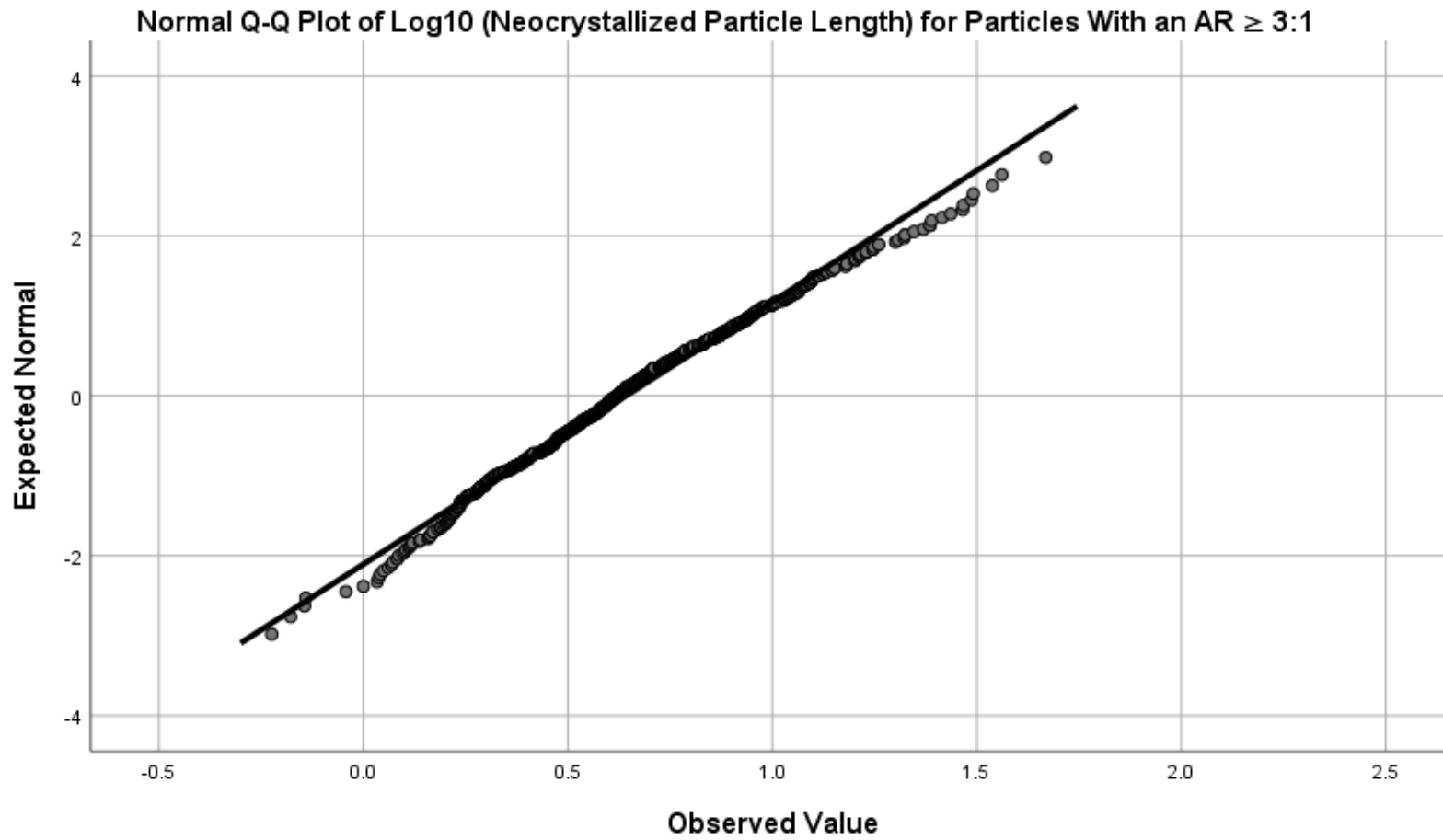


Figure 21. Normal Q-Q Plot of Log10 (Neocrystallized Particle Length) for Particles with an AR \geq 3:1

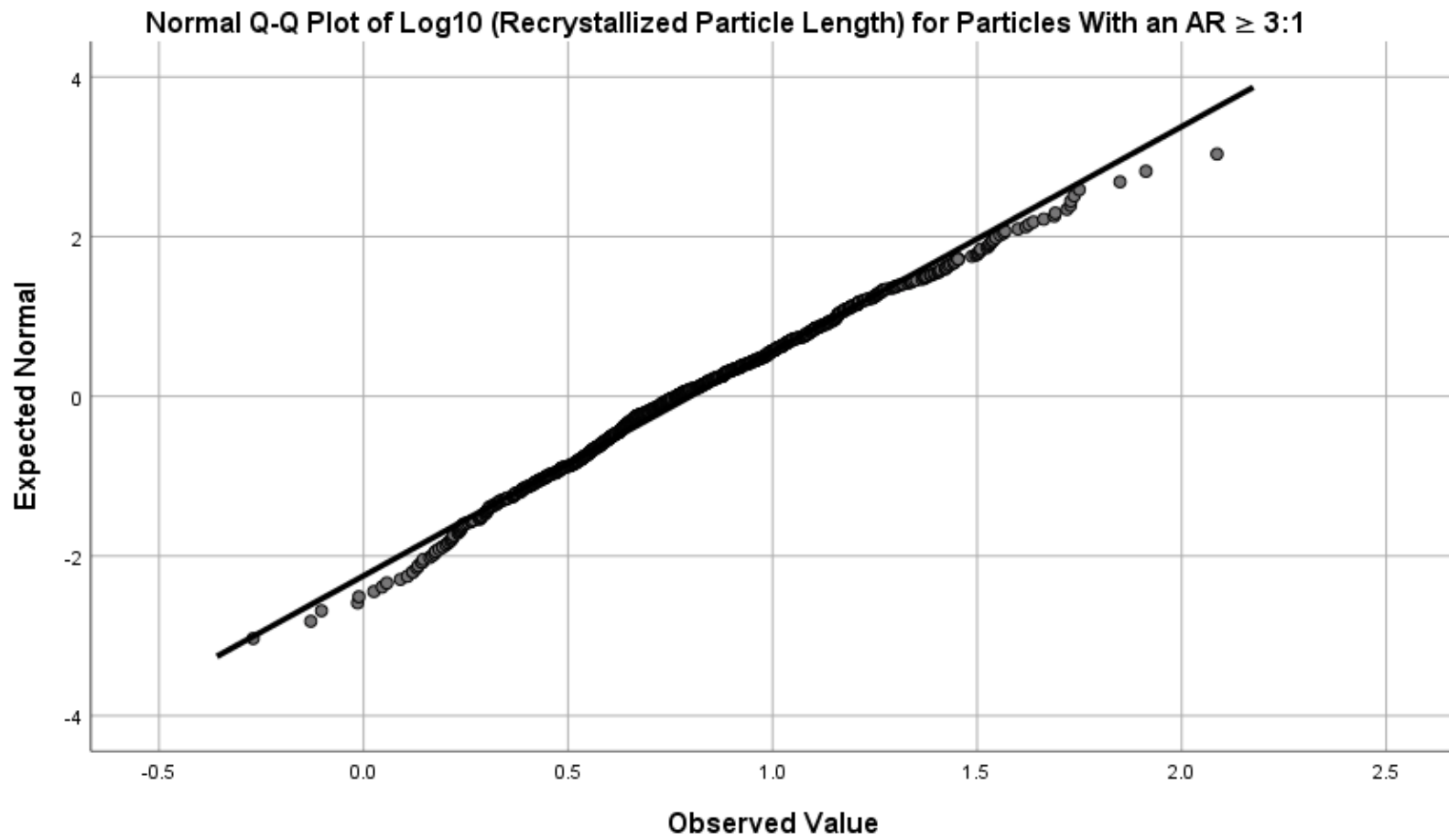


Figure 22. Normal Q-Q Plot of Log10 (Recrystallized Particle Length) for Particles with an AR \geq 3:1

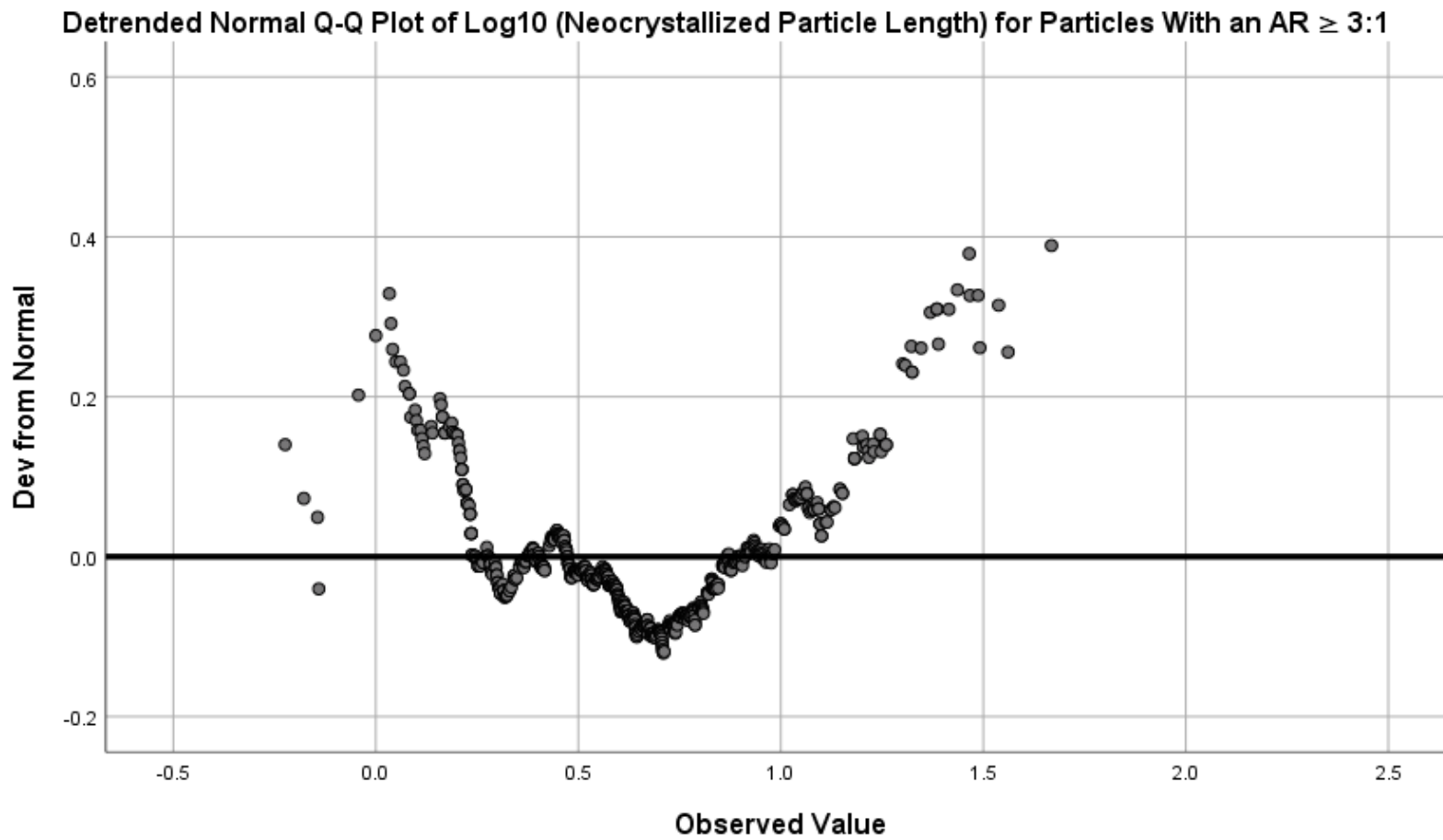


Figure 23. Detrended Normal Q-Q Plot of Log10 (Neocrystallized Particle Length) for Particles with an AR \geq 3:1

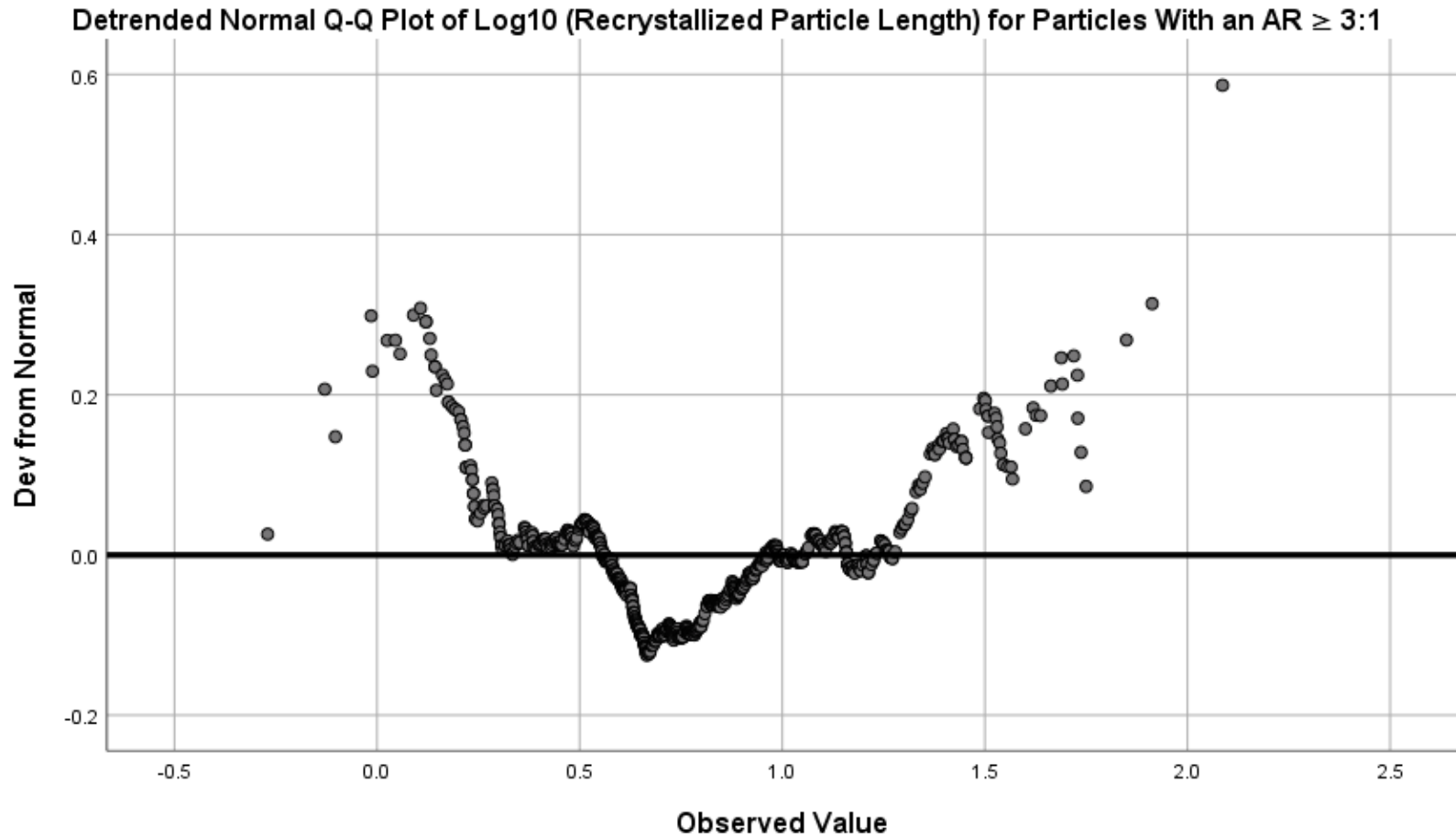


Figure 24. Detrended Normal Q-Q Plot of Log10 (Recrystallized Particle Length) for Particles with an AR \geq 3:1

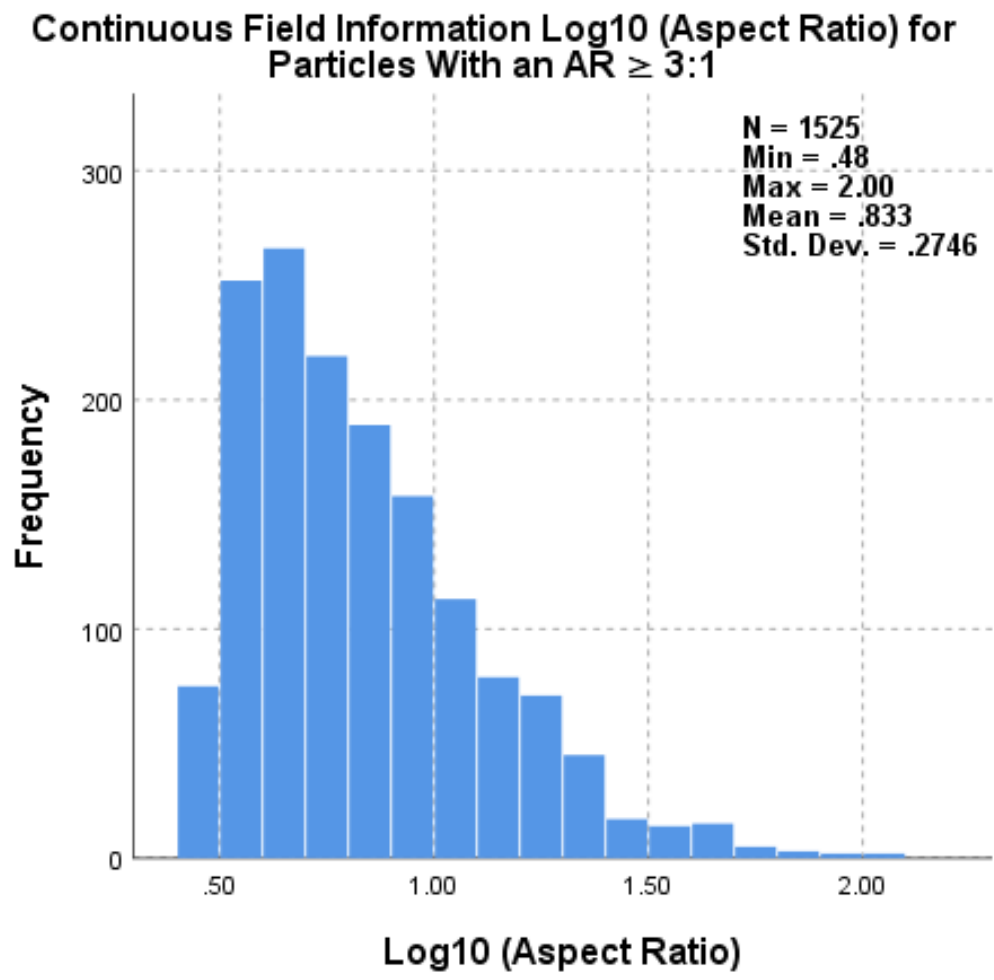


Figure 25. Continuous Field Information for Log10 (Particle Aspect Ratio) for Particles with an AR $\geq 3:1$ Across Crystallization Process

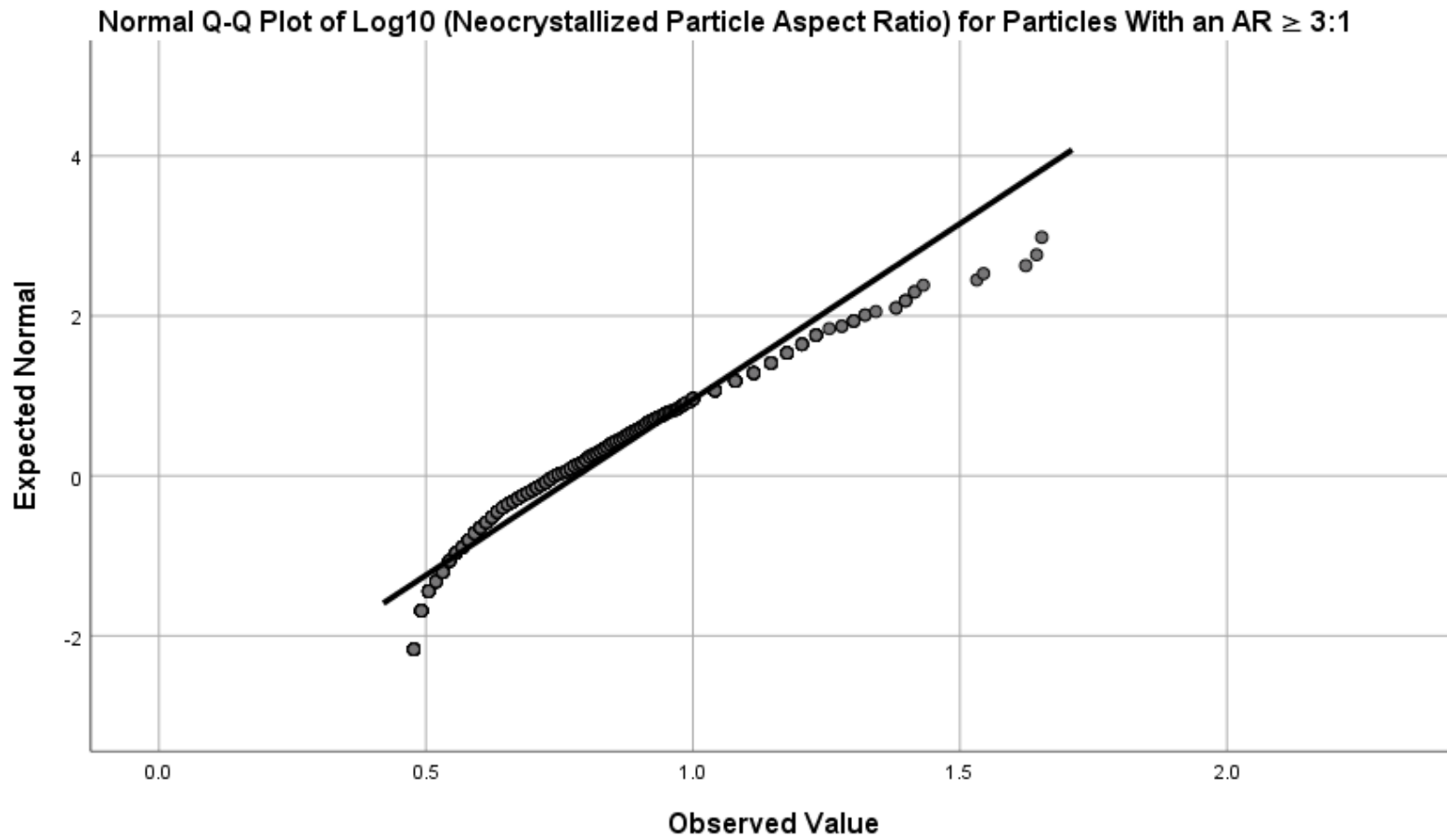


Figure 26. Normal Q-Q Plot of Log10 (Neocrystallized Particle Aspect Ratio) for Particles with an AR $\geq 3:1$

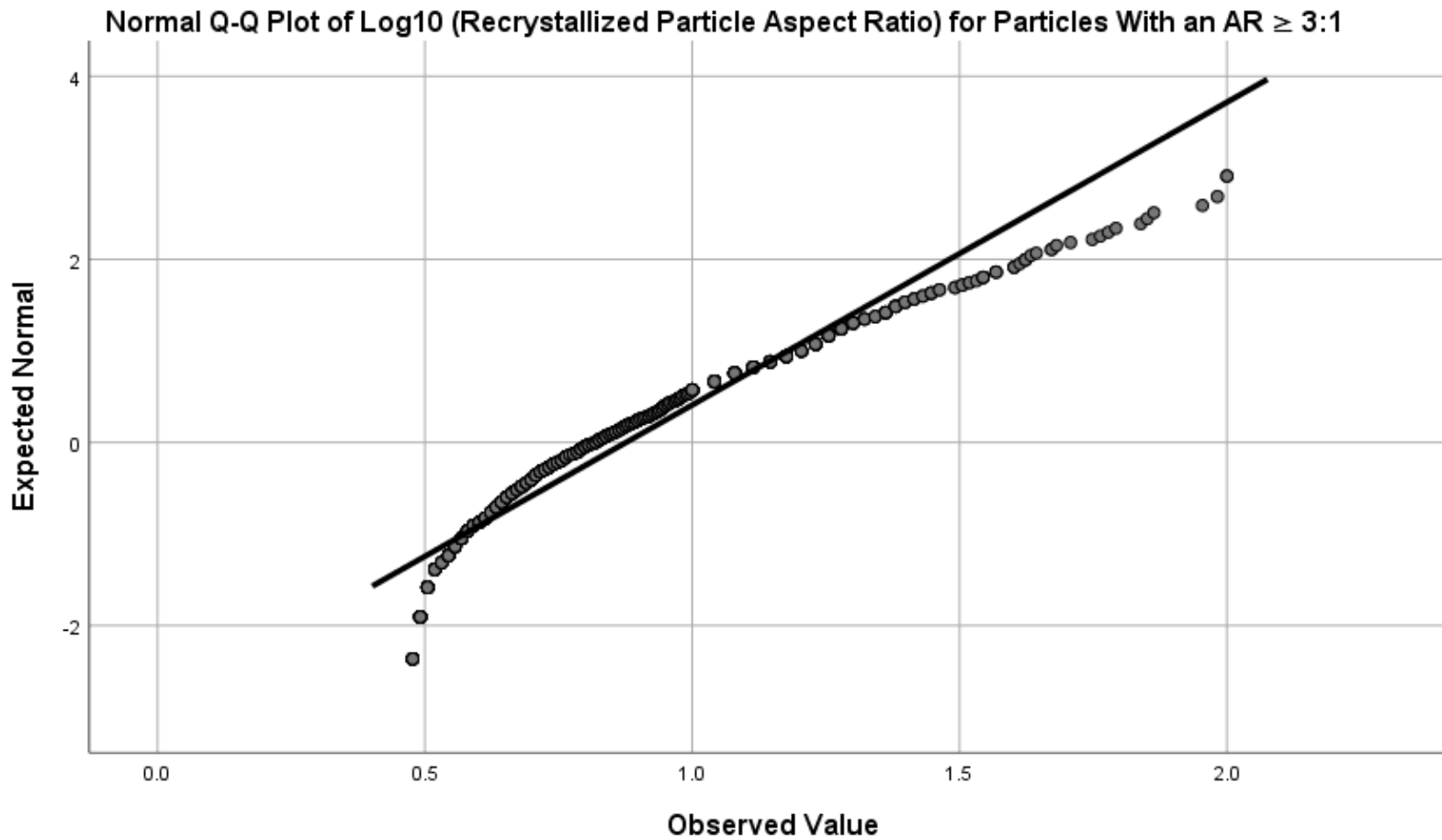


Figure 27. Normal Q-Q Plot of Log10 (Recrystallized Particle Aspect Ratio) for Particles with an AR \geq 3:1

Detrended Normal Q-Q Plot of Log10 (Neocrystallized Particle Aspect Ratio) for Particles With an AR \geq 3:1

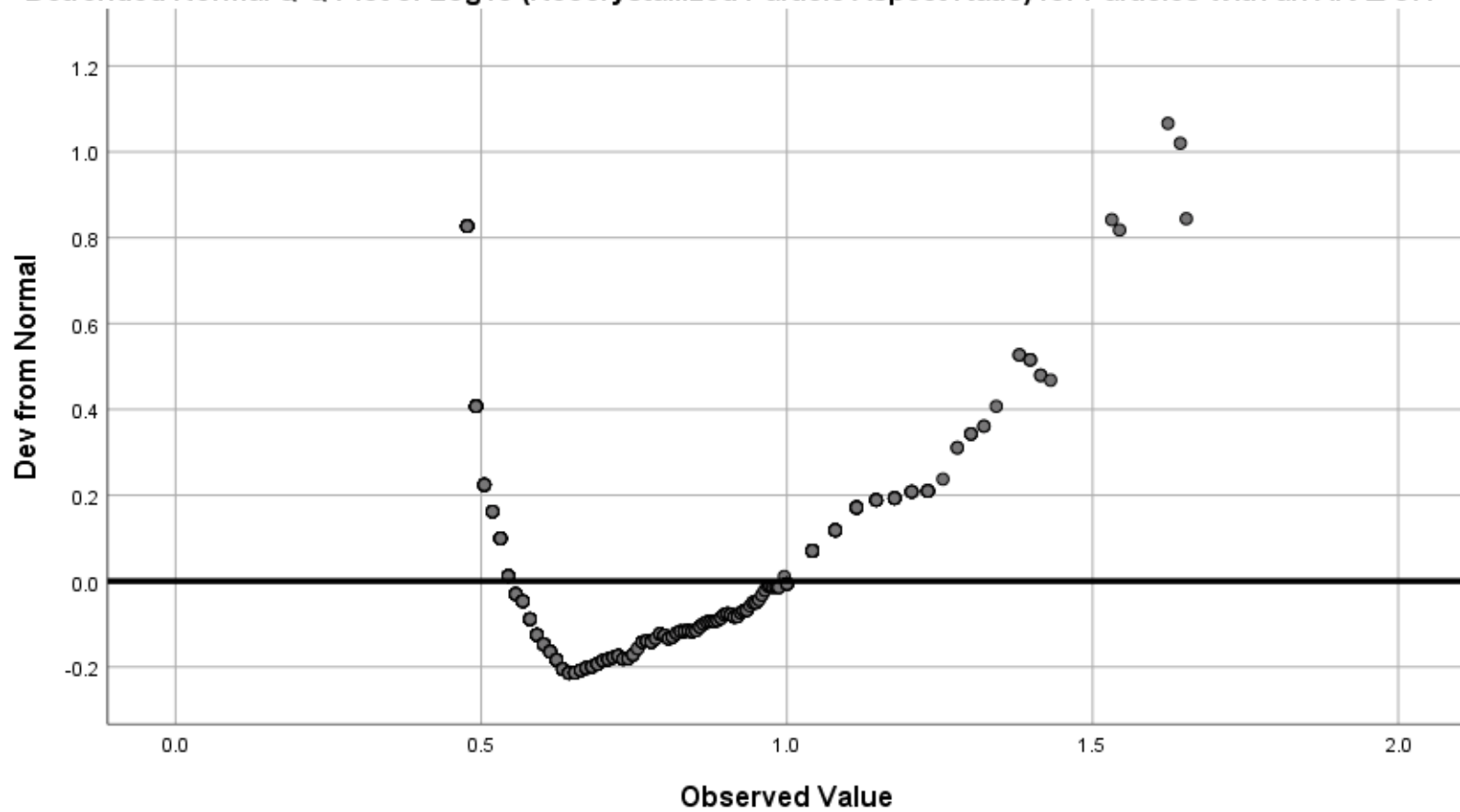


Figure 28. Detrended Normal Q-Q Plot of Log10 (Neocrystallized Particle Aspect Ratio) for Particles with an AR \geq 3:1

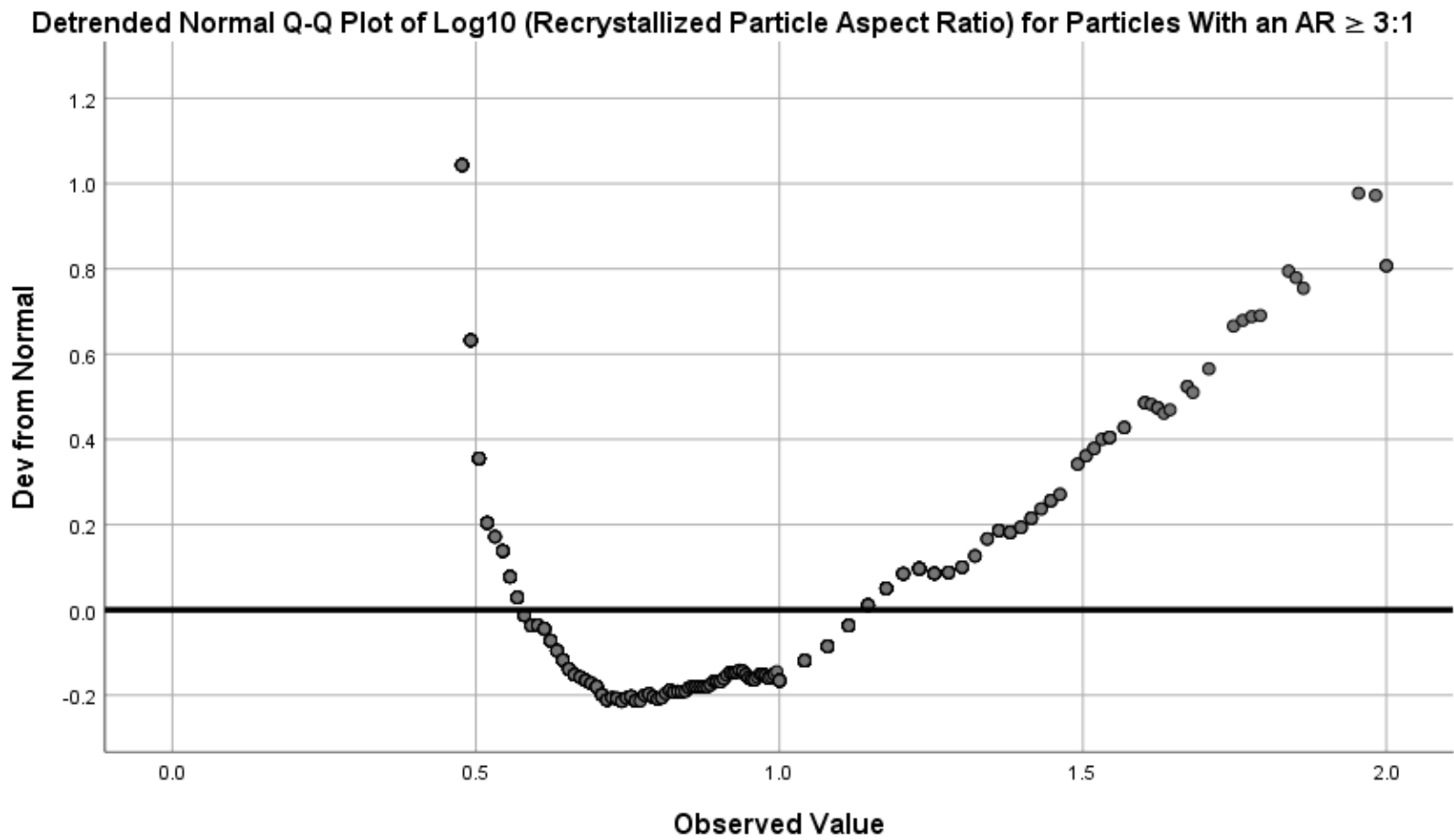


Figure 29. Detrended Normal Q-Q Plot of Log10 (Recrystallized Particle Aspect Ratio) for Particles with an AR $\geq 3:1$

Mann Whitney U-Test Formula:

$$U_1 = R_1 - \frac{n_1(n_1 + 1)}{2}$$

$$U_2 = R_2 - \frac{n_2(n_2 + 1)}{2}$$

Where:

R_1, R_2 are the sum of ranks in sample 1 and 2 respectively

n_1, n_2 are population sizes in sample 1 and sample 2 respectively

Figure 30. U-Test formula that will be used to compare neocrystallized (population 1) and recrystallized (population 2) fibrous amphibole fibers to see if they are significantly different or similar.

U-Test Analyses

All Data Neocrystallized Vs. Recrystallized	SEM Neocrystallized Vs. SEM Recrystallized	FESEM Neocrystallized Vs. FESEM Recrystallized	FESEM Data Vs. SEM Data
Neocrystallized Particles (population 1) Vs. Recrystallized Particles (population 2)	SEM Neocrystallized Particles (population 1) Vs. SEM Recrystallized Particles (population 2)	FESEM Neocrystallized Particles (population 1) Vs. FESEM Recrystallized Particles (population 2)	FESEM Particles (population 1) Vs. SEM Particles (population 2)
Test 1: Population 1 lengths Vs. Population 2 lengths	Test 1: Population 1 lengths Vs. Population 2 lengths	Test 1: Population 1 lengths Vs. Population 2 lengths	Test 1: Population 1 lengths Vs. Population 2 lengths
Test 2: Population 1 widths Vs. Population 2 Widths	Test 2: Population 1 widths Vs. Population 2 Widths	Test 2: Population 1 widths Vs. Population 2 Widths	Test 2: Population 1 widths Vs. Population 2 Widths
Test 3: Population 1 aspect ratios Vs. Population 2 aspect ratios	Test 3: Population 1 aspect ratios Vs. Population 2 aspect ratios	Test 3: Population 1 aspect ratios Vs. Population 2 aspect ratios	Test 3: Population 1 aspect ratios Vs. Population 2 aspect ratios

Figure 31. Plan for statistical comparison between neocrystallized and recrystallized fibrous amphiboles for McCullough Range, NV.

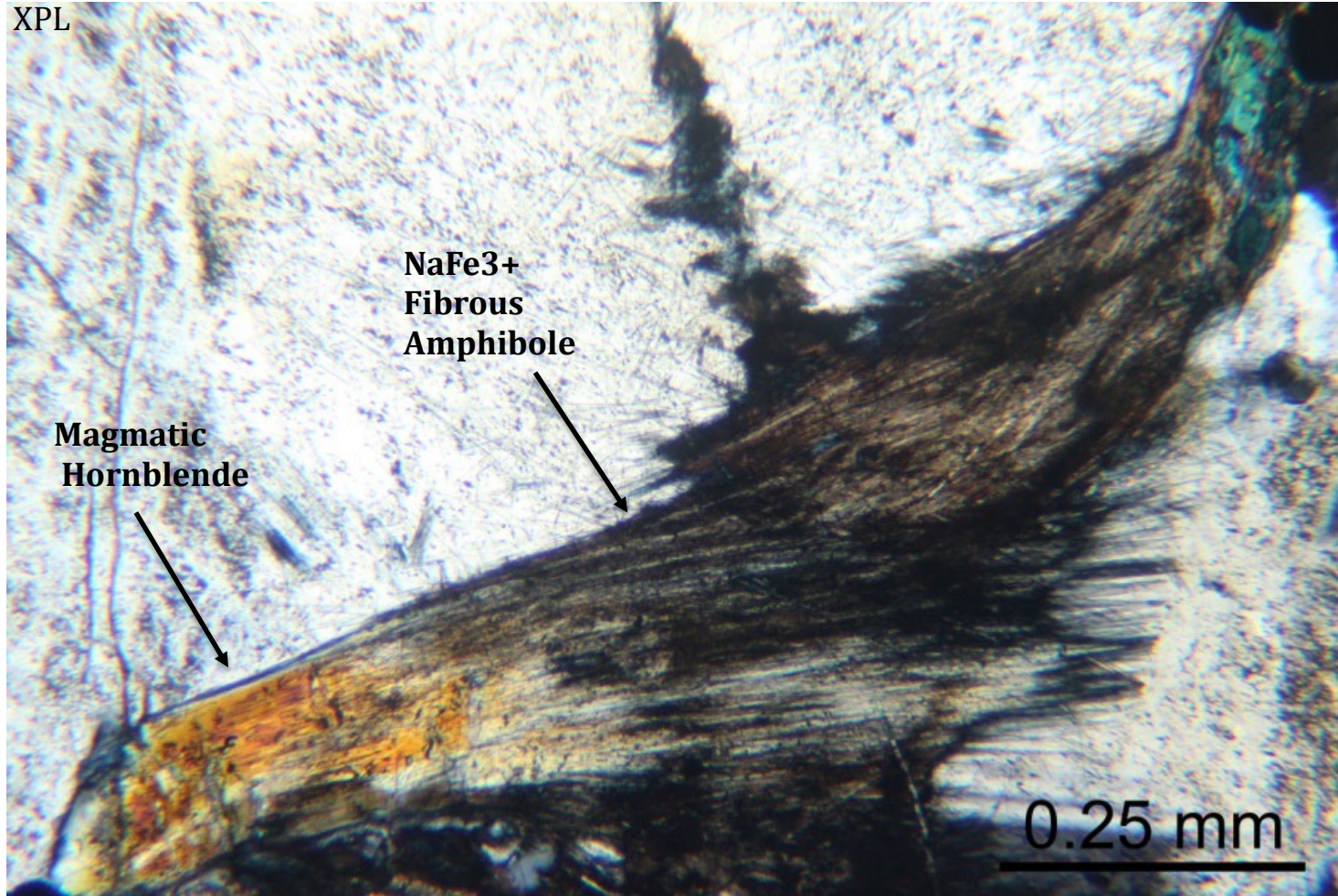


Figure 32. NOA formed via replacement of magmatic magnesio-hornblende (left arrow) into NaFe³⁺ fibrous amphibole (right arrow) asbestos surrounded by altered albite. Fibrous amphibole is intergrown with albite (right edge) along the amphibole pseudomorph boundary. Cross polarized light. Photo courtesy of Rodney Metcalf. Modified from Austin et al. (2019).

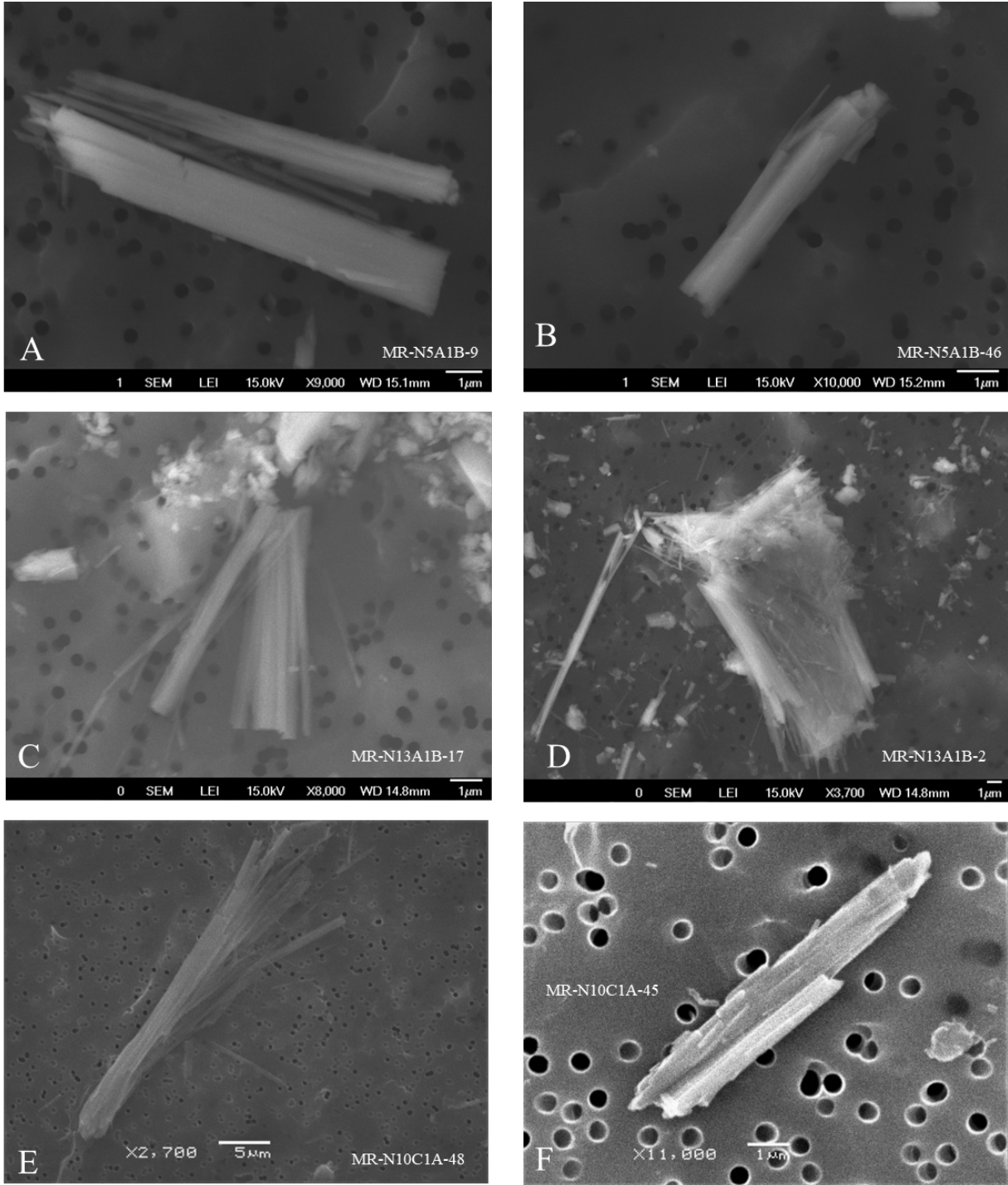


Figure 33. FESEM (A-D) and SEM (E-F) photomicrographs of neocrystallized fibrous amphibole bundles.

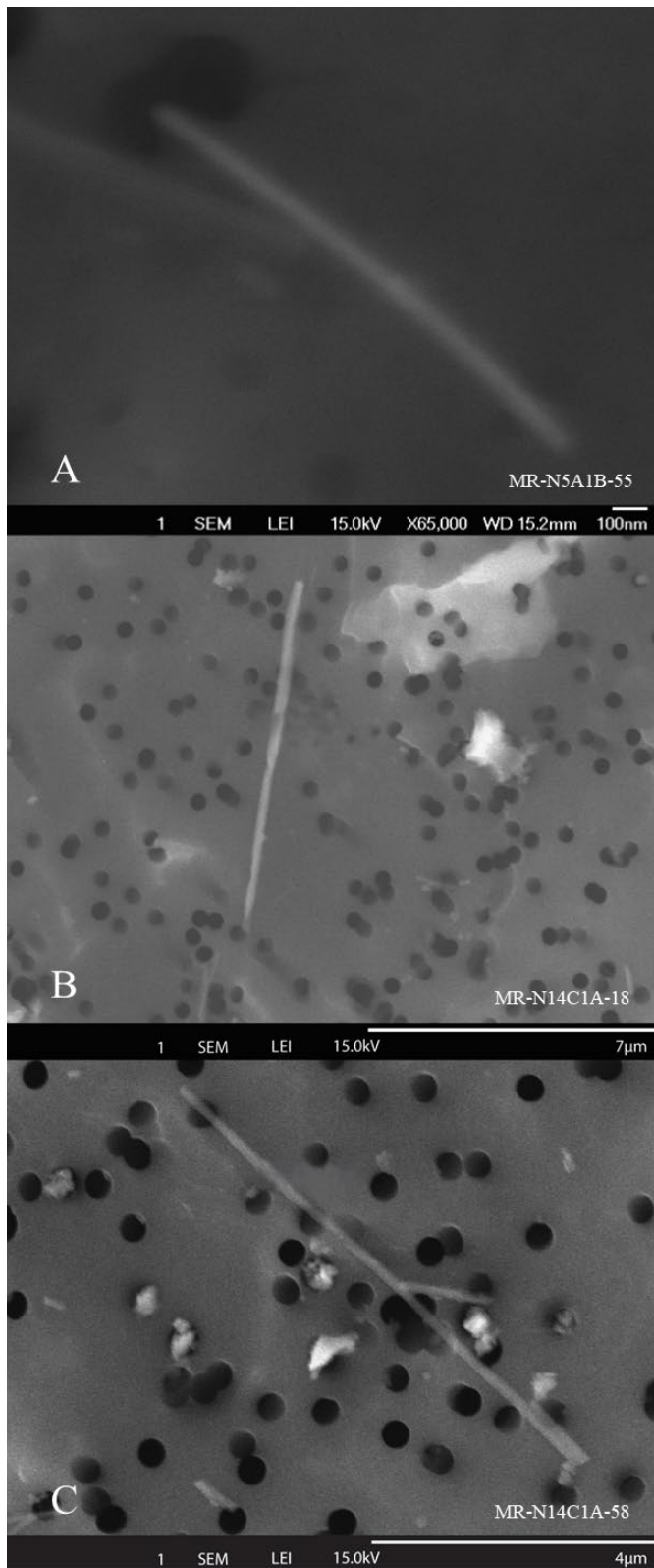


Figure 34 (A-C). FESEM photomicrographs of neocrystallized fibrous amphibole fibers.

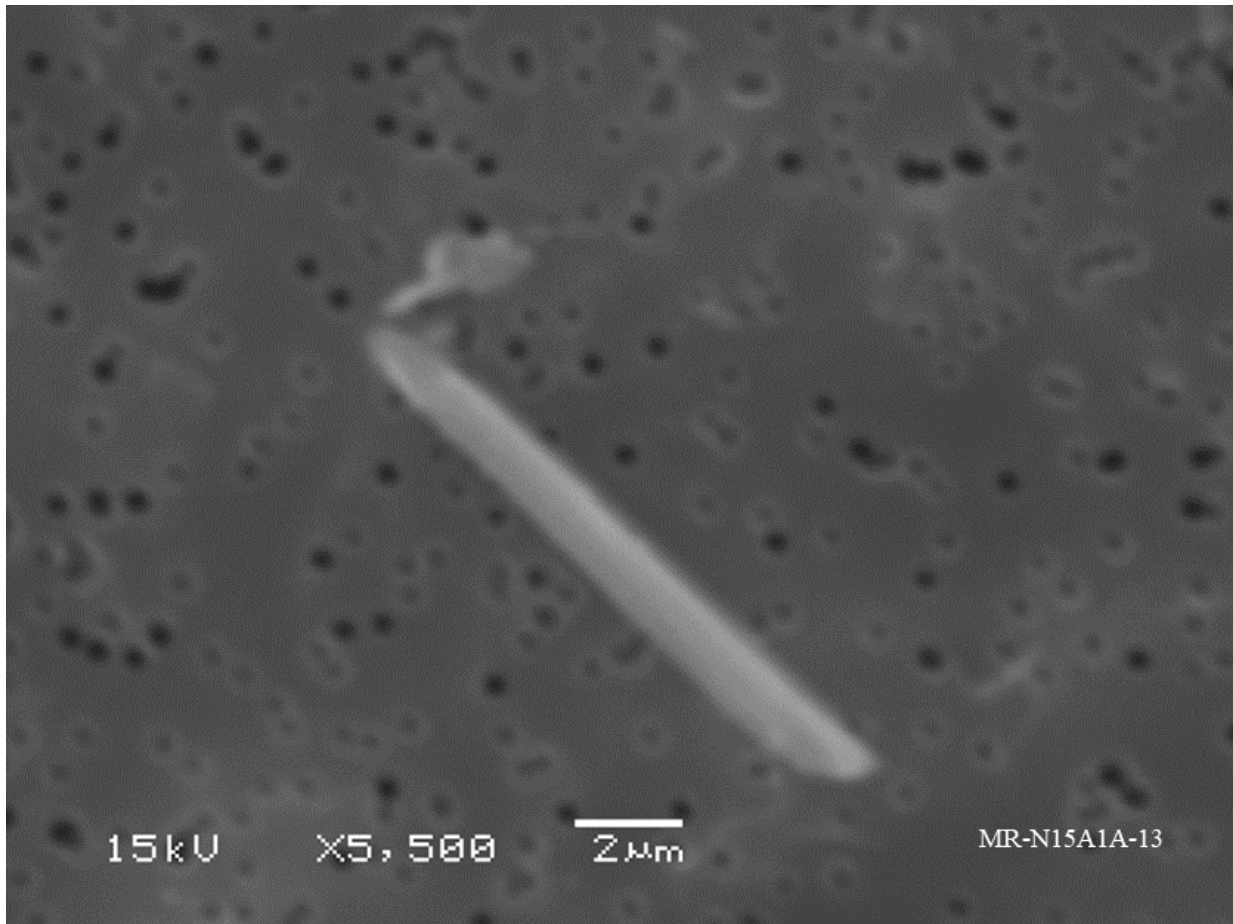


Figure 35. SEM photomicrograph of a neocrystallized prismatic crystal.



Figure 36(A-C). FESEM photomicrographs of recrystallized fibrous amphibole bundles.

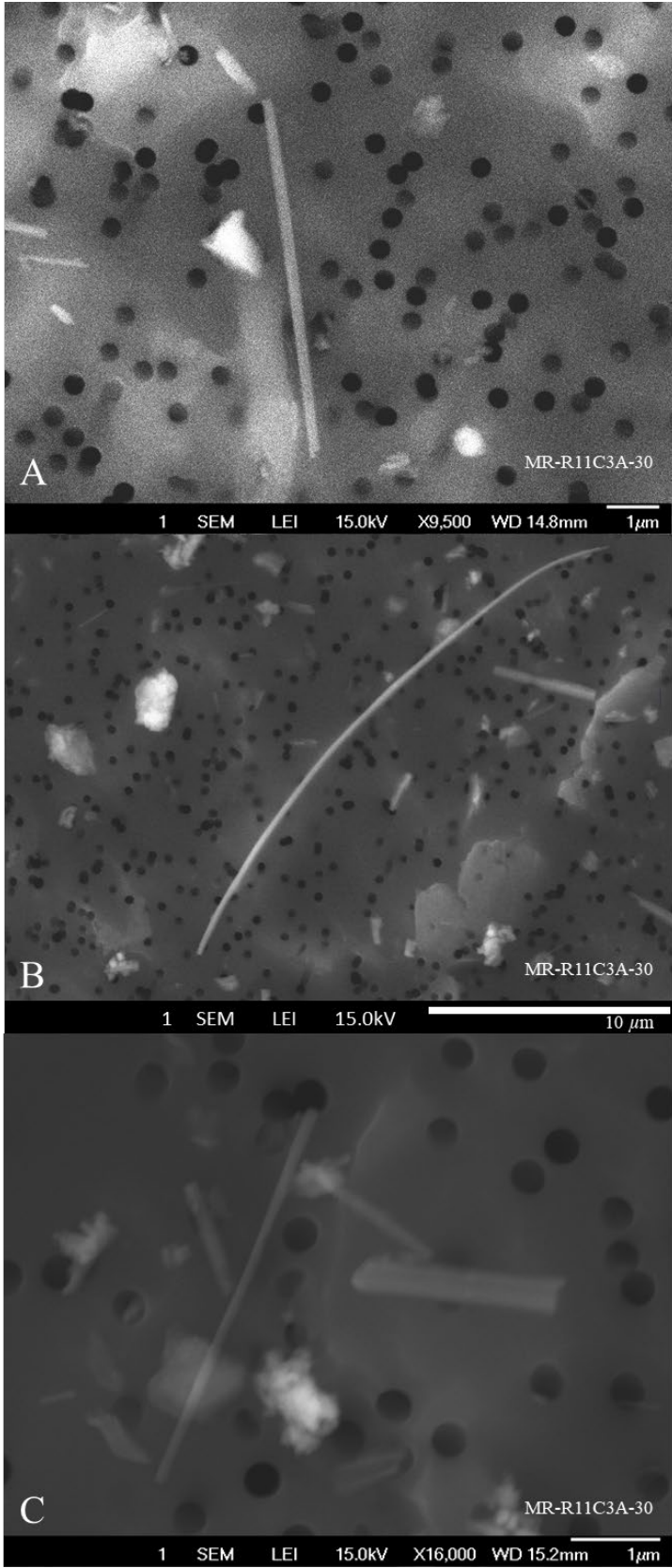


Figure 37(A-C). FESEM photomicrographs of recrystallized fibrous amphibole fibers.

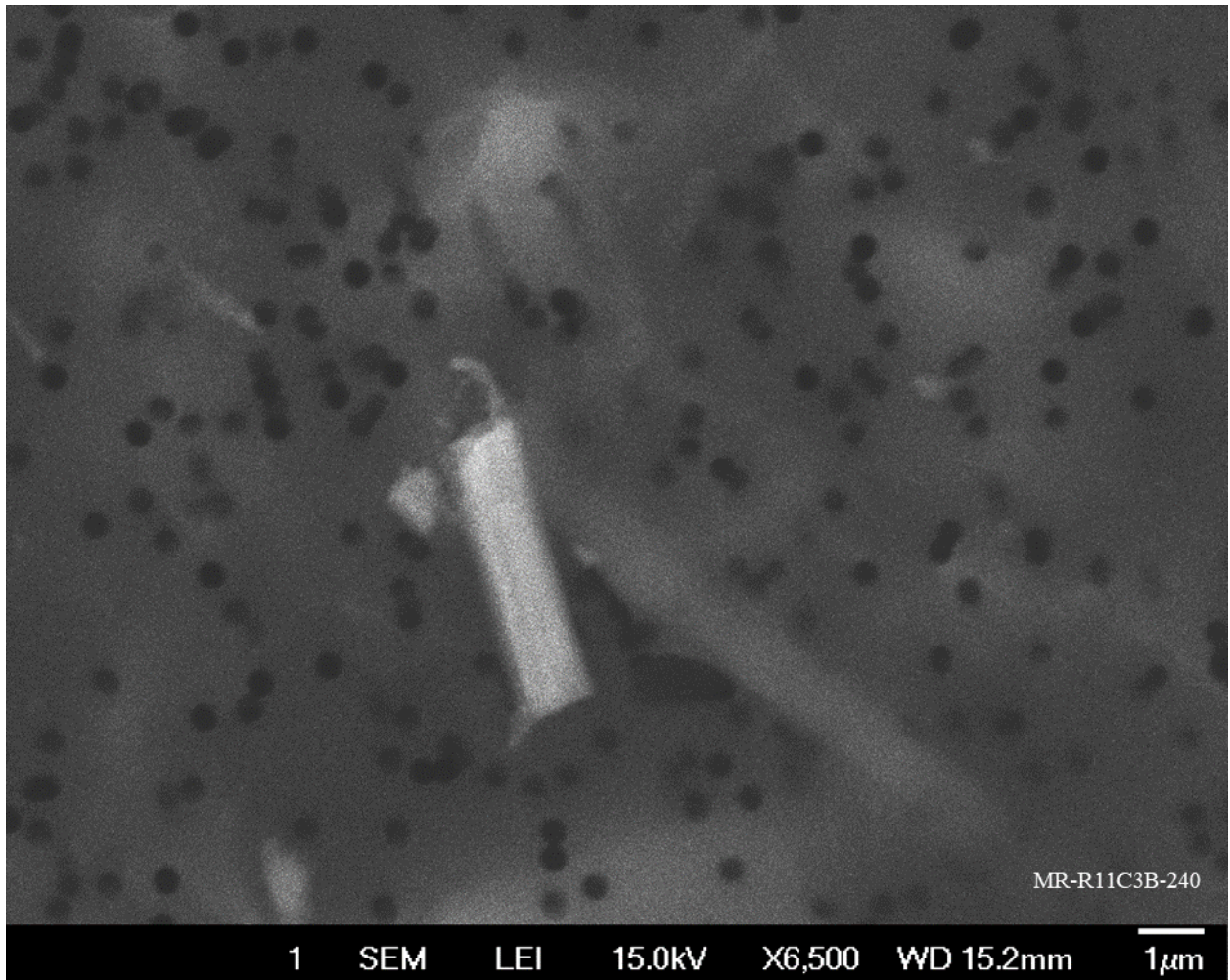


Figure 38. FESEM photomicrographs of recrystallized prismatic crystal.

MR data set

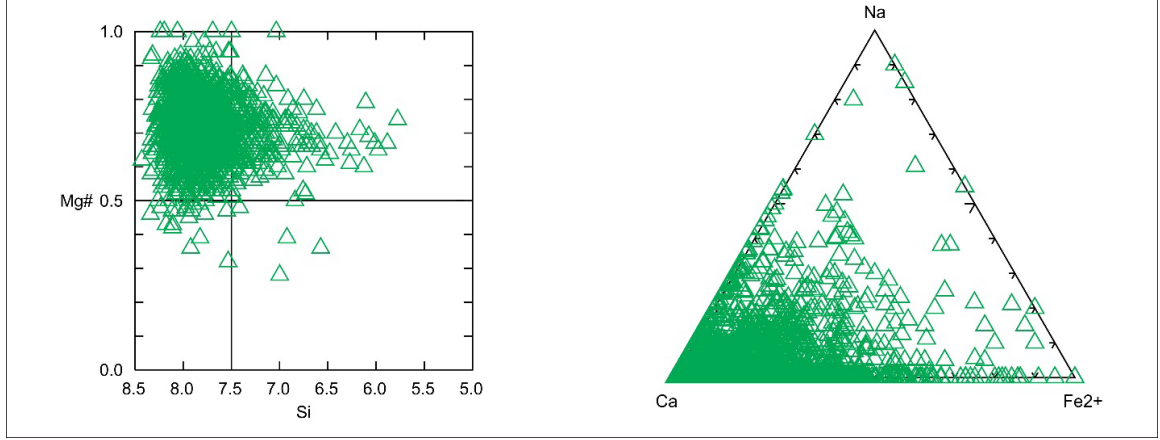


Figure 39. SEM EDS analysis of my data set showing particles plotting mainly as calcic amphiboles.

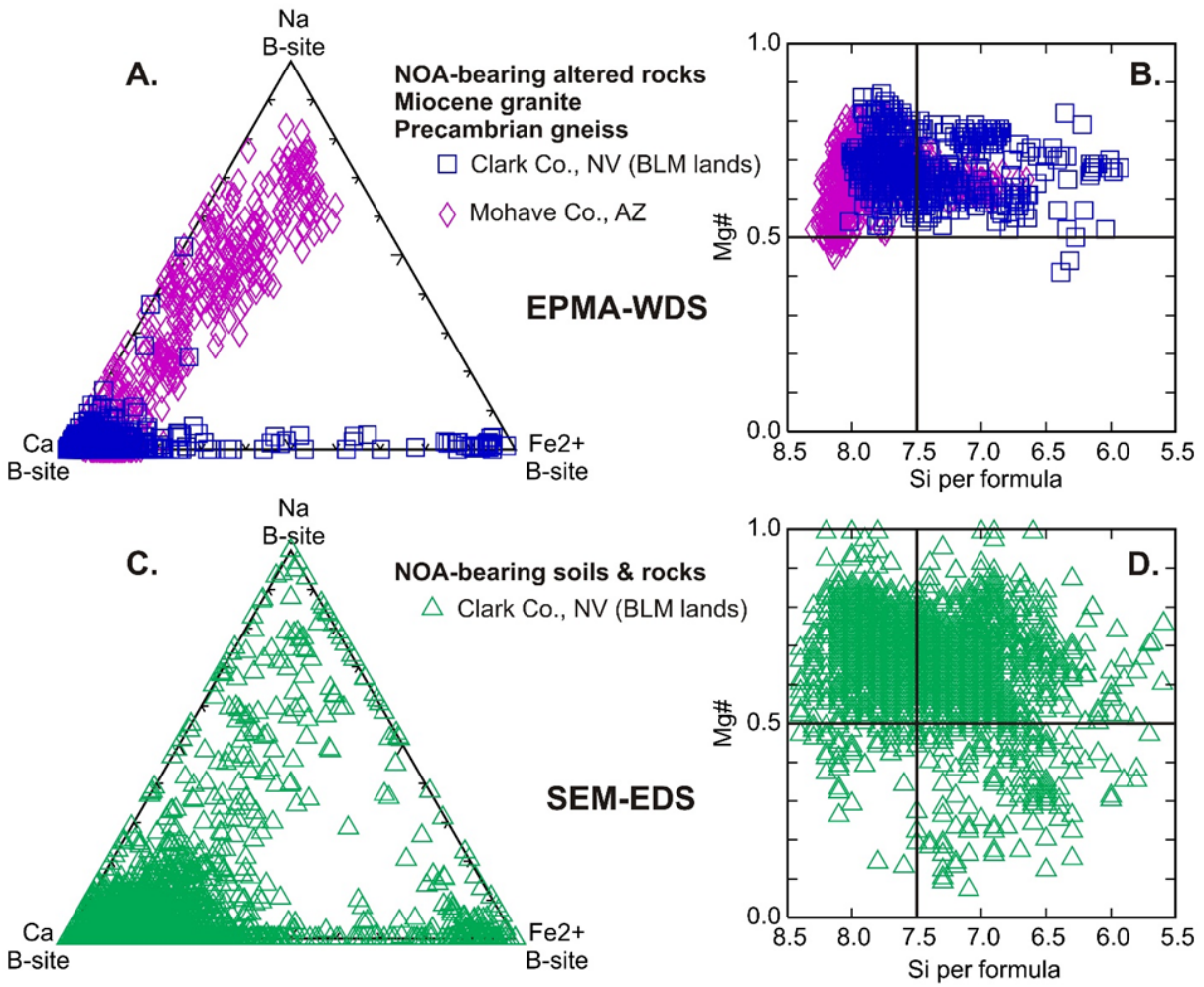
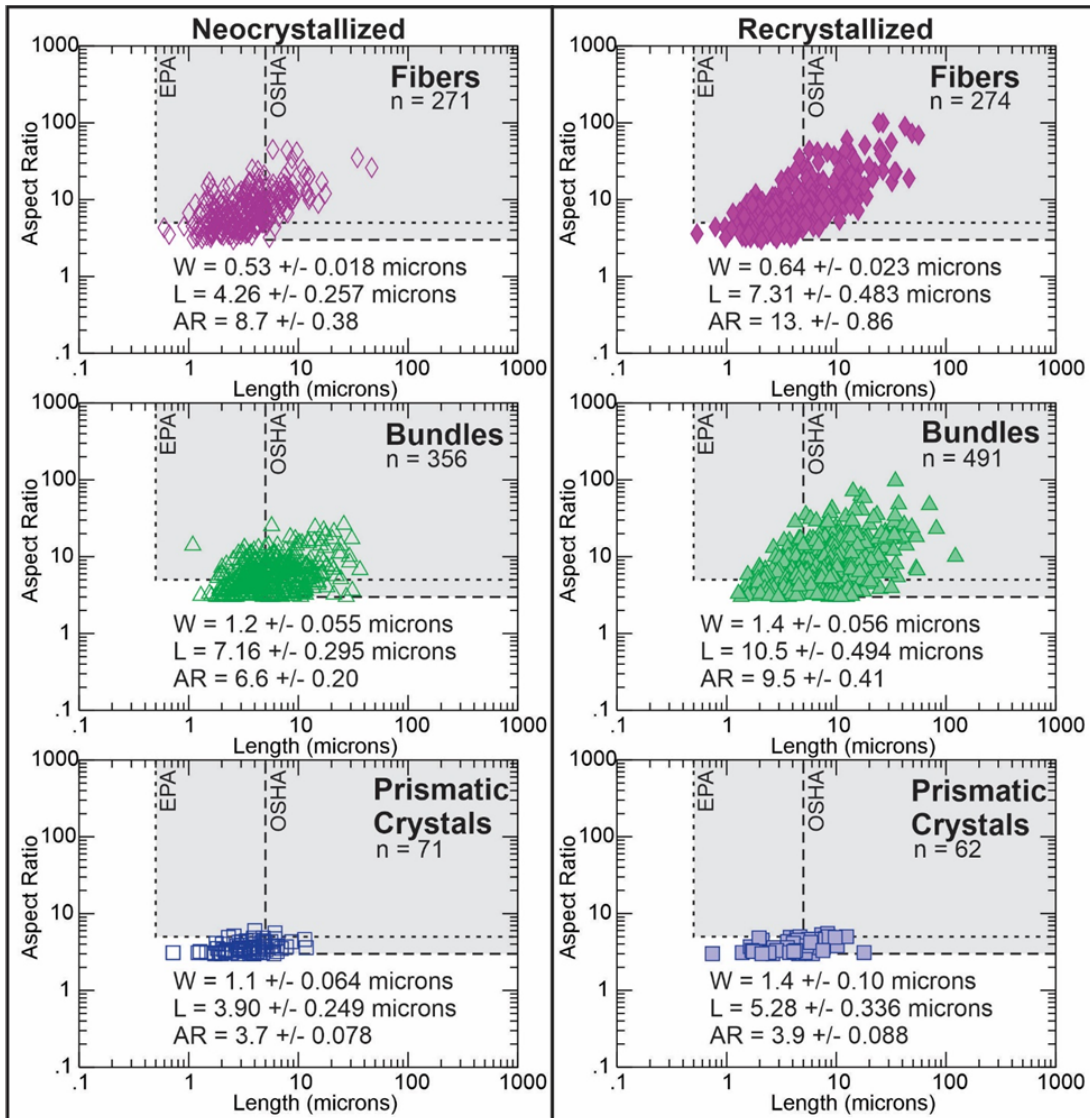


Figure 40. A/B) EPMA-WDS analyses from Metcalf et al. (2018). C/D) SEM EDS analyses from Metcalf et al. (2018). All figures show NV samples plotting mainly as calcic amphiboles.



OSHA Asbestos Fiber Regulation: $L \geq 5 \mu\text{m}$ and $AR \geq 3:1$
 EPA TEM Asbestos Fiber Dimensions: $L \geq 0.5 \mu\text{m}$ and $AR \geq 5:1$

Figure 41. All Neocrystallized (open shapes) and recrystallized (solid shapes) amphibole data plotted aspect ratio vs. length. All plots contain both OSHA's regulatory definition and EPA TEM Counting definition of an asbestos fiber.

Appendix C: Supplemental Data

All supplemental data can be found in ProQuest.

References

- Addingley, C. G. (1996). Asbestos dust and its measurements. *The Annals of Occupational Hygiene*, 9(2), 73-82.
- Ahn, J. H., & Buseck, P. R. (1991). Microstructures and fiber-formation mechanisms of crocidolite asbestos. *The American Mineralogist*, 76(9-10), 1467-1478.
- Akai, J. (1982). Polymerization process of biopyribole in metasomatism at the Akatani ore deposit, Japan. *Contributions to Mineralogy and Petrology*, 80(2), 117-131.
- Alder, Roessler, & Roessler, Edward B. (1964). Introduction to probability and statistics (3d ed.). W. H. Freeman.
- Allen, L. P., Baez, J., Stern, M. E. C., Takahashi, K., & George, F. (2018). Trends and the economic effect of asbestos bans and decline in asbestos consumption and production worldwide. *International Journal of Environmental Research and Public Health*, 15(3), 531. doi:10.3390/ijerph15030531
- American Society for Testing and Materials. (1995) Standard test method for microvacuum sampling and indirect analysis of dust by transmission electron microscopy for asbestos structure number concentrations: West Conshohocken, Pa., ASTM 5755-95, 13 p.
- Agency for Toxic Substances and Disease Registry. (2001). Toxicological profile for asbestos. ATSDR, Atlanta, GA. <https://www.atsdr.cdc.gov/toxprofiles/tp61.pdf> (accessed 7 Mar. 2023).
- Aust, A. E., Cook, P. M., & Dodson, R. F. (2011). Morphological and chemical mechanisms of elongated mineral particle toxicities. *Journal of Toxicology and Environmental Health. Part B, Critical Reviews*, 14(1-4), 40-75. doi:10.1080/10937404.2011.556046
- Austin, T. (2019). Petrogenesis of unusual occurrence of amphibole asbestos in mohave county, arizona and clark county, nevada (Order No. 22583757). Available from Dissertations & Theses @ University of Nevada Las Vegas; ProQuest One Academic. (2312585188). Retrieved from

<https://www.ezproxy.library.unlv.edu/login?url=https://www.proquest.com/dissertations-theses/petrogenesis-unusual-occurrence-amphibole/docview/2312585188/se-2>

- Bailey, K.F., Kelse, J., Wylie, A.G., and Lee, R.J. (2004). Prismatic and Asbestiform Growth Habit. www.cdc.gov/niosh/docket/archive/pdgs/NIOSH-099A/0099A-030104-PictorialPresentation.pdf. Accessed 8 Apr 2018.
- Baumann, F., Ambrosi, J., & Carbone, M. (2013). Asbestos is not just asbestos: An unrecognised health hazard. *The Lancet Oncology*, 14(7), 576-578.
- Beard, M.E., Crankshaw, O.S., Ennis, J.T., and Moore, C.E. (2001). Analysis of crayons for asbestos and other fibrous materials, and recommendations for improved analytical definitions: Research Triangle Park, North Carolina, Research Triangle Institute, Center for Environmental Measurements and Quality Assurance, Earth and Mineral Sciences Department, [informal report], 23 p., plus appendices A-H.
- Beaven, L. (2014). FINAL EPA ASSESSMENT OF LIBBY ASBESTOS EASES NON-CANCER RISK FINDINGS. *Inside EPA's Risk Policy Report*, p. Inside EPA's Risk Policy Report, Dec 9, 2014, Vol.21(48).
- Boulanger, G., Andujar, P., Paireon, J., Billon-Galland, M., Dion, C., Dumortier, P., . . . Jaurand, M. (2014). Quantification of short and long asbestos fibers to assess asbestos exposure: A review of fiber size toxicity. *Environmental Health*, 13(1), 59.
- Buck, B., Goossens, D., Metcalf, R., McLaurin, B., Ren, M., & Freudenberger, F. (2013). Naturally occurring asbestos: Potential for human exposure, southern Nevada, USA. *Soil Science Society of America Journal*, 77(6), 2192-2204. doi:10.2136/sssaj2013.05.0183
- Buck, B. J., Londono, S. C., McLaurin, B. T., Metcalf, R., Mouri, H., Selinus, O., . . . Institutionen för biologi och miljö (BOM). (2016). The emerging field of medical geology in brief: Some examples. *Environmental Earth Sciences*, 75(6), 1-13. doi:10.1007/s12665-016-5362-6

- Buck, B. J., Metcalf, R. V, & McLaurin, B. T. (2018). *Naturally-Occurring Asbestos in Southern Nevada*.
https://www.unlv.edu/sites/default/files/page_files/27/Sciences-NaturallyOccurringAsbestos-FinalReport.pdf
- Camargo, M., L. Stayner, K. Straif, M. Reina, U. Al-Alem, P. Demers, and P. Landrigan. (2011). Occupational exposure to asbestos and ovarian cancer. *Environ. Health Perspect.* 119:1211–1217.
doi:10.1289/ehp.1003283
- Clinkenbeard, J.P., Churchill, R.K., and Lee, K. (2002). Guidelines for Geologic Investigations of Naturally Occurring Asbestos in California. California Department of Conservation.
http://www.conservation.ca.gov/cgs/minerals/hazardous_minerals/asbestos/documents/asbestos_guidelines_sp124.pdf.
- Cooper, C. D., & Alley, F. C. (2011). *Air pollution control: A design approach*, 4th Edition. Waveland press.
- Davis, J., Addison, J., McINTOSH, C., Miller, B., & Niven, K. (1991). Variations in the Carcinogenicity of Tremolite Dust Samples of Differing Morphology. *Annals of the New York Academy of Sciences*, 643(1), 473-490.
- Dement, J. M., & Wallingford, K. M. (1990). Comparison of phase contrast and electron microscopic methods for evaluation of occupational asbestos exposures. *Applied Occupational and Environmental Hygiene*, 5(4), 242-247.
- Dodson, R., Atkinson, M., & Levin, J. (2003). Asbestos fiber length as related to potential pathogenicity: A critical review. *American Journal of Industrial Medicine*, 44(3), 291-297.
- D. Egilman, J. E. Steffen, T. Tran, K. Clancy, M. Rigler, and W. Longo, “Health Effects of Censored Elongated Mineral Particles: A Critical Review,” in *Detection Limits in Air Quality and Environmental Measurements*, ed. M. J. Brisson, (2019), (West Conshohocken, PA: ASTM International, 192–239). <http://doi.org/10.1520/STP1618201800805>

- Erskine, B., & Bailey, M. (2018). Characterization of asbestiform glaucophane-winchite in the Franciscan Complex blueschist, northern Diablo Range, California. *Toxicology and Applied Pharmacology*, 361, 3-13.
- Gamble, J.F. and Gibbs, G.W. (2008). An evaluation of the risks of lung cancer and mesothelioma from exposure to amphibole cleavage fragments. *Regulatory Toxicology and Pharmacology*, 52(1), S154-S186.
- Goldstein, J., Newbury, D., Joy, D., Lyman, C., Echlm, P., Lifshin, E., Sawyer, L., & Micheal, J. (2003). Scanning Electron Microscopy and X-ray Microanalysis - Third Edition. In *Springer*. https://doi.org/10.1007/978-1-4615-0215-9_5
- Gunter, M., Belluso, E., & Mottana, A. (2007). Amphiboles; environmental and health concerns. *AMPHIBOLES: CRYSTAL CHEMISTRY, OCCURRENCE, AND HEALTH ISSUES*, 67(1), 453-516.
- Harper, M. (2008). 10th Anniversary critical review: Naturally occurring asbestos. *J. Environ. Monit.* 10:1394–1408. doi:10.1039/b810541n International Agency for Research on Cancer, 2012
- Holmes, S. (1965). DEVELOPMENTS IN DUST SAMPLING AND COUNTING TECHNIQUES IN THE ASBESTOS INDUSTRY. *Annals of the New York Academy of Sciences*, 132(1), 288-297.
- IBM Corp. Released 2021. IBM SPSS Statistics for Windows, Version 28.0. Armonk, NY: IBM Corp.
- International Agency for Research on Cancer. (2012). Asbestos. In: *A review of human carcinogens*. IARC Monogr. Eval. Carcinogenic Risks to Humans 100C. WHO Press, Lyon, France. p. 219– 294.
- Langer, A.M., (1970). Electron microprobe analysis study of asbestos fibers and bodies from lung tissue Lab. Diagn.Dis. Caused Toxic Agents, Ed., Proc. Appl. Semin. 126-136.
- Langer, A.M., Selikoff, I., & Sastre, A. (1971). Chrysotile Asbestos in the Lungs of Persons in New York City. *Archives of Environmental Health*, 22(3), 348-361.

- Langer, A. M., Ashley, R., Baden, V., Berkley, C., Hammond, E. C., Mackler, A. D., ... & Selikoff, I. J. (1973). Identification of asbestos in human tissues. *Journal of Occupational Medicine*, 15(3), 287-295.
- Langer, A., Wolff, M., Rohl, A., & Selikoff, I. (1978). Variation of properties of chrysotile asbestos subjected to milling. *Journal of Toxicology and Environmental Health*, 4(1), 173-188.
- LAERD Statistics. (2018). Mann-Whitney U Test using SPSS Statistics. URL: <https://statistics.laerd.com/spss-tutorials/mann-whitney-u-test-using-spss-statistics.php>
- Leake, B., Woolley, A., Arps, C., Birch, W., Gilbert, M., Grice, J., . . . Youzhi, G. (1997). Nomenclature of amphiboles: Report of the subcommittee on amphiboles of the international mineralogical association, commission on new minerals and mineral names. *Canadian Mineralogist*, 35(1), 219-246.
- Lee, R., Strohmeier, B., Bunker, K., & Van Orden, D. (2008). Naturally occurring asbestos—A recurring public policy challenge. *Journal of Hazardous Materials*, 153(1), 1-21.
- Lippmann, M. (1988). Asbestos exposure indices. *Environmental research*, 46(1), 86-106.
- Lowers, H., and G. Meeker. (2002). Tabulation of asbestos-related terminology. USGS Open-File Rep. 02-458. USGS, Reston, VA. <http://pubs.usgs.gov/of/2002/ofr-02-458/index.html> (accessed 18 Apr. 2013).
- LYNCH, J. R., AYER, H. E., & JOHNSON, D. L. (1970). The interrelationships of selected asbestos exposure indices. *American Industrial Hygiene Association Journal*, 31(5), 598-604.
- Meeker, G.P., Bern, A.M., Brownfield, I.K., Lowers, H.A., Sutley, S.J., Hoefen, T.M., and Vance, J.S. (2003). The Composition and Morphology of Amphiboles from the Rainy Creek Complex, Near Libby Montana: *American Mineralogist*, v. 88, p. 1955.

- Meeker, G., H. Lowers, G. Swayze, B. Van Gosen, S. Sutley, and I. Brownfield. (2006). Mineralogy and morphology of amphiboles observed in soils and rocks in El Dorado Hills, California. USGS Open-File Rep. 2006-1362. USGS, Reston, VA.
- Merewether, E. R. A., & Price, C. W. (1930). Report on Effects of Asbestos Dust on the Lungs and Dust Suppression in the Asbestos Industry. Part I. Occurrence of Pulmonary Pibrosis and Other Pulmonary Affections in Asbestos Workers. *Report on Effects of Asbestos Dust on the Lungs and Dust Suppression in the Asbestos Industry. Part I. Occurrence of Pulmonary Pibrosis and Other Pulmonary Affections in Asbestos Workers.*
- Metcalf, R. and Buck, B. (2015). Genesis and health risk implications of an unusual occurrence of fibrous NaFe³⁺-amphibole. *Geology*, 43(1), 63-66. doi:10.1130/G36199.1
- Metcalf et al., 2018 in Buck, B. J., Metcalf, R. V, & Mclaurin, B. T. (2018). *Naturally-Occurring Asbestos in Southern Nevada*. https://www.unlv.edu/sites/default/files/page_files/27/Sciences-NaturallyOccurringAsbestos-FinalReport.pdf
- Miller, A., Langer, A. M., Teirstein, A. S., & Selikoff, I. J. (1975). “Nonspecific” interstitial pulmonary fibrosis: association with asbestos fibers detected by electron microscopy. *New England Journal of Medicine*, 292(2), 91-93.
- Mortureux, M. ANSES (The French Agency for Good, Environmental and Occupational Health & Safety). (2015). OPINION of the French Agency for Food Environmental and Occupational Health & Safety on “Health Effects and the identification of cleavage fragments of amphiboles from quarried minerals. Available from: <https://www.anses.fr/en/content/opinion-anses-health-effects-and-identification-cleavage-fragments-amphiboles-quarried>
- NIOSH recommends asbestos research plan. (2011). *Professional Safety*, 56(5), 20.
- NIOSH. (1990). Testimony of the National Institute for Occupational Safety and Health on the Occupational Safety and Health Administration’s Notice of Proposed Rulemaking on Occupational

- Exposure to Asbestos, Tremolite, Anthophyllite, and Actinolite. Docket No. H-033d, May 9, 1990. https://www.osha.gov/FedReg_osha_pdf/FED19920608.pdf. Accessed 14 June 2018.
- NIOSH. (1972). Occupational exposure to asbestos; criteria for a recommended standard. (1972). U. S. Dept. of Health, Education, and Welfare, Public Health Service, Health Services and Mental Health Administration, National Institute for Occupational Safety and Health; for sale by the Supt. of Docs., U. S. Govt. Print. Off., 1972.
- Occupational Safety and Health Administration. (1987) Code of Federal Regulations 29 CFR 1910.1001 subpart Z(b). Washington, D.C. 1987.
- Perkins, R.L. and Harvey, B.W. (1993). Method for the determination of asbestos in bulk building materials: U.S. Environmental Protection Agency EPA/600/R-93/116, Office of Research and Development, Washington, D.C.
- Perry, A. (2004). A discussion of asbestos detection techniques for air and soil. *US Environmental Protection Agency, Office of Solid Waste and Emergency Response, Office of Superfund Remediation and Technology Innovation Program*.
- Pfau, J. C., Sentissi, J. J., Li, S. A., Calderon-Garciduenas, L., Brown, J. M., & Blake, D. J. (2008). Asbestos-induced autoimmunity in C57BL/6 mice. *Journal of immunotoxicology*, 5(2), 129-137.
- Pfau, J., Serve, K., & Noonan, C. (2014). Autoimmunity and Asbestos Exposure. *Autoimmune Diseases*, 2014(2014), 1-11.
- Pfau, J. C., Serve, K., Woods, L., & Noonan, C. (2016). Asbestos exposure and autoimmunity. *Biological effects of fibrous and particulate substances*, 181-194.
- Pfau, J.C. Immunotoxicity of Asbestos, *Current Opinion in Toxicology*. (2017). doi: 10.1016/j.cotox.2017.11.005.

- Pfau, J.C., Buck, B., Metcalf, R.V., Kaupish, Z., Stair, C., Rodriguez, M., and Keil, D.E. (2017). Comparative health effects in mice of Libby amphibole asbestos and a fibrous amphibole from Arizona. *Toxicology and Applied Pharmacology*, 334, 24-34.
- Jean C. Pfau, Tracy McNew, Kerensa Hanley, Lindsay Swan, Brad Black. (2018) Autoimmune markers for progression of Libby amphibole lamellar pleural thickening. *Inhalation Toxicology* 31:11-12, pages 409-419.
- Plumlee, G. S., Morman, S. A., & Ziegler, T. L. (2006). The toxicological geochemistry of earth materials: An overview of processes and the interdisciplinary methods used to understand them. *Reviews in Mineralogy and Geochemistry*, 64, 5–57. <https://doi.org/10.2138/rmg.2006.64.2>
- POOLEY, F. (1970). THE DETECTION OF ASBESTOS IN TISSUES FD POOLEY, PD OLDHAM, CHANG-HYUN UM and JC WAGNER. In *Pneumoconiosis: Proceedings of the International Conference, Johannesburg, 1969* (p. 108). Oxford University Press.
- Rasband, W.S., ImageJ, U. S. National Institutes of Health, Bethesda, Maryland, USA, <https://imagej.nih.gov/ij/>, 1997-2018.
- Shannahan, J., M. Schladweiler, R. Thomas, W. Ward, A. Ghio, S. Gavett, and U. Kodavanti. (2012). Vascular and thrombogenic effects of pulmonary exposure to Libby amphibole. *J. Toxicol. Environ. Health A* 75:213–231. doi:10.1080/15287394.2012.652055
- Sokal, R., & Rohlf, F. (1969). *Biometry: the principles and practice of statistics in biological research* (2nd ed.). W.H. Freeman and Company.
- Stanton, M. F., Layard, M., Tegeris, A., Miller, E., May, M., Morgan, E., & Smith, A. (1981). Relation of particle dimension to carcinogenicity in amphibole asbestoses and other fibrous minerals. *Journal of the National Cancer Institute*, 67(5), 965–975.
- Tetra Tech. (2014) Final phase 1 site characterization report for Boulder City bypass naturally occurring asbestos (NOA) Project phase 1 (Railroad pass to Silverline Road).

- http://www.nevadadot.com/uploadedFiles/NDOT/Micro-Sites/BoulderCityBypass/NOS/Final_NDOT_Phase_I_Report-10-6-14.pdf. Accessed 8 Apr 2018.
- Thompson, C.S. (1974), Discussion of the mineralogy of industrial talcs: U.S. Bureau of Mines Information Circular 8639, p. 22-42.
- Tweeddale, G. (2000). Science or public relations?: The inside story of the Asbestosis Research Council, 1957-1990. *American Journal of Industrial Medicine*, 38(6), 723-734.
- Taber, S. (1916). The Origin of Veins of the Asbestiform Minerals. *Proceedings of the National Academy of Sciences - PNAS*, 2(12), 659-664.
- U.S. EPA. (2011). U.S. Code of Federal Regulations. 40 CFR 763 subpart E, App. A. Washington, D.C. 2011.
- U.S. EPA. (2014). Toxicological review of Libby Amphibole asbestos, EPA/635/R-11/002F. <http://1.usa.gov/1SvBqoe>. Accessed 8 Apr 2018.
- U.S. Geological Survey. (2020). Mineral commodity summaries 2020: U.S. Geological Survey, 200 p., <https://doi.org/10.3133/mcs2020>
- Van Gosen, B. S. (2007). The geology of asbestos in the United States and its practical applications. *Environmental and Engineering Geoscience*, 13(1), 55-68. doi:10.2113/gsegeosci.13.1.55
- Veblen, D., Buseck, P., & Burnham, C. (1977). Asbestiform chain silicates: New minerals and structural groups. *Science (New York, N.Y.)*, 198(4315), 359-365.
- Virta, R. (2002). Asbestos: Geology, mineralogy, mining, and uses. USGS OpenFile Rep. 02-149. USGS, Reston, VA.
- Van Gosen, B. (2007). The geology of asbestos in the United States and its practical applications. *Environmental & Engineering Geoscience*, 13(1), 55-68.

- Wheater, C. P., and Cook, P. A. (2000). *Using Statistics to Understand the Environment*, Routledge, Routledge Introductions to Environment Series
- WHO Regional Office. (2000). Air Quality Guidelines. In F. Theakston (Ed.), *Air Quality Guidelines* (Second, Vol. 22, Issue 8). <https://doi.org/10.1007/BF02986808>
- Wolfe, C., B. Buck, A. Miller, J. Lockey, C. Weis, D. Weissman, A. Jonesi, and P. Ryan. (2017). Exposure to naturally occurring mineral fibers due to off-road vehicle use: A review. *Int J Hyg Environ Health*.
- Wylie, A. G., and Schweitzer, P. (1982). The effects of sample preparation and measuring techniques on the shape and shape characterization of mineral particles; the case of wollastonite: *Environmental Research* (New York, N.Y.), v. 27, no. 1, p. 52.

Curriculum Vitae

Natalie Renkes

email: natalie.renkes@unlv.edu

Education & Certifications

University of Nevada,
Las Vegas (UNLV)
Masters in Geoscience
Expected Graduation Date:
May 2023

Grand Valley State
University (GVSU)
Bachelor of Science in
Geology, Minor in
Anthropology
Graduated: April 2016

Department of Homeland
Security
Office of Accessibility
Systems and Technology,
Trusted Tester Certified

Work Experience

Junior Project Manager/ Program Coordinator and Student Supervisor, Forest Service

Cooperator, University of Nevada Las Vegas- Forest Inventory and Analysis, Las Vegas, NV | May 2022 to Present.

- Works as a junior project manager to operate and maintain the DATIM and EVALIDator web applications. Both projects are included in the Joint Venture Agreement between UNLV and the Forest Service. The purpose of DATIM is to assist resource program managers to develop statistically valid natural resource monitoring plans and analyses. The purpose of EVALIDator is to produce a large variety of population estimates and their sampling errors based on the current Forest Inventory and Analysis Database (FIADB). Also project manager for Urban EVALIDator, Science Strategy, and Nonresponse bias in estimations projects.
- Performs project management duties: executed, maintained, and updated project plan and schedule, task management and tracking, submitted application security review documentation, quality assurance testing, technical documentation, web accessibility compliance assessment, and handles customer support requests.
- Supervises and manages student employees and staff. Conducts coaching sessions, resolves conflicts and performance issues, assigns tasks, oversees recruitments, handles onboarding/offboarding.
- Performs program coordination duties as follows: provides program and project management support, participates in professional recruitments, handles purchasing needs, maintains software licenses and equipment upgrades, manages asset/ equipment inventories, assists with customer support, training, and outreach activities, performs quality assurance/ quality control testing, updates HMTL through GitHub to assist in the ETL process, and performs other administrative duties as assigned.
- Researches Section 508 of the Rehabilitation Act of 1973 ((29 U.S.C § 794 (d)), generates annual VPAT report for DATIM, creates lessons plans, and teaches staff best practices for following and programming 508 compliance standards across all UNLV-FIA web pages and applications. Tests all UNLV-FIA web pages and applications to ensure compliance of Section 508 by using the World Wide Web Consortium (W3C) Web Content Accessibility Guidelines (WCAG) and the Department of Homeland Security Trusted Tester Conformance Test Process for the Web. Performs other duties based on FIA National Operations Priorities.
- Manages the Section 508 remediation projects for multiple web applications including, DATIM, UMaestro, and EVALIDator.
- Became certified by the Department of Homeland Security (DHS) Office of Accessibility Systems and Technology as a Trusted Tester. The Applied DHS Trusted Tester method provides a code-

inspection based test approach for evaluating web content conformance by utilizing Web Content Accessibility Guideline's (WCAG) Level A and AA standards. This certification promotes a common understanding of the Section 508 compliance standards, unifies the test process, tools, and reporting, and improves the ability for developers to reproduce test results expediting remediation of nonconformance. The certification test process incorporates all tests in the information and communications technology (ICT) testing baseline in accordance with Section 508 and the Web Content Accessibility Guidelines (WCAG) Level A and AA standards.

Research Associate and Student Supervisor, Forest Service Cooperator, University of Nevada Las Vegas- Forest Inventory and Analysis, Las Vegas, NV | May 2020 to April 2022.

- Supervised and managed student employees, provided program and project management support, conducted recruitments and acquisitions, handled all purchasing and traveling needs, maintained software licenses and equipment upgrades, managed asset/ equipment inventories, coordinated office space, assisted with customer support, training, and outreach activities, performed quality assurance/ quality control testing, updated HMTL through GitHub to assist in the ETL process, and performed other administrative duties as assigned.
- Researched Section 508, generated annual VPAT report for DATIM, created lessons plans, and taught staff best practices for following and programming 508 compliance standards across all UNLV-FIA web pages and applications. Tested all UNLV-FIA web pages and applications to ensure compliance of Section 508 by using the World Wide Web Consortium (W3C) Web Content Accessibility Guidelines (WCAG) and the Department of Homeland Security Trusted Tester Conformance Test Process for the Web. Performed other duties based on FIA National Operations Priorities.

Graduate Teaching Assistant, University of Nevada Las Vegas, Las Vegas, NV | August 2017 to 2020

- Served as head graduate teaching assistant for physical geography labs. Responsibilities included preparing lab materials, instructing other graduate teaching assistants on the subject matter, and how to teach the material to students. As a TA, I prepared lab lectures and instructed students on the basic applications in geography and geology.

Courses taught: Physical Geography.

Billing Coordinator and Administrative Assistant, Netech Corporation and Presidio INC., Caledonia, MI | May 2012 to June 2017.

- Responsible for managing and creating new customers and vendors within our systems; managed order and engagement status with sales, purchasing, engineering, and project management; coordinated shipping activity and sales tax with vendors; reviewed and submitted vendor invoices for payment; generated customer-facing invoices; performed other duties as assigned.
- Managed multiple phone lines and directed calls to appropriate personal, conducted proof of deliveries, and revamped and maintained the accounts payable filing system.

Teaching Assistant, Grand Valley State University, Allendale, MI | August 2013 to 2016.

- Responsible for answering students' inquiries, setting up lab materials, and grading papers.

Courses taught: Mineralogy, Earth History, and Exploring the Earth.

Geology Departmental Assistant, Grand Valley State University, Allendale, MI | August 2013 to 2016.

- Responsible for prepping and cleaning up lab spaces, sorting the rocks & mineral kits, filing fossils and specialty pieces, returning topography maps to the respected places.

Museum Collections Intern, National Park Service and AmeriCorps Volunteer, Jimmy Carter National Historic Site, Plains, GA | May to August 2014, 450 hours of Service.

- AmeriCorps and Student Conservation Association (SCA) member. Completed museum inventory; updated locations and catalog data in Interior Collections Management System (ICMS); identified, labeled, and packaged artifacts for curation; photographed the entire museum collection.

- Performed regular collections management duties, such as housekeeping and integrated pest management (IPM). Received training on the care and handling of museum objects, museum housekeeping, IPM, and operation of ICMS and other programs.

Research Experience

UNLV M.S. Thesis: Morphology of Recrystallized Vs Neocrystallized Fibrous Amphibole: Implications for Potential Health Risk | *Masters Advisor:* Dr. Brenda Buck | *Duration of Study:* 2017 to Present | *Expected Graduation:* May 2023.

- Conducting medical geology research on naturally-occurring amphibole asbestos (NOA) and the health risk potential in McCullough Range, NV. Analyzed amphibole fiber morphology via the field emission scanning electron microprobe to understand its potential toxicity. Independently and frequently handled hazardous asbestos waste.
- Previously 40-hr HAZWOPER certified and understands procedures and necessary personal protective equipment (PPE) for handling hazardous waste. Familiar with many contaminants and the methods for remedial action, especially when regarding asbestos.

Radon Emissions and Potentials within the Michigan Natural Storage Facility (Gypsum Mine) | *Faculty Mentor:* Dr. Peter Wampler | *Duration of Study:* 2015 to 2016.

- Responsible for radon air quality emission data collection, sampling for isotopic analysis, literature searches, data visualization and interpretation, final report, and poster presentation.

High Resolution, Optical Simulated Luminescence, and Granulometry Analysis of Stratigraphic Sections at Tel-Yarmut within the Central Shephelah, Israel | *Faculty Mentor:* Dr. Oren Ackermann | Bar Ilan University, Israel | *Duration of Study:* June to August 2015.

- Responsible for creation of stratigraphic sections, collection of samples for Granulometry, High Resolution, OSL dating methods/ analyses, and collection of archaeological artifacts (i.e. pottery, stone tools, etc.) with proper documentation.

Laboratory and Field Skills

DHS Trusted Tester certified for section 508 accessibility standards, previously 40-hr HAZWOPER certified, hazardous substance sampling, handling of toxic substances (asbestos/ radon), use of proper PPE, air quality data collection, environmental data collection, data analysis/interpretation, petrographic microscope, scanning electron microscope, field emission scanning electron microscope, Microsoft Office, and technical writing.

Honors/Awards

UNLV Graduate Teaching Assistantship (2017-2020), Bernada French Scholarship (2018-2020), Graduate Access Scholarship (2017-2020), GSA G&H Best Poster Award (2018, 2019), UNLV Geosymposium Best Graduate Poster (2019), GSA Travel Award (2018), Edwards & Olswang Scholarship (2017), GVSU Distinguishing Promise Award (2016).